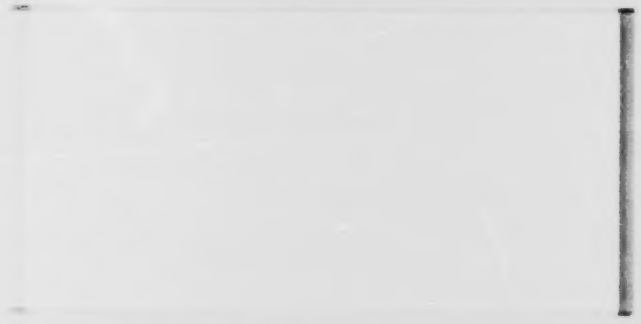

ARCTIC SCIENCES LTD

CA1
DTC 801
87
E82
c.2

88-00309/

Library and Information Centre / Centre de Documentation (CSLA)
RECEIVED / REÇU LE
JUL 30 1987
Transport Canada / Transports Canada

TP 8461E

AN EVALUATION OF THE FEASIBILITY OF ACOUSTIC RADAR DETECTION OF ICEBERGS IN PACK ICE

Prepared for

Transportation
Development Centre

Transport Canada

by

J.R. Marko

Arctic Sciences Ltd.
1986 Mills Road
R.R. #2, Sidney, B.C.
V8L 3S1

(604) 656-0177

ASL File 39-113-M

May 11, 1987

DISCLAIMER The contents of this report reflect the views of Arctic Sciences Ltd. and not necessarily the official view or opinions of the Transportation Development Centre of Transport Canada.

LANGUAGE NOTICE Un sommaire en français de ce rapport est inclus avant la Table des matières.

PROJECT TEAM

Dr. J.R. Marko	- Overall direction, field and interpretative work.
Mr. R.D. Huston	- Theoretical analysis.
Mr. D.D. Lemon	- Acoustical technique critique.
Mr. W.J.B. Wallace	- Electrical engineering, instrument maintenance and modification, field measurements.
Mr. R.A.J. Chave	- Software development.

Transport Canada / Transports Canada
Development / Développement

REPORT DOCUMENTATION FORM

1. Transport Canada Report No.	2. TDC Project No.	3. Recipient's Catalogue No.
TP 8461 E	6418	

4. Title and Subtitle	5. Report Date
An Evaluation of the Feasibility of Acoustic Radar Detection of Icebergs in Pack Ice	May 1987
	6. Performing Organization Report No. ASL 39-113-M

7. Author(s)	8. Transport Canada File No.
J.R. Marko	D1460-224

9. Performing Organization Name and Address	10. DSS File No.
Arctic Sciences Ltd. 1986 Mills Road, RR#2 Sidney, BC V8L 3S1	11SB.T8200-4-4588
	11. DSS or Transport Canada Contract No. 1SB85-00200

12. Sponsoring Agency Name and Address	13. Type of Report and Period Covered
Transportation Development Centre (TDC) 200 Dorchester Blvd., West West Tower, Suite 601 Montreal, Quebec H2Z 1X4	14. Sponsoring Agency Code

15. Supplementary Notes	16. TDC Project Officer
	H. Posluns

17. Abstract

A previous theoretical evaluation of the feasibility of using acoustic radar to detect small iceberg fragments in the midst of sea ice was extended to include field tests on man-made targets at temperate latitudes. A commercial SODAR instrument was used in a horizontal configuration to obtain transmission, return signal and noise data under a variety of atmospheric and other environmental conditions. Data were in qualitative agreement with present understandings of long-range sound propagation. Return signal data were well characterized by an empirical model which was combined with environmental and estimated noise source data to assess feasibility of detecting 50 m^2 iceberg surfaces under worst case conditions in sea ice and on the open ocean. Detection range estimates were 1 to 1.5 km with the "as is" system with a high probability for further range extension through the optimization of frequency and other transmission parameters, noise reducing design changes and the addition of processing gain. It was concluded that a commercial navigation instrument based on the tested concept is feasible. Recommendations for future related research and development were provided.

18. Key Words	19. Distribution Statement
Acoustic radar, iceberg detection, Sodar, sound distance and ranging	Limited number of copies available from the Transportation Development Centre

20. Security Classification (of this report)	21. Security Classification (of this page)	22. No. of Pages	23. Price
Unclassified	Unclassified	135	

Canada

Transports Canada / Transport Canada
Développement / Development

FORMULE DOCUMENTAIRE DU RAPPORT

1. Nº du rapport Transports Canada	2. Nº de l'étude — CDT	3. Nº de catalogue du destinataire
TP 8461 E	6418	

4. Titre et sous-titre	5. Date du rapport
An Evaluation of the Feasibility of Acoustic Radar Detection of Icebergs in Pack Ice	Mai 1987
	6. Nº du rapport de l'organisme exécutant: ASL 39-113-M

7. Auteur(s)	8. Nº de dossier Transports Canada
J.R. Marko	D1460-224

9. Nom et adresse de l'organisme exécutant	10. Nº de dossier — ASC
Arctic Sciences Limited 1986 Mills Road, RR#2 Sidney, C.B. V8L 3S1	11SB.T8200-4-4588
	11. Nº de contrat — ASC ou Transports Canada: 1SB85-00200

12. Nom et adresse de l'organisme parrain	13. Genre de rapport et période visée
Centre de développement des Transports (CDT) 200 boul. Dorchester ouest Suite 601, Tour ouest Montréal, Québec H2Z 1X4	14. Code de l'organisme parrain

15. Remarques additionnelles	16. Agent de projet — CDT
	H. Posluns

17. Résumé

Nous avons élargi la portée d'une évaluation théorique précédente sur la possibilité d'utiliser des ondes acoustiques pour détecter la présence de petits icebergs au milieu des glaces marines afin d'inclure des tests effectués sur le terrain avec des cibles artificielles, à des latitudes tempérées. Un appareil SODAR a été utilisé dans diverses conditions atmosphériques et environnementales pour émettre horizontalement des ondes et capter les ondes réfléchies et le bruit ambiant. Les données obtenues sont en assez bon accord avec la compréhension actuelle de la propagation des sons à long portée. Le signal réfléchi est bien décrit par un modèle empirique, lequel est combiné avec des données environnementales et des données approximatives sur les sources de bruit pour évaluer la possibilité de détecter des icebergs d'une surface de 50 m^2 dans les conditions les moins favorables, en présence de glaces marines et en pleine mer. La portée de la détection a été évaluée à environ 1 à 1,5 km avec le système actuel; on pourra fort probablement accroître cette portée en optimisant le choix de la fréquence et de certains autres paramètres de transmission, et en modifiant l'appareil de façon à réduire le bruit et à accroître le gain. Nous en sommes venus à la conclusion qu'il était possible de concevoir un appareil de navigation basé sur ce principe. Nous terminons par certaines recommandations sur la recherche et le développement dans ce domaine.

18. Mots-clés	19. Diffusion
Ondes acoustiques, détection des icebergs, SODAR, télémétrie acoustique	Un nombre limité de copie est disponible auprès du Centre de développement des transports

20. Classification de sécurité (de ce rapport)	21. Classification de sécurité (de cette page)	22. Nombre de pages	23. Prix
non classifié	non classifiée	135	-

Canada

ACKNOWLEDGEMENTS

The author would first like to express his appreciation and gratitude to Arctic Sciences Ltd. staff members, Bill Wallace and René Chave, who actively participated in the experimental and data-processing work. Additional useful discussions of results were also carried out with David Lemon of Arctic Sciences and Del Huston of the University of Victoria. Numerous other individuals outside of the company also contributed important advice and insights relevant to both experimental design and data interpretation. Most prominent in this respect were Drs. Tony Embleton and Gilles Daigle of the National Research Council, Mr. Tant Priestly of the NOAA Wave Propagation Laboratory and, of course, Dr. Ken Underwood of Xontech Inc., who made significant contributions to the solution of innumerable small technical difficulties.

SUMMARY

The report addresses the feasibility of using sound transmitted and reflected in the atmosphere to detect the presence of icebergs in the vicinity of a marine vessel or offshore platform in the presence of sea ice or high sea-state conditions. Experience has shown that the detection of such navigational hazards with conventional marine radar is highly uncertain because of the relatively higher per unit area radar cross-sections of the sea ice and sea surface relative to the icebergs of freshwater origin. It was suggested that detection through atmospheric sound reflection would circumvent this "clutter" problem by offering return signals which are more or less directly proportional to the projection of the area of the reflecting object onto a plane normal to the insonifying beam.

This alternative approach to detection was tested, using the theoretical basis outlined in an earlier preliminary report* and transmission, reflection and noise data gathered during a series of temperate latitude field experiments. These experiments utilized a commercial Sodar (sound distance and ranging) instrument, normally used in a vertical configuration to measure atmospheric winds and boundary layer structure.

The instrument was operated with its antenna axis directed horizontally at a series of man-made reflectors extending upward from cement- and sea water-covered earth planes, transmitting 70 acoustic watts of power in a 7° beam. Instrument data output consisted of 128 consecutive samples, taken at .05 or .1 second intervals, of the logarithmically amplified voltage signals generated by the reflection of .2 second duration sound pulses.

Sound level measuring equipment was used both for calibration and to observe the dependence of the incident sound levels (at the target) on wind and atmospheric thermal structure. Comparisons of both incident and return signal level data indicated that reflected signals were obtained almost exclusively from surfaces with normals deviating by less than 25 to 30° from the incident beam axis. Moreover, major changes in both recorded levels were primarily associated with alterations of the vertical profile of sound propagation speed relative to the stationary earth reference frame. In particular, upwind sound propagation and propagation through a boundary layer with a negative vertical temperature gradient (air temperatures decreasing with elevation) coincided with reduced sound levels because of upward refraction of the detected sound beams. This effect resulted in the formation of acoustic shadow zones where, according to

---

* Marko, J.R. and Huston, R.D. An Evaluation of the Feasibility of Air Acoustic Detection of Icebergs in Pack Ice. Interim Report, 1985.

ray theory, zero sound levels should have been recorded. Nevertheless, the considerable sound levels observed in such zones were consistent with earlier short-range measurements and the postulated existence of underlying mechanisms associated with diffraction and forward scattering.

It was found that most of the return signal data could be understood in terms of the transmitted acoustic power levels and relatively small (in terms of decibels) deviations from free propagation or "free field plus pressure doubling" (FPPD) values for ranges up to 1 km. In terms of an empirical model or description developed from the data, signals recorded at such ranges were found to be, on average, about 13 dB below expectations from simple calculations assuming reflection of the incident sound by smooth planar surfaces and conventional geometric and attenuation loss mechanisms. The extreme deviations from the FPPD values were -3 and -19 dB. At ranges larger than 1 km (tested up to R=1645 m) the deviations from the corresponding R=1 km value were, on average, well described by additional losses of 5 or 10 dB depending on, respectively, the absence or the presence of upward refraction conditions in at least one leg of the two-way reflected sound path. This deviation from the primarily $1/R^4$ geometric falloff rate of the return signals was evident particularly under overall downward refracting conditions in terms of:

a) returns from very distant targets (at ranges up to 3.5 km) outside the nominal sampling range of the instrument (these returns appeared as reflections of previously transmitted pulses and hence were notable as anomalous structure in the normal return observations); and

b) frequent instances in which stronger returns were received from the more distant member of a pair of targets of similar nominal cross-sections.

Use of these observations to characterize performance of an acoustic radar in Arctic and sub-Arctic marine environments required additional data on both the sensitivity of the Sodar to environmental noise sources and on the strength of those sources. The study reconciled previously reported noise data with new measurements to obtain estimates of ambient noise levels as a function of frequency for vessels moving through open-water and on an icebreaker moving through level first year ice. In the former case, the noise levels were found to be dominated by stack and fan noise and would have their contributions to the Sodar output noise level greatly reduced by the rejection figure of the detector's highly directional, forward-looking antenna. Estimation of the wind-generated noise in this configuration was made by comparisons of instrument signal output noise levels with simultaneous wind and ambient sound level measurements. It was found that the output noise levels (in dB) were approximately proportional to the wind component directed into and along the antenna axis. Moreover comparisons with ambient noise data indicated that the source of this noise was local generation in the vicinity of the unscreened Sodar transducer/horn installation. The experimental data on the relationship between the wind components and the noise levels were used to establish system noise levels under anticipated operating conditions.

The above-outlined empirical return signal model, the experimental noise/wind relationship and an icebreaker noise versus frequency extrapolation were used to evaluate detection ranges for a 50 m^2 reflection surface (corresponding to a face of a 5,000 tonne rectangular parallelipiped-shaped bergy bit). Evaluations were carried out for the in-ice (icebreaking) case and for a marine vessel under full speed in the open ocean. Approximate worse case scenarios were considered for a 350 acoustic watt transmitter/receiver without any obvious modifications to reduce local noise generation. The criterion for detection, derived from our field data was that reflected return output signal levels exceed the noise level by 0.1 volt.

Calculations for the in-ice case were carried out separately for 1,000, 2,000, and 8,000 Hz assuming the validity of the 2000 Hz signal data at other frequencies with the exception of an additional 6 dB loss at 8 kHz in the presence of upward refraction. It was also assumed the wind-related noise component was inversely proportional to the square of the transmission frequency. Scenario data were derived for an icebreaker travelling at 5 m/s into 15 m/s and 3 m/s headwinds. The dominant factor, namely the wind related noise, was found to limit detection to approximately 1, 1.25 and 1.5 km for 1, 2 and 8 kHz respectively.

Estimates made for open sea conditions with a 10 m/s (20 knot) vessel speed and several different headwinds indicate the likelihood of detection out to the 1 to 1.5 km ranges deduced for the in-ice case. It was concluded that acoustic radar detection of small icebergs was feasible to the levels required by operational conditions aboard a vessel moving through first year ice or open water.

Among the alternatives suggested to improve performance beyond the estimated levels, were the use of wind-screening materials and the addition of processing gain. The report's primary recommendation was that data be obtained as soon as possible on the actual detectibility of icebergs under realistic Arctic conditions. It was proposed that this additional study be carried out in 1987 in the Arctic from either the M.V Arctic, a Canada Coast Guard icebreaker, or from some other icebreaking vessel. It was suggested that the efficiency and effectiveness of this study would be maximized by initial system tests with a Sodar instrument, modified to include real-time display and transmission frequency flexibility, in the Victoria, BC area. These initial tests would focus on instrument shakedown and determination of the dependence of detectibility on transmission frequency. Resolution of the latter issue is fundamental to many design questions and could strain program resources if left solely to Arctic testing.

SOMMAIRE

Ce rapport étudie la possibilité d'utiliser des ondes sonores émises et réfléchies dans l'atmosphère en vue de détecter la présence d'icebergs au voisinage d'un navire ou d'une plate-forme en mer, en présence de glaces marines ou en haute mer. L'expérience a démontré que la détection de ces dangers pour la navigation au moyen d'un radar maritime ordinaire est très aléatoire car la glace d'eau de mer et l'eau de mer ont des surfaces radar équivalentes sensiblement plus grandes que celles de la glace d'eau douce et de l'eau douce. On a cru que l'utilisation d'ondes acoustiques permettrait d'éviter ce parasitage du signal réfléchi en donnant des signaux réfléchis plus ou moins directement proportionnels à la projection de l'aire de l'objet réflecteur sur un plan normal au faisceau acoustique.

Cette méthode de détection a été testée à l'aide de la théorie décrite dans un rapport* préliminaire antérieur, et des données ont été recueillies sur les signaux émis et réfléchis ainsi que sur le bruit lors d'une série d'expériences sur le terrain à latitudes tempérées. Ces expériences ont été effectuées avec un appareil SODAR ("Sound Distance And Ranging"), lequel est ordinairement utilisé à la verticale pour mesurer les vents atmosphériques et la structure des couches limites.

L'antenne de l'appareil a été orientée à l'horizontale vers une série de réflecteurs artificiels érigés en hauteur au-dessus de plans de sol recouverts de ciment et d'eau de mer; le faisceau avait une puissance acoustique de 70 watts et une ouverture de 7°. Les données recueillies par l'appareil étaient constituées de 128 mesures consécutives, prises à intervalles de 0,05 ou 0,1 seconde, des tensions amplifiées logarithmiquement produites par la réflexion d'impulsions acoustiques d'une durée de 0,2 seconde.

Un sonomètre a été utilisé pour faire l'étalonnage ainsi que pour mesurer la variation du niveau des ondes sonores incidentes (sur la cible) avec la vitesse du vent et la température atmosphérique. La comparaison des niveaux des ondes incidentes et réfléchies a révélé que les signaux réfléchis provenaient presque exclusivement de surfaces dont la normale faisait un angle ne dépassant pas 25 à 30° avec la direction du faisceau incident. Par ailleurs, les variations importantes constatées dans les deux types de niveau étaient dues principalement aux variations du profil vertical de la vitesse du son par rapport à un système de référence fixé à la terre. En particulier, la propagation du son contre le vent et la propagation à travers une couche limite avec un gradient de température vertical négatif (c'est-à-dire lorsque la température diminue avec l'altitude) coincidaient avec une réduction des niveaux sonores en raison de la réfraction vers le haut des faisceaux sonores détectés. Cet effet a occasionné la formation de zones d'ombrage acoustique où, d'après la théorie géométrique de la propagation, on devrait observer un niveau sonore nul. Néanmoins, les niveaux sonores élevés mesurés dans ces zones concordaient avec ceux mesurés précédemment à courte portée [2,3] et avec l'hypothèse de l'existence de mécanismes de diffraction et de diffusion avant.[4]

* Marko, J.R. and Huston, R.D. An Evaluation of the Feasibility of Air Acoustic Detection of Icebergs in Pack Ice. Rapport intermédiaire 1985.

La plus grande partie des données fournies par le signal réfléchi peut être expliquée au moyen du niveau de puissance de l'onde acoustique émise et d'écarts relativement faibles (en décibels) par rapport à la propagation en l'espace libre ou à la propagation "en espace libre avec doublage de pression" pour des distances allant jusqu'à 1 kilomètre. Dans le cadre d'un modèle empirique élaboré à partir des données, les signaux captés à ces distances étaient en moyenne à 13 dB au-dessous du niveau prévu au moyen d'un calcul à hypothèses simples: réflexion des ondes incidentes par des surfaces planes uniformes, propagation géométrique et mécanismes d'affaiblissement réguliers. Les écarts extrêmes par rapport aux valeurs de propagation en espace libre avec doublage de la pression étaient de -3 et -19 dB. Aux distances supérieures à 1 km (distance maximale des tests: 1645 m), les écarts par rapport aux valeurs obtenues à une distance de 1 km étaient en général assez bien décrits par des affaiblissements supplémentaires de 5 ou 10 dB selon l'absence ou la présence respectivement de réfraction vers le haut dans l'une au moins des deux moitiés du trajet aller-retour des ondes sonores. Par rapport à la décroissance de premier ordre en $1/R^4$, due à la propagation géométrique, cet écart des signaux réfléchis étaient particulièrement évident dans la réfraction vers le bas et se manifestait par:

a) la réception d'ondes réfléchies par des cibles très éloignées (à des distances allant jusqu'à 3,5 km) en dehors de la gamme d'échantillonnage nominale de l'appareil (ces ondes réfléchies apparaissaient sous la forme de réflexions d'impulsions émises antérieurement et leur structure anormale était par conséquent facile à distinguer de la structure des ondes réfléchies normales);

b) le grand nombre de fois où le signal réfléchi par une cible était plus fort que celui réfléchi par une cible plus proche de même surface équivalente nominale.

L'utilisation de ces observations pour caractériser la performance d'un télémètre acoustique en milieu arctique et sub-arctique nécessitait des données additionnelles sur la sensibilité de l'appareil SODAR aux sources de bruit ambiant et sur l'intensité de ces mêmes sources. Cette étude concilie avec de nouvelles mesures des données sur le bruit publiées précédemment et évalue le niveau du bruit ambiant en fonction de la fréquence pour des navires se déplaçant en pleine mer et pour un brise-glace se déplaçant dans des glaces de l'année. Dans le premier cas, les bruits dominants sont ceux produits par les cheminées et les hélices et leur contribution aux bruits captés par l'appareil SODAR est fortement réduite par la grande directivité de l'antenne du détecteur. Le niveau du bruit produit par le vent a été évalué dans cette configuration en comparant le niveau du bruit de sortie (en db) est approximativement proportionnel à la composante du vent en direction de l'antenne et dans l'axe de cette dernière. D'autres comparaisons avec les données sur le bruit ambiant ont révélé que la source de ce bruit se trouvait au voisinage du transducteur et du cornet non protégés de l'appareil SODAR. Des données expérimentales sur la relation entre les composantes du vent et les niveaux de bruit ont permis de déterminer le niveau de bruit du système dans les conditions de fonctionnement anticipées.

Le modèle empirique du signal réfléchi décrit ci-dessus, la relation expérimentale entre le bruit et le vent et une extrapolation du bruit d'un brise-glace en fonction de la fréquence ont été utilisés pour évaluer la distance de détectabilité d'une surface réfléchissante de 50 m^2 (ce qui correspond à la section de face d'un "bergy bit" de 5 000 tonnes en forme de parallélipipède rectangle). Les évaluations ont été effectuées pour un brise-glace se frayant un chemin dans les glaces et pour un navire filant à toute vitesse en pleine mer. Des scénarios correspondant approximativement aux situations les plus défavorables ont été examinées pour un émetteur-récepteur d'une puissance acoustique de 350 watts sans modification en vue de réduire le bruit local. D'après les données obtenues pour le terrain, le niveau du signal réfléchi doit dépasser le niveau du bruit de 0,1 V pour qu'un objet puisse être détecté.

En ce qui concerne le brise-glace, les calculs ont été effectués à 1000, 2000 et 8000 Hz en supposant que les données recueillies à 2000 Hz étaient valides aux autres fréquences, sauf pour un affaiblissement naturel de 6 db à 8 kHz en présence d'une réfraction vers le haut. On a également supposé que le bruit occasionné par le vent était inversement proportionnel au carré de la fréquence de transmission. Les calculs ont été effectués pour un brise-glace se déplaçant à 5 m/s avec des vents contraires de 15 m/s et 3 m/s. Les résultats indiquent que le facteur dominant, c'est-à-dire le bruit produit par le vent, limite la portée de la détection à environ 1, 1,25 et 1,5 km à 1, 2 et 8 kHz respectivement.

Des calculs approximatifs ont été effectués pour un navire se déplaçant à 10 m/s (20 noeuds) en pleine mer avec plusieurs vitesses de vent contraire et, dans ce cas, les résultats indiquent que les portées de détection se trouvent à peu près dans la même gamme de 1 à 1,5 km obtenue pour le brise-glace. D'où la conclusion que la détection de petits icebergs par télémétrie acoustique était possible avec la précision exigée par les conditions opérationnelles sur un navire traversant des glaces de l'année ou se déplaçant en pleine mer.

Parmi les possibilités suggérées en vue d'améliorer la performance du détecteur, on remarque l'utilisation de pare-vent et l'accroissement du gain de traitement. La principale recommandation du rapport était qu'on obtienne aussitôt que possible des données sur la détectabilité des icebergs dans des conditions arctiques réelles. Il a été proposé de faire effectuer cette étude additionnelle en 1987, dans l'Arctique, en utilisant le brise-glace ARCTIC de la Garde côtière canadienne ou un autre brise-glace. Le rendement et l'efficacité de cette étude pourraient probablement être optimisés par des tests préliminaires dans la région de Victoria (C.-B.) sur un appareil SODAR modifié de façon à donner des affichages temps réels et offrir un meilleur choix de fréquences de transmission. Ces tests préliminaires auraient pour but de mettre l'appareil à l'épreuve et de déterminer la variation de la détectabilité avec la fréquence de transmission. La réponse à cette dernière question serait de la plus haute importance pour la solution d'un grand nombre de problèmes de conception et pourrait drainer les ressources du programme si elle ne devait être obtenue qu'à partir des tests effectués dans l'Arctique.

TABLE OF CONTENTS

		Page
LIST OF FIGURES		xiv
LIST OF TABLES		xviii
1.	INTRODUCTION	1
2.	BACKGROUND	3
	EXPERIMENTAL RESULTS	15
3.1	INITIAL QUALITATIVE OBSERVATIONS OF REFLECTED ACOUSTIC SIGNALS	15
3.2	INCIDENT BEAM CHARACTERISTICS	17
3.3	RETURN SIGNAL RECEPTION	32
3.4	NOISE	72
3.5	INTERPRETATION AND COMPARISON WITH MODELS	86
4.	EVALUATION OF ACOUSTIC ICEBERG DETECTION	101
4.1	BACKGROUND	101
4.2	IN-ICE ICEBERG DETECTION	103
4.3	OPEN SEA DETECTION	108
4.4	SUMMARY AND RECOMMENDATIONS	108
5.	REFERENCES	116
APPENDIX A	RELATIONSHIP BETWEEN SODAR OUTPUT VOLTAGE AND SOUND PRESSURE LEVELS (SPL) RE: 20 μ PA AT THE RECEIVING ANTENNA	119
APPENDIX B	METEOROLOGICAL DATA AND MAPS OF OAK BAY AND BOUNDARY BAY AIPRORT SITES	123
APPENDIX C	OPEN MARKET EVALUATION	133

LIST OF FIGURES

		Page
Figure 2-1:	Block diagram of the Xontech Sodar instrument.	5
Figure 2-2:	Block diagram of the signal processing stages applied to Sodar preamplifier output.	8
Figure 2-3:	The Sodar antenna, shield and electronics at field site.	10
Figure 3-1:	a) Return signals as a function of range. b) Plan view of the experimental site.	16
Figure 3-2:	Return Sodar signals recorded on the end of the Institute of Ocean Sciences pier.	18
Figure 3-3:	Geometry and notation used in characterizations of direct and indirect transmission paths.	19
Figure 3-4:	Plan view of experimental configurations at Boundary Bay Airport site June 6, 1986.	23
Figure 3-5:	Sound level meter recorder output recorded at the Oak Bay site May 30, 1986.	24
Figure 3-6:	Average sound pressure level as function of antenna rotation angle.	25
Figure 3-7:	Polar diagram of beam pattern.	26
Figure 3-8:	Sound pressure levels measured as a function of range at the target.	28
Figure 3-9:	Sound pressure levels measured as a function of range at the Oak Bay site.	30
Figure 3-10:	Sound pressure levels measured as a function of range for horizontal, and slightly inclined Sodar antenna settings.	31
Figure 3-11:	Distance converted logarithmic intensities of reflected signal returns as a function of range/time at 11:30 PDT and 18:40 PDT, June 24, 1986	35
Figure 3-12:	Distance converted logarithmic intensities of reflected signal returns as a function of range/time at 15:15 PDT and 15:36 PDT June 24, 1986.	36

Page

Figure 3-13: Interval averaged signals recorded for: 11:44-12:19 PDT, 18:00-18:19 PDT, and 18:20-18:35 PDT on May 16, 1986. 38

Figure 3-14: Interval average signals for the periods: 11:26-11:56, 11:59-12:19, 15:05-15:24 and 15:51-16:09 May 21, 1986. 39

Figure 3-15: Interval average signals for the periods: 13:27-13:44 and 15:21-15:31, May 23, 1986. 40

Figure 3-16: Interval average signals for the periods: 11:03-11:15, 12:49-13:12, 15:03-15:11 and 16:45-16:52 PDT May 30, 1986. 41

Figure 3-17: Interval average signals for the periods 11:26-11:45, 13:41-14:00, 15:51-16:12, 17:14-17:32, 17:50-18:09, and 18:59-19:17 PDT, June 24, 1986. 42

Figure 3-18: Interval average signals for the periods 15:11-15:18, 15:29-15:47, 16:07-16:17, 16:56-17:22, and 17:38-18:10 PDT, June 30, 1986. 43

Figure 3-19: Sound pressure levels detected at Sodar receiver during representative daily periods as recorded at the Oak Bay Marina. 47

Figure 3-20: The detectability (elevation above background) of signals associated with reflectors from markers 1, 2 and 3 for the period 15:03-15:11 May 30, 1986. 48

Figure 3-21: The detectability (elevation above background) of signals associated with reflectors from markers 1, 2 and 3 for the period 16:45-16:52 May 30, 1986. 49

Figure 3-22: The detectability (elevation above background) of signals associated with reflectors from markers 1, 2 and 3 for the period 15:02-16:11 June 24, 1986. 50

Figure 3-23: The detectability (elevation above background) of signals associated with reflectors from markers 1, 2 and 3 for the period 17:50-19:17 June 24, 1986. 51

Figure 3-24: The detectability (elevation above background) of signals associated with reflectors from markers 1, 2 and 3 for the period 15:28-15:46, June 30, 1986. 52

Page

Figure 3-25: Marker 2 detectability originally plotted in Figure 3-24, after averaging over groups of 4 consecutive voltage samples. 53

Figure 3-26: Plots of near-simultaneous SPL values associated with reflected returns from marker 1 and windspeed component along Sodar antenna axis. 54

Figure 3-27: Plots of Sodar-received SPL values for markers 1, 2 and 3 as a function of wind component parallel to the transmitting antenna axis. 56

Figure 3-28: Interval average signal returns obtained with a horizontal beam at height 1.2 m directed at a 2.25 m^2 steel plate target mounted at ground level on airport runway, June 5. 59

Figure 3-29: Interval average signal returns from horizontal beam at height 1.2 m directed at 2.25 m^2 steel plate mounted at ground level on airport runway, June 6, 1986. 60

Figure 3-30: The detectability of the June 6, 1986 return signal from the 2.25 m^2 target included at 90° at a range R=462 m. 61

Figure 3-31: Interval average signal returns obtained on June 21, 1986 with the 2.25 m^2 target mounted at ground level on the airport runway. 63

Figure 3-32: Interval average signal returns obtained on June 26, 1986 from the 2.25 m^2 target mounted at ground level on the runway at R=715 m: 20:35-20:45 PDT target inclination 90°; 20:45-20:57 PDT target inclination at 90°; and 20:57-21:02 PDT target inclination at 90°. 66

Figure 3-33: Interval average signal returns obtains on June 26, 1986 from the 2.25 m^2 target mounted at ground level on the runway at R=715 m: 21:03-21:10 PDT; and 21:10-21:14 PDT. 67

Figure 3-34: Interval average signal returns obtained on June 26, 1986 from the 2.25 m^2 target mounted at ground level on the runway at R=715 m: 21:14-21:19 PDT; and 21:19-2: PDT. 69

Page

Figure 3-35: The detectability (elevation above local background) associated with signals recorded at 20:34-21:21 PDT June 26, 1986 with the 2.25 m^2 target mounted on the runway surface at R=715 m with an inclination of 90°. 35

Figure 3-36: Ambient noise sound pressure spectrum levels measured on The Oceanographer. 73

Figure 3-37: Wind-generated noise measured within a 100 Hz bandwidth in the Sodar receiver on the Planet. 74

Figure 3-38: Spectral characteristics measured during motion of an icebreaker. 74

Figure 3:39: Octave band sound pressure levels as measured on the CCGS Radisson in open water. 76

Figure 3-40: Octave band sound pressure levels as measured on the CCGS Radisson when moving through level (first year) ice. 77

Figure 3-41: Sound pressure spectrum levels measured on the upper forward deck of the Queen of Sidney, July, 1986. 79

Figure 3-42: Estimated noise spectrum levels on a forward deck (i.e. fo'c'sle) for an icebreaker moving through level ice and open water. 81

Figure 3-43: Experimental Sodar output values obtained at the Sheringham Lighthouse site as a function of the noise spectrum levels measured adjacent to the cylindrical side of the detecting transducer. 83

Figure 3-44: Experimental data on Sodar noise level at Sheringham Lighthouse site as a function of wind velocity component anti-parallel to Sodar antenna. 85

Figure 3-45: Detailed temperature and velocity versus height data measured above an airport runway during a day day. 88

Figure 3-46: Data points represent sound pressure levels measured above hard ground. 91

Figure 3-47: Experimental return signal ranges versus spatial target range recorded during high propagation periods. 97

Page

Figure 4-1: Plots of estimated noise and signal levels in the presence of icebreaking noise and 3 m/s and 15 m/s headwinds. 105

Figure 4-2: Plots of estimated noise and signal levels for a vessel moving at 20 knots (10 m/s) into 10.5 and 0 m/s headwinds. 109

Figure 4-3: Side- and plan-views of the M.V. Arctic, a potential platform for an acoustic detection instrument. 111

Figure 4-4: A representative modern marine radar display screen. 113

LIST OF TABLES

Table 2-1: Sodar field experiments. 11

Table 2-2: Experiments using Bruel and Kjaer sound level measurement equipment. 13

Table 3-1: Sound pressure levels measured at Sodar receiver (Oak Bay Marina site). 45

Table 3-2: Reduction of May 21, 1986 marker 1 reflect signal as a function of the angular deviation of the Sodar atenna axis. 45

Table 3-3: Sound pressure levels values corresponding to traget-reflected signals. 65

Table 3-4: Model calculated and measured mean sound pressure levels at the target in dB re 20 μPa. 89

Table 3-5: Model calculated and measured mean sound pressure levels at the Sodar antenna in dB re 20 μPa. 90

Table 3-6: Experimental and free propagation model calculated values of the sound pressure level at the Sodar antenna. 94

1. INTRODUCTION

Theoretical arguments have been presented[1]* for the feasibility of acoustic radar detection of small iceberg fragments in the midst of a surrounding sea-ice cover. Calculations indicated that backscattered acoustic beams would allow the discrimination of iceberg fragments as small as 5,000 tonnes at ranges as large as a few kilometres. The main advantages of the new technique relative to conventional marine radar would derive from an approximate proportionality between the area of a reflecting surface and the strength of the received reflected acoustic signal. In the marine radar case, the electromagnetic reflectivity of the freshwater iceberg surface is generally smaller per unit area than that of the surrounding saline sea-ice or open-sea surfaces. As a result, one might expect acoustic, as opposed to electromagnetic, radar to be less sensitive to non-iceberg-related reflections or 'clutter', hence offering superior detection in the close-in (less than a few kilometres) zone surrounding a moving vessel or a stationary drilling platform.

The present report contains the results of a major extension of the earlier work including the performance of actual acoustic detection tests using simulated iceberg reflectors at temperate latitudes. Such tests were recommended by the project review committee to assess the accuracy of theoretical predictions of performance and of the assumed dependences on instrument and environmental parameters. The motivation for such a testing program was to achieve an understanding of the acoustic reflector detection mechanism without incurring the expenses and logistical difficulties of Arctic testing which only would be necessary should initial field data support the feasibility of the detection concept.

Investments in major instrument design, component acquisition and, usually inevitable, 'debugging' efforts were avoided by the use of a commercial Sodar (sound distance and ranging) system manufactured by Xontech Inc. of Van Nuys, CA, for conventional use as a detector of turbulence and wind velocity profiles in the atmospheric boundary layer. The present usage required the writing, by Xontech, of new system software and physical modifications by ourselves of the antenna mount to allow horizontal beam orientation.

The Xontech instrument will be described in some detail in the following Section 2, after a brief summary of the essentials of the acoustic detection technique. Appropriate terminology and parameter definitions will be introduced with reference to the earlier theoretical development[1] and in preparation for the presentation and interpretation of field-test data in Section 3. The latter section will begin with a description of the locations and rational associated with

---

* Numbers in brackets designate references listed at the end of the report.

each of the experiments carried out during the course of the study. Data and conclusions drawn from this experimental work will be related to the feasibility of iceberg detection in Section 4, which also summarizes the study's results and presents recommendations with regard to prospects and major design choices.

2. BACKGROUND

The principle behind the use of atmospheric sound to detect icebergs or other hazardous objects is straightforward. A highly directional (focused) pulsed beam of sound is generated to propagate horizontally over the ocean surface. Reflected portions of this beam, usually detected by a common transmitting/receiving unit, are classified according to their magnitude, timing and direction of their arrival, providing a measure of relative reflecting strength of objects at different ranges along each interrogated direction. Obviously the technique has much in common with the blowing horn and ringing bell echo-ranging long used by whalers, fishermen and merchant vessels to avoid ice and other hazards. The new elements in this application are the great advances which have subsequently been made in the technology of acoustic beam generation and detection and in the understanding of atmospheric sound propagation and reflection.

The quantitative basis of the understanding is most easily expressed in terms of the sonar equation:

$$EL_{ref} = SL - TL_1 - TL_2 + TS \qquad (2.1)$$

where the echo level EL represents the returned signal intensity expressed in decibels (dB) relative to a standard intensity $\sim 10^{-12}$ watt/m^2 (equivalent to a reference sound pressure of 20 μPa associated with the average human audibility threshold in air).

The first term on the right-hand side of Eq. 2.1 represents the source level and, when expressed in decibels relative to the 20μPa level, can be written as:

$$SL_{20\mu Pa} = 20 \log \frac{P_e(r=1m)}{(20\ \mu Pa)} = 10 \log \Pi + DI + 109\ dB \qquad (2.2)$$

where $P_e(r=1\ m)$ is the pressure level recorded 1 m from the source, Π is the total emitted source power and DI is the directional index defined through

$$DI = 10 \log D \text{ and}$$

$$D = \frac{4\pi}{\int_{4\pi} H^2(\theta,\phi)\, d\Omega}$$

$$\text{where } H(\theta,\phi) = \frac{P(r, \theta, \phi)}{P_{ax}(r)}$$

represents the ratio of the pressure signals at (r, θ, φ) and at a distance r on the transducer axis (the pressure beam pattern). As defined, DI is a measure of the additional intensity introduced by the

focusing properties of the antenna at a point on the beam axis. This additional intensity is measured relative to the level which would be received from an isotropically emitting point source of equal power. The terms TL_1 and TL_2 represent the signal loss in decibels associated with the paths from the source to the scatterer and from the scatterer to the source, respectively.

The final term in Eq. 2.1, TS, is the target strength defined in terms of sound intensities (average power/unit area) by the relationship:

$$TS = 10 \log \frac{I(r'=1)}{I_p(r)} = 10 \log \frac{\sigma}{4\pi} \qquad (2.3)$$

where $I(r'=1)$ is the backscattered beam intensity 1 m from the target as inferred from the received backscattered signal and the $1/R^2$ far field relationship and $I_p(r)$ is the incident intensity at the target. We have introduced the backscattering cross-section, σ, through the definition:

$$\frac{I(r'=1)}{I_p(r)} = \frac{\sigma}{4\pi} \qquad (2.4)$$

In the field experiments carried out in this study the generation, transmission and reception of acoustic signals utilized a Xondar Mk-1 Sodar unit. This instrument is normally used in a vertical configuration to:

(a) detect the height of the atmospheric boundary layer through turbulence-generated reflections of transmitted sound waves; and

(b) to extract vertical profiles of the atmospheric wind velocity from the so-called Doppler frequency shifts of the received relative to the transmitted signals.

As indicated in the schematic of the instrument components in Figure 2-1, the Xondar instrument is built around an IBM PC microcomputer equipped with an 8087 math coprocessor, two serial and one parallel ports, a battery-backed calendar clock and two 320 Kbyte floppy disk drives. The key environmental signal processor (ESP) board plugs into the PC expansion bus and, through direct memory access technology (DMA), utilizes the faster 5 million instructions/second (mips) rate of the Texas Instruments TMS digital signal processing chip. (The PC itself operates at only 0.1 mips.) The board operates asynchronously from the PC to carry out the key functions of:

(1) initiating the generation of an acoustic pulse transmitted by the antenna transducer;

(2) determining the PRI (pulse repetition interval) separating successive signal pulse transmissions;

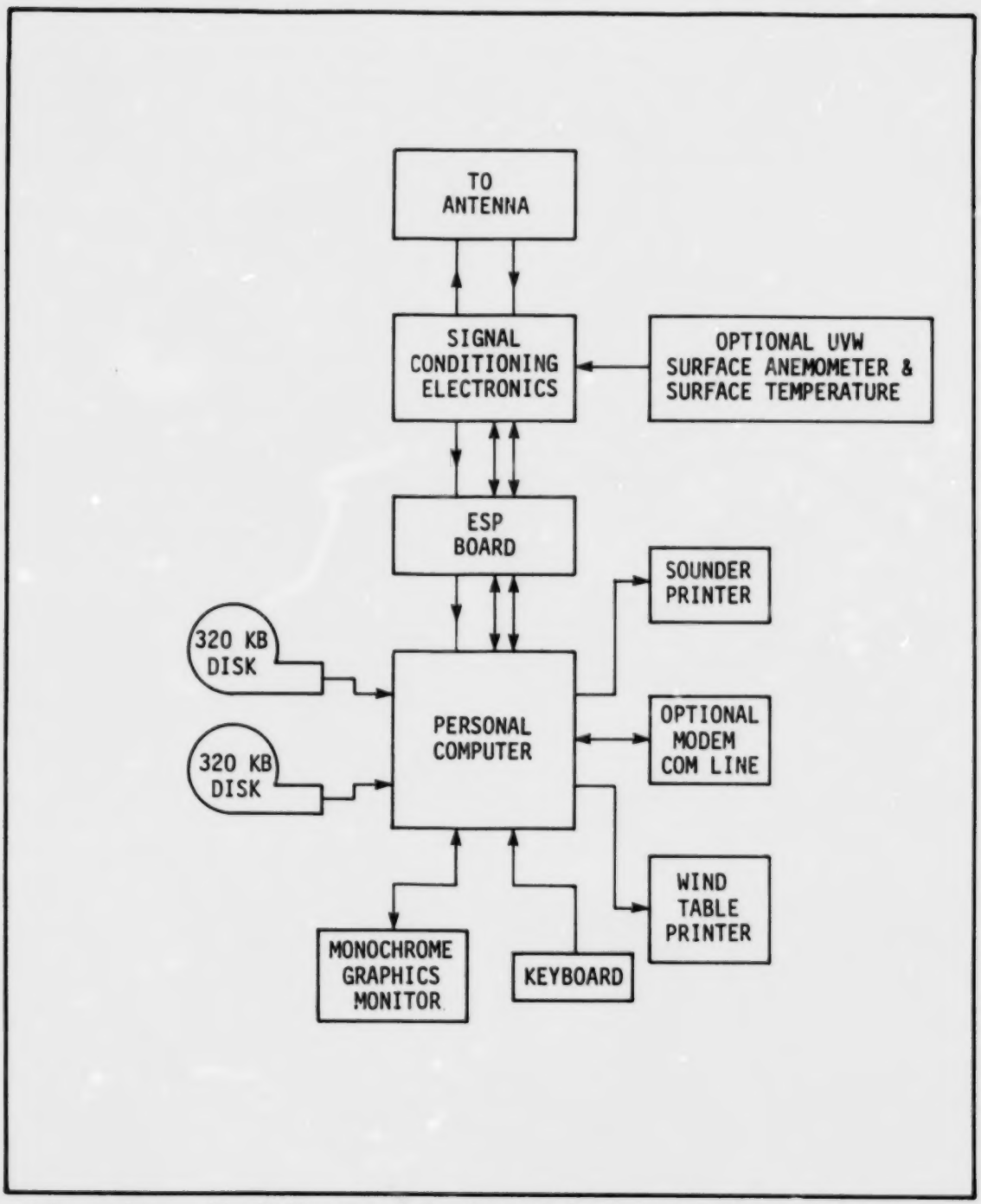

Figure 2-1: Block diagram of the Xontech Sodar instrument used in the field testing programs.

(3) digitizing the bandpass-filtered analog return signal received by the antenna. A double precision FFT (Fast Fourier Transform) is applied to the data before the passing of results to the PC for further processing in order to derive vertical wind profiles from Doppler shift values; and

(4) digitally sampling a logarithmically amplified version of a second portion of the bandpass-filtered antenna signal, thus providing a measure of the time-dependent strength of the received acoustic returns.

Although, as will be seen, the Doppler measurement capability (item 3) would have been useful in the interpretative portions of the study and may have additional practical utility*, the project measurement program concentrated on the use of the Xondar sounder output (item 4). This output represented the amplitude of the returned signals as a function of the time lag after pulse transmission. Since the time delay in the arrival of a signal reflected from an object is proportional to its spatial separation from the transmitter/receiver, signal strength versus time data are directly translatable into representations of reflector strength as a function of range along each interrogated horizontal line. Studies of the transmitted sound signals at various points along such lines and of the corresponding return signals as functions of meteorological conditions and surface reflector properties constituted the bulk of the feasibility evaluation program.

Modifications of the original Xondar system control software were necessary to allow both its use with a single transmitting/receiving antenna beam (three beams are used in its conventional application) and the shift in emphasis to the recording of sounder data. Key operating parameters such as the pulse repetition interval, the timing of the initial pulse and the Doppler sampling and integration periods were menu selectable. Other operational options, such as the transmitted acoustic

---

* During the course of this study, we were made aware of a Transportation Development Centre (TDC) project to use a very high-frequency, downward-looking Doppler velocimeter to measure icebreaker speed in pack ice. Such a capability is needed to optimize the efficiency of the icebreaking function. The required velocity data would be directly obtainable from a Sodar-like iceberg detection device by utilizing the output of the Doppler processing channel generated by backscattered sound reflections of the transmitted sound pulse by the foreground ice-cover topography. This approach would avoid the necessity for large acoustic projectors to compensate for the fact that, in the recommended configuration[2], signal reception is completely dependent upon non-specular reflection (scattering) of the incident beam.

frequency or the rate at which the analog sounder output is digitally sampled, required changes in hardware components (passive filter boards) and separate system disks.

The sounder signal is taken (see Figure 2-2) from the antenna and, after an initial stage of amplification and band-pass filtering (540 Hz bandwidth), is passed through a narrower (45 Hz), digitally-switched capacitive filter prior to full wave rectification, additional amplifications and low-pass filtering necessary for envelope detection. The envelope or amplitude signal is then passed through a logarithmic amplifier to increase system dynamic range before additional amplification and A/D (analog-to-digital) conversion.

Using the known gains of the circuit on the input side of the log amplifier together with transducer parameters, the latter signal can be used to derive the magnitude of the generating pressure oscillation at the transducer. In our case, the relationship between the digitized output voltage and the input pressure signal was established more directly by calibration of the Xondar with reflected directed acoustic signals of known (measured) sound pressure levels (the echo level, EL, of Eq. 2-1). Our procedure in this case is described in Appendix A.

The sounder output is digitized with 12-bit precision (1 sign bit and 11 amplitude bits) at either 10 Hz or 20 Hz. Following each transmitted pulse, 128 receiver voltage samples are taken and recorded at uniformly spaced time intervals. To avoid saturation of the receiver the first of these samples is taken 300 ms after the start of the 200 ms transmission pulse. For the 10 Hz sampling rate, this means that returns were recorded up to 13 seconds after the onset of the pulse. For a sound velocity of 335 m/s, returns could be recorded from objects at distances as large as 2.18 km. For the 20 Hz sampling rate, the maximum range of recorded returns was 1.11 km. Since this limit was often smaller than the range of significant reflecting targets, special care had to be taken to insure that the pulse repetition interval was large enough to avoid confusion from the detection of distant object returns from earlier transmission pulses. Avoidance of such difficulties was found to be possible in most instances by the use of the 10 Hz sampling rate and a 15 second PRI. In this case, successive digital signal values corresponded in principle to samples of returns from 33.5 m deep range cells centred on points separated by 16.8 m along the beam propagation direction. The 33.5 m 'range cell' figure represents the maximum spatial resolution possible with a transmission pulse duration or Δt i.e.:

$$\Delta r = \frac{c\Delta t}{2} \qquad (2.5)$$

Evidence will also be presented to show that even with the above choice of parameters, the presence of particularly strong reflectors and/or appropriate meteorological conditions can still introduce spurious reflections of earlier pulses into the recorded echo.

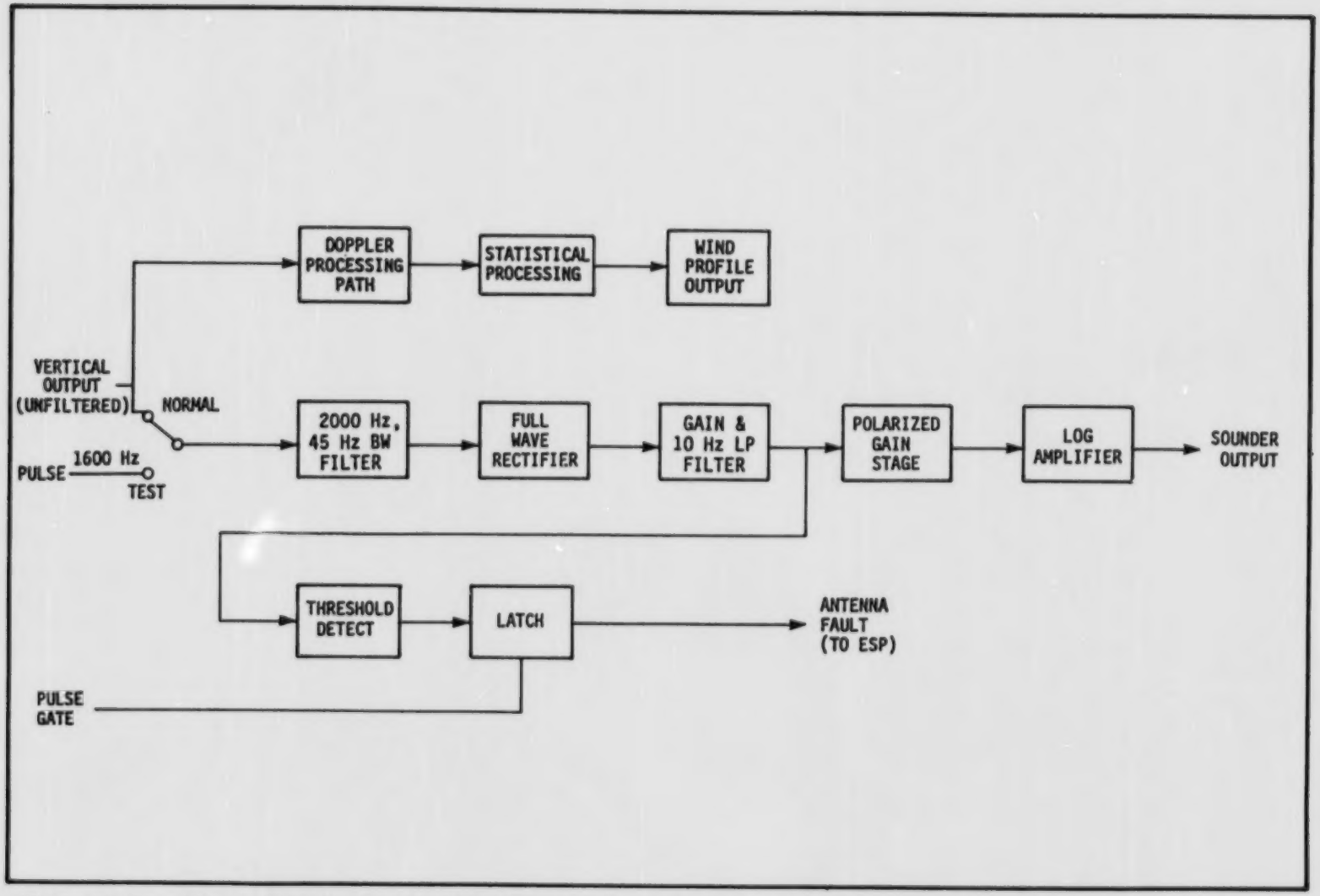

Figure 2-2: Block diagram of the signal processing stages applied to Sodar preamplifier output. After further amplification indicated sounder output is digitized to provide instrument output signal.

Digital sounder output voltages (in millivolts) were written into a 'sounder' data file in which each set of 128 sampled entries was labelled according to the sequential number and time of the immediately preceding transmission pulse (ping). A second 'wind' file was also to be created to record, at specified intervals, the end results of the processing path followed by the second portion of the original analog return signal (Figure 2-2). This Doppler processing chain included high-speed 8 kHz A/D conversion, FFT analysis, averaging and data quality testing. Its products were to be representative of the relative velocity components along the beam axis of major reflecting objects located within specified range intervals. Each velocity component, when associated with wind-generated turbulence or waves for example, could have been of use in interpreting sounder results. Unfortunately, an inadvertent mix-up of 'old' and 'new' versions of the system control disks only allowed the creation of such files for the 1600 Hz transmission experiment which was very brief and limited in content.

A typical field set-up of the Sodar apparatus is shown in Figure 2-3. The sensitive electronic components were protected under the canopy of the pickup truck which was used to transport the heavy and bulky Sodar antenna and acoustic shield which, together with a mounting base, an attached power amplifier, relays and front-end filter electronics (contained in a weatherproof cabinet), were fixed to a specially designed trailer unit.

Other instruments used during the study included an Anderaa automatic recording weather station which provided air temperature, wind speed and wind direction data at two vertical levels (usually 2 and 8 m) and several Bruel and Kjaer (B&K) acoustic instruments, including the 2218 and 2230 sound level meters, the 1621 tunable band-pass filter, the 1625 1/3 octave filter set and a portable graphic level recorder. A 5 kW Honda generator in conjunction with a Sonderstrom line conditioner was used to provide a stable, portable power source for several experiments.

Horizontal Sodar transmission experiments were made at five different locations. Individual sites are listed in Table 2-1 together with associated descriptions, motivations and test dates. Maps of the two most important, Oak Bay and Boundary Bay, sites are included in Appendix B (Figure B-5 and B-6) together with temperature and wind data records contemporary with all experiments.

Other experimental measurements, carried out solely with the Bruel and Kjaer sound level instruments, are summarized in Table 2-2.

With the exception of the CCGS Sir John Franklin noise measurements, none of the experimental tests were carried out under conditions which duplicated the polar and subpolar operating environments of iceberg detection devices. As indicated in the introduction (Section 1), this circumstance was the result of a deliberate decision that the heavy logistical and economic costs of Arctic or sub-Arctic testing should be incurred only if and when less taxing and more efficient measurements at temperate latitudes provided strong indications of feasibility.

Figure 2-3: The Sodar antenna, shield and electronics at field site

Table 2-1: Sodar field experiments.

Location	Date(s)	Site Description	Objectives
Glamorgan Road, Sidney, B.C.	Apr. 9/86	Level 720 m asphalt road bounded at its ends by a 4 m rise and two identical 3 m high flat-roofed cement block buildings. Sodar located on rise and directed perpendicular to front walls of the building	Initial test of system operation and observations of return signal magnitude from cement analog of vertical sided ridge/iceberg.
Institute of Ocean Sciences, Sidney, B.C.	Apr. 23/86	Sodar located on end of dock elevated by 4-5 m and looking out over sea surface. Reflections measured from 4'x8'x1/8" steel sheet mounted on adjustable wooden frame on raft with 1.5' freeboard.	Measurement of return signal strength from plane target as a function of range, sea state, etc.
	May 1/86	As per Apr. 23, but to avoid directional alignment difficulties, plane target replaced by 8'x1' diameter or 10'x1' diameter cylindrical wooden posts.	As per Apr. 23 for cylindrical target.
	May 13/86	At location of earlier IOS experiments but without towed target.	Measurement of noise level dependence on on orientation relative to wind and presence of fishnet spoiler.
Oak Bay Marina, Oak Bay Municipality, B.C.	May 16/86	Sodar located in parking lot immediately overlooking at 4 to 5 elevation, sheltered bay and several natural and man-made reflecting targets in more exposed waters at ranges of 0.6 to 3 km. Initial experiments semi-permanent set-up of weather station at nearby location.	Measurement strengths as function of target and beam orientation meteorological conditions.
	May 21/86	Sodar located in parking lot immediately overlooking at 4 to 5 elevation, sheltered bay and several natural and man-made reflecting targets in more exposed waters at ranges of 0.6 to 3 km.	Measurements made under high wind and sea-state conditions using both 20 and 10 Hz sampling. Sound-level meter measurements of noise and echo strength adjacent to Sodar.
	May 23/86	Sodar located in parking lot immediately overlooking at 4 to 5 elevation, sheltered bay and several natural and man-made reflecting targets in more exposed waters at ranges of 0.6 to 3 km.	10 Hz and 20 Hz 15 sec PRI measurements.

Table 2-1 Cont'd : Sodar field experiments.

Location	Date(s)	Site Description	Objectives
	May 30/86	Sodar located in parking lot immediately overlooking at 4 to 5 elevation, sheltered bay and several natural and man-made reflecting targets in more exposed waters at ranges of 0.6 to 3 km.	As previously except used only 10 Hz, 15 sec PRI measurement to determine dependence on Sodar elevation/depression angle. Sound-level measurements in boat and of noise level and reflected ping levels at Sodar.
	June 24/86	Sodar located in parking lot immediately overlooking at 4 to 5 elevation, sheltered bay and several natural and man-made reflecting targets in more exposed waters at ranges of 0.6 to 3 km.	As previously except weather station mounted on island in beam at range = 0.9 km. Again sound-level measurements made from boat.
	June 30/86	Sodar located in parking lot immediately overlooking at 4 to 5 elevation, sheltered bay and several natural and man-made reflecting targets in more exposed waters at ranges of 0.6 to 3 km.	More measurements with island-mounted weather stations.
Sheringham Point Lighthouse	June 13/86	High elevation site (~14 m above highest H.W.) on cliff behind lighthouse.	Measurements of noise and Sodar signals levels as function of look direction and wind speed and direction. No usable targets.
	June 18/86	Repeated measurements of June 13 and, as well, at a nearby, higher elevation (24 m above highest H.W.) site looking directly westward.	More Sodar and sound-level noise measurements at 14 m and 24 m elevation sites. Short period of 1600 Hz measurements was carried out.
Boundary Bay Airport, Ladner, B.C.	June 5,6/86	Quiet abandoned airport runway (usable length ~1 km) located in Fraser River delta.	Measurements of antenna and sound propagation characteristics over an acoustically hard surface. Determination of reflected signal dependence upon height and orientation of plane target and meteorological parameters.
	June 26/86		Measurements of sound levels and target signal returns during a pre-sunset period when minimal thermal gradients were expected to minimize refractive effects.

Table 2-2: Experiments using Bruel and Kjaer sound level measurement equipment.

Location	Date(s)	Site Description	Objectives
Strait of Belle board the HMCS Sir John Franklin	Apr. 15-16/86	Although data were needed on noise and vibration levels in more typical 1-2 m ice, schedule delays and very light ice conditions limited tested ice conditions to thickness of 1' or less.	Establishment of noise and vibration levels typical of various locations on a working icebreaker.
Strait of Georgia and archipelago of Gulf of Georgia	June 27, July 10/86	Aboard a large ferry transport vessel travelling between Tswassen, B.C. and Swartz Bay, Vancouver Island.	Measurement of noise level as a function of frequency and relative wind speed on board a large motor vessel.

Nevertheless, while none of the experiments actually demonstrated the detection of real icebergs from a vessel in the midst of sea ice or violent or fog-shrouded North Atlantic seas, each of them was intended to provide further data on aspects of the acoustic iceberg detection process immediately relevant to evaluating performance under such typical operating conditions and as identified in the scenarios of [1]. The results of these experiments are presented and discussed in Section 3. Further interpretation and application to feasibility evaluation are given in Section 4.

3. EXPERIMENTAL RESULTS

3.1 INITIAL QUALITATIVE OBSERVATIONS OF REFLECTED ACOUSTIC SIGNALS

Familiarization with the horizontally-directed Sodar instrument in the immediate vicinity of Arctic Sciences Ltd.'s Sidney, B.C. location provided an early opportunity to obtain data relevant to evaluating the reflection strength of objects above both hard and intermediately hard (water) horizontal surfaces.

In the first instance (field experiment 1 of Table 2-1), the Sodar was mounted to transmit a horizontal beam from the top of a gradual rise in a 10 m wide asphalt road which extended away from the lower-end of the sloped segment on a level line before ending in a crossroad 'tee' some 700 m along the length of the transmitted beam. The primary targets of interest at this site were two flat-roofed rectangular cement buildings oriented with their vertical front faces perpendicular to and approximately in the centre of the 7° wide Sodar beam at a range of 725 m. The vertical alignment of these faces and their combined frontal areas of ~100 m^2 provided a fair physical realization of the 50 m^2, 80° slope iceberg fragment reflectors considered in the theoretical evaluation[1].

The resulting 2,000 Hz Sodar data were recorded in air temperatures ranging from 8.9° to 9.3° under gusty 7 kt (3.5 m/s) winds directed easterly antiparallel to the transmitted acoustic beam. Comparison with an appropriately scaled plan view of the experimental site (Figure 3-1b) shows a consistent direct correspondence between the peaks in the detected signal and the presence of localized reflectors. The return from the targeted building was most obvious and superseded in magnitude only by the reflected signals associated with the closest (R<300 m) members of a roadside line of 18" diameter (at base) x 36' high tapered telephone poles.

The building signal was 850 to 900 mv above the relatively high (compared to most other later experiments) noise background levels associated with the proximity of the site to a major highway and an airport. Using the calibration technique of Appendix A, the reflected building signal corresponded to a sound pressure level exactly equal to the 44 dB value predicted[1] for the echo level (EL) associated with a perpendicularly oriented (in the horizontal plane) iceberg surface 50 m^2 in area and 80° inclination under the conditions of the meteorological scenario 3[1] which most closely resembled the moderate, wind-dominated refraction conditions associated with the April 9 measurements. Although corrections to the theoretical model calculations could be made to account for the higher (2,000 Hz) transmitter frequency and the larger surface area and inclination angle of the target, a truly detailed analysis of the observed returns is precluded by the absence of any data on the vertical temperature and wind profiles end as well by the absence of good data on the sound pressure levels at the target.

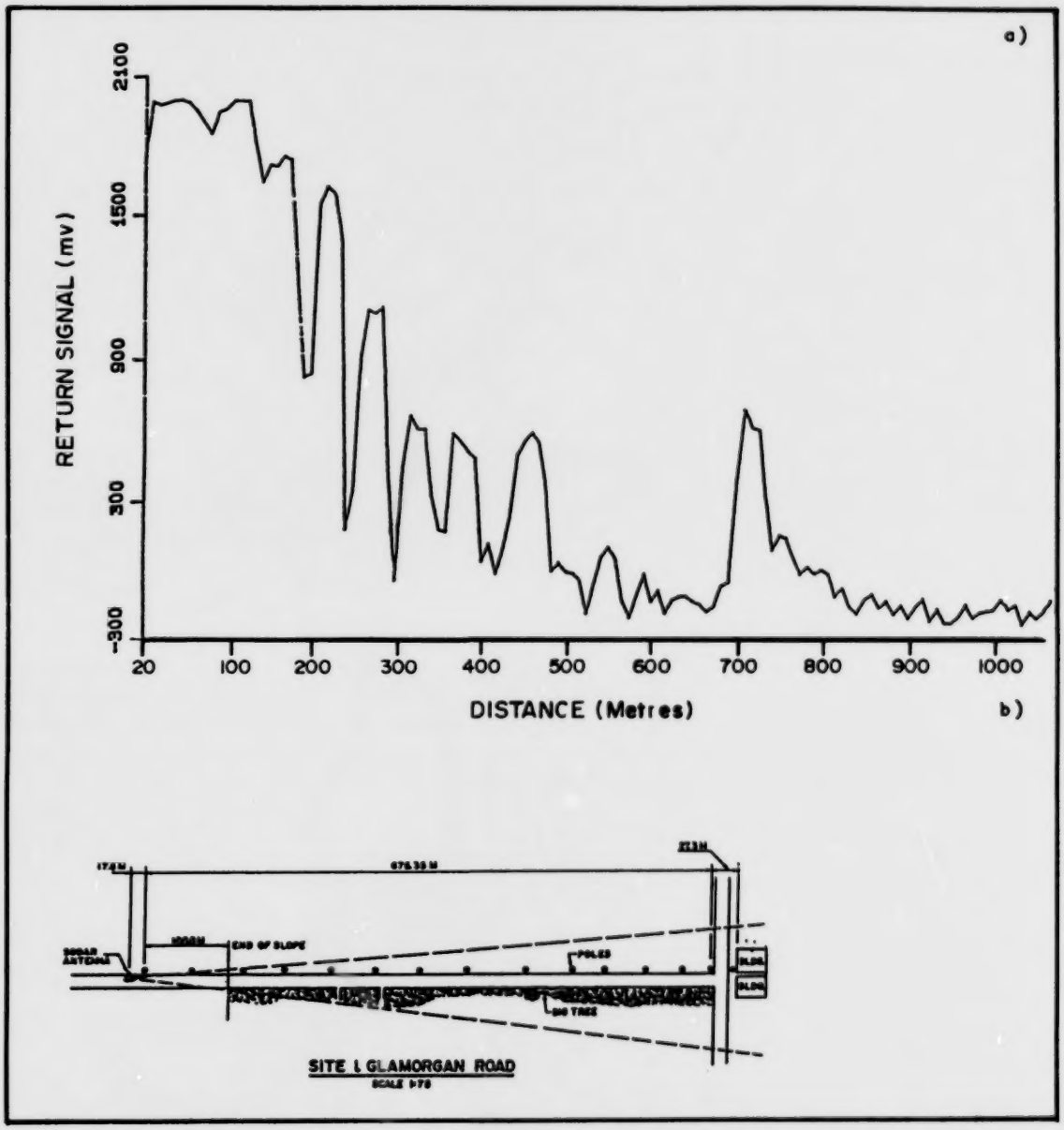

Figure 3-1: a) Return signals as a function of range (averaged over n= transmitted pulses) obtained for Sodar measurements at the Glamorgan Road site.
b) Plan view of the experimental site with horizontal scale identical to that of a). The elevations of the Sodar antenna axis relative to the level section of the road was approximately 4 m.

Other early field tests were specifically directed at measuring the strength of the returns from similar but shorter (2 and 3 m) cylindrical wooden poles vertically mounted on a towable raft deployed in the beam of the Sodar instrument mounted on the end of a deep-water pier at the Institute of Ocean Sciences, Sidney, B.C. Unfortunately, detailed cross-section measurements were contaminated by the presence of significant signal contributions from the sides of the raft which were, moreover, very sensitive to relative beam and raft orientation. The uncertainty in this last respect was, of course, most significant at large target ranges. Such difficulties were also encountered earlier with a raft-mounted planar sheet steel reflector 2.25 m^2 in area deployable at 45°, 60°, 80° and 90° inclination angles. The strong returns obtained from this reflector inclined at 90° and approximately perpendicularly oriented in the horizontal plane (Figure 3-2) again qualitatively confirmed the capability of detecting even small planar surfaces in the less than 1 km range. More quantitative interpretation of this capability, particularly in the presence of the intended Arctic shipboard operational environment required the extraction of transmitted and received reflected beam- and noise-data from subsequent experiments with stable targets and more complete measurements of the time-varying environmental and sound propagation conditions. Relevant details of the three primary sites used in these experiments are provided in Appendix B for easy reference together with the meteorological records cited in interpretation and discussions of the experimental results.

Our remaining presentation of experimental results in this section is organized according to three major data categories:

(a) incident beam characteristics and variability (subsection 3.2);

(b) received acoustic signal characteristics and variability (subsection 3.3); and

(c) noise (subsection 3.4).

An evaluation and interpretation of these data in terms of the theoretical model[1] is provided in a final subsection 3.5.

3.2 INCIDENT BEAM CHARACTERISTICS

3.2.1 BACKGROUND

As previously discussed[1], the acoustic intensity incident on a given test area in the far-field (i.e. where the intensity falls off as $1/R^2$) of a transmitting Sodar antenna will be determined by the following factors:

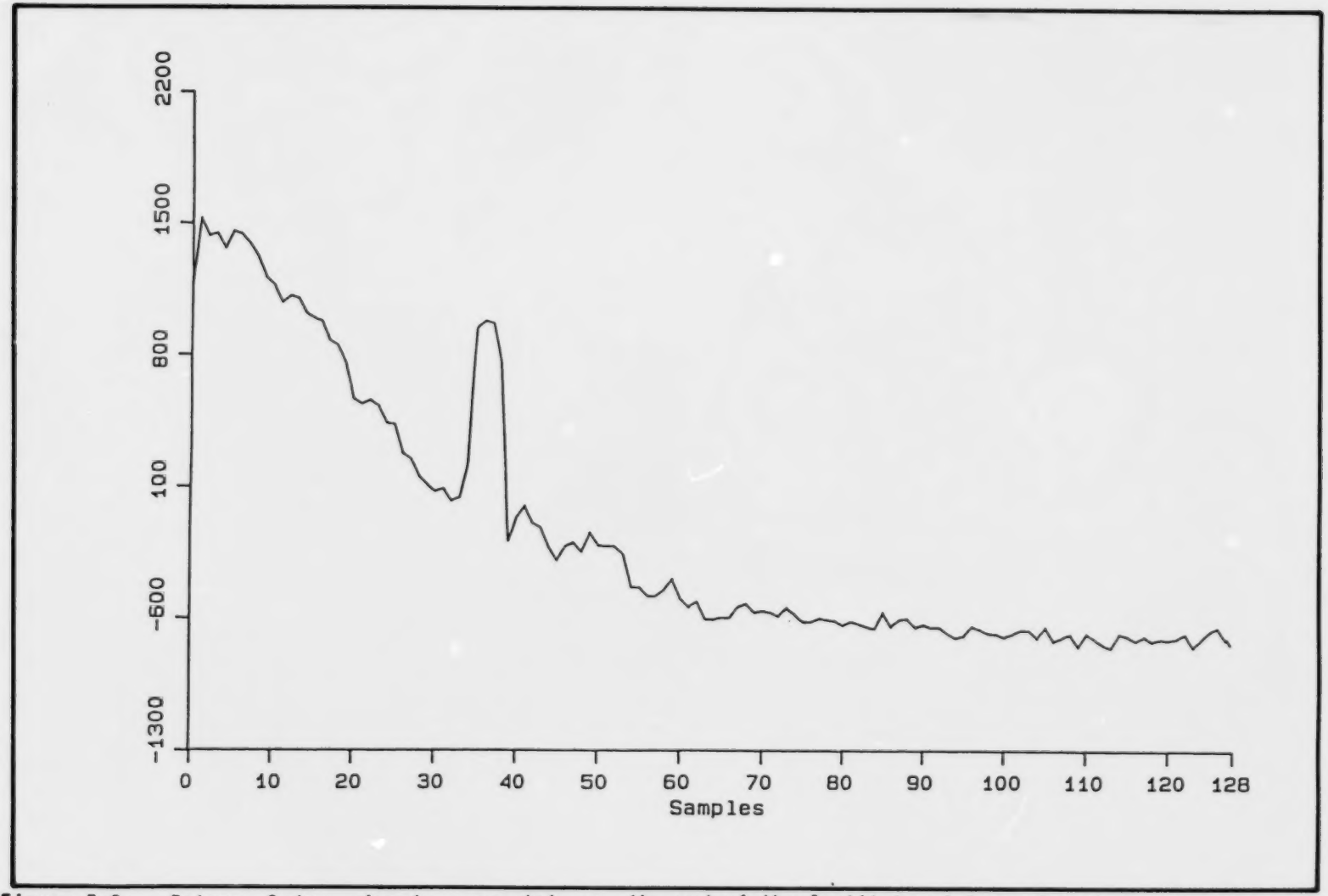

Figure 3-2: Return Sodar signals recorded on the end of the Institute of Ocean Sciences pier. Returns measured at successive samples correspond to range-cells shifted by 8.4 m. The prominent return in this trace (an average of n= pulse returns) arose from reflections off a raft-mounted 8' high wood post 12" in diameter at a range R = 359 m.

(a) the electrical power (at the transmitted sound frequency) supplied to the transducer and transducer efficiency (ratio of acoustic power/electrical power);

(b) the focusing properties of the paraboloidal reflector and its surrounding lead- and lossy foam-lined shield (which was intended to suppress the off-axis side-lobes of the bare reflector beam pattern);

(c) the detailed amplitude and phase behaviour of those components of the transmitted beam which undergo reflection from the intervening ice-, water-, cement- or asphalt earth surface; and

(d) the refraction of the direct and surface reflected beams by vertical gradients in sound speed.

The first two of these factors are relatively simple to characterize for a given Sodar instrument and once established should vary negligibly as a function of measurement conditions, location, etc.

The surface-reflection factor is potentially a source of large variability in beam propagation because of interference between sound wave components which reach a given down-beam point by alternative direct and indirect (reflected) paths (Figure 3-3).

The reflection coefficient of the indirect beam can be written as:

$$R = \frac{\sin\Psi - Z_1/Z_2}{\sin\Psi + Z_1/Z_2} \qquad (3.1)$$

where Ψ is the grazing angle relative to the planar earth surface and $Z_1=R_1+jX_1$, $Z_2=R_2+jX_2$ are the complex acoustic impedance of the air (Z_1) and earth surface (Z_2) media. For a perfectly reflecting hard surface, $Z_2=\infty$ and $R=1$ corresponding to neither amplitude loss nor phase change upon reflection.

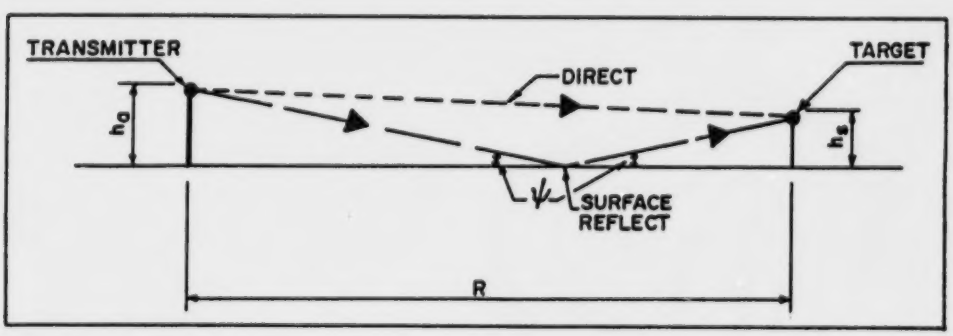

Figure 3-3: Geometry and notation used in characterizations of direct and indirect transmission paths.

However, for realizable reflecting surfaces z_2 remains finite and for angles Ψ such that $\sin \Psi << (z_1/z_2)$, nearly lossless reflection occurs with a 180° phase reversal. Since at ranges R>500 m, the difference in path length between the direct and reflected beam, i.e.

$$\Delta PL = \frac{2h_a h_s}{R} \qquad (3.2)$$

(see Figure 3-3) is usually an order of magnitude or more smaller than the transmitted sound wave length (0.15 m at f = 2,000 Hz); the phase reversal at small angles can cause a sudden drop in the combined (direct plus surface-reflected component-) signal detected at a receiver in the incident beam. Differences in the impedances of ice and sea water could have visible effects in the relative amounts of down beam loss measured over these alternative surfaces.

A secondary category of surface-related effects on beam intensity is associated with the presence of 'roughness' sufficient to reduce the intensities associated with those sound ray components which undergo surface reflection. In the limit where this roughness is large enough to produce a uniform scattering over the above-surface hemisphere, interference effects vanish at the cost of the loss of half of the original transmitted acoustic power.

Nevertheless, the presence of refraction associated with wind-and temperature-gradient induced sound speed gradients is in most circumstances, the main source of long-, intermediate- and short-term variability in the intensity of a propagating acoustic beam.

In the simplest case of a constant vertical gradient in the sound velocity, i.e.

$$c(z) = c_o(z=0) + Kz \qquad (3.3)$$

where c_o=(sound speed in still air at z=0) + $u_o \cos\theta_w$, and u_o and θ_w represent the speed and directionality of the wind respectively with respect to the beam axis. An acoustic ray originally propagating at an angle γ_w to the horizontal follows a circular trajectory with a radius of curvature

$$r = c_o/|K|\cos \gamma_w \qquad (3.4)$$

Depending upon the sign of the quantity K (i.e. a positive or negative gradient in the sound propagation speed), an originally horizontal beam is directed either downward (+) or upward (-). In the latter case, intensities, measured at heights comparable to the elevation of the undeflected beam axis, fall off much more rapidly than $1/R^2$ with range, since all forward propagating rays increase in inclination (relative to the ground plane) with distance. A well-defined shadow region should

appear[2] characterized by negligible measured sound intensities. More recent studies[4-6] have demonstrated that sound penetrates this region through both diffraction and turbulence-induced forward scattering. In the former case the sound in the shadow region originates from a creeping wave which enters the region at the shadow edge and is confined to the region between the surface and a height

$$\ell = \frac{\lambda^2 c}{8\pi^2 \frac{dc}{dz}}$$

Propagation into the shadow region at heights $>\ell$ is describable by the rays of ordinary geometric acoustics.

Forward scattering by atmospheric turbulence becomes of importance for frequencies >500 Hz and lowers the levels of attenuation from those predicted by the purely diffractive propagation mechanism. Recent data[6] suggest that maximum (for $f \leq 4$ kHz) reduction in sound level relative to the zero refraction case is about 30 dB. This reduction was about 10 dB larger than the saturation value previously deduced[7] from experimental results[4].

On the other hand, positive vertical sound propagation speed gradients can, in some cases, increase acoustic intensities by increasing the fraction of arriving rays which have undergone one or more surface bounces thereby reducing the effects of direct/reflected ray interferences. Nevertheless, the possibilities for multipath propagation in this configuration can introduce complex spatial dependences into measured intensity distributions.

As noted earlier[1], separate recognition must be given to the different effects of the gradient components associated alternatively with vertical changes in temperature (through the temperature dependence of the still air sound speed) and the height dependences of the beam-parallel or antiparallel wind components. In the former case, the effect is independent of sound propagation direction. A positive temperature gradient always forces a horizontally propagating sound ray downward. Typical positive vertical wind gradients, on the other hand, force such rays downward or upward according to whether the propagation direction has a parallel or antiparallel wind component, respectively. In the absence of compensating temperature gradient effects, upwind propagation losses may be expected to be considerably in excess of those associated with downwind modes.

In addition to its above-cited role in scattering sound into shadow regions, atmospheric turbulence also affects sound propagation in the directly insonified regions by broadening the beam from its still-air value and by introducing "excess" attenuation associated with the scattering of sound into directions outside the nominal beam pattern[8]. The magnitude

of the additional attenuations can be as large as or greater than 10 dB/km and is proportional to the cube root of the frequency.

3.2.2 EXPERIMENTAL RESULTS

Due to the relatively well-characterized acoustic properties of cement and asphalt surfaces [impedances approaching infinity and negligible phase changes in reflection[9]], the major portion of our experimental measurements of acoustic beam parameters were carried out over an abandoned cement runway at the Boundary Bay airport (see Table 2-1 and Appendix B for site details).

Under these circumstances, the assumption of perfect earth plane reflection was justified on the basis of previous quantitative comparisons of observed and model-predicted propagation properties. Additionally, the presence of a perfectly hard surface plane also provided an excellent representation of the acoustic properties of the continuous sea-ice cover characteristic of the polar and subpolar areas which are the venue for a major use of the acoustic iceberg detection technique. Other experimental propagation data obtained in the marine experiments at the Oak Bay Marina will also be presented and discussed relevant to a second set of detection applications, namely in open- or lightly ice-infested waters. These latter tests can be used, as well, to help evaluate the extent to which propagation is dependent on the properties of the reflecting earth plane.

The acoustic power output of the Sodar unit used in all transmission tests was specified by the manufacturer as 70 watts. This quantity was not directly measured in our experiments, although it was consistent with the measured 88 volt peak-to-peak input to the 4 Ω transducer coil and a typical 30% figure for the transducer efficiency.

Measurements of the angular distribution of acoustic intensity in the horizontal plane containing the beam axis were carried out on June 6. A B&K 2230 sound-level meter was used in a fast response, rms mode from a fixed, 1-m high platform, 462 m from the Sodar transmitter (with its axis, horizontal at 1.1 m height). Changes in angle were made by rotating the Sodar antenna in the horizontal plane (Figure 3-4). This arrangement allowed sound pressure levels to be measured at different angular deviations from the beam axis over a common acoustical path.

Sound pressure levels corresponding to each angle represented the average over at least 50 consecutive transmission pulses in order to minimize the effects of the characteristically large short-term variability in the incident intensity. Examples of this variability are included in Figure 3-5a,b as taken from the recorder output during measurements at the Boundary Bay runway site (a) and over the Oak Bay water surface (b). (The latter measurements were made from small boats with the sound-level meter hand-held approximately 1 m above the water surface.) As these traces suggest, the amplitudes of adjoining pulses were correlated and there were some indications, in both the terrestrial and marine data, of prominent

contributions to variability at periods on the order of 1.5 to 2 minutes. In all cases, the maximum range of variability was about 20 dB.

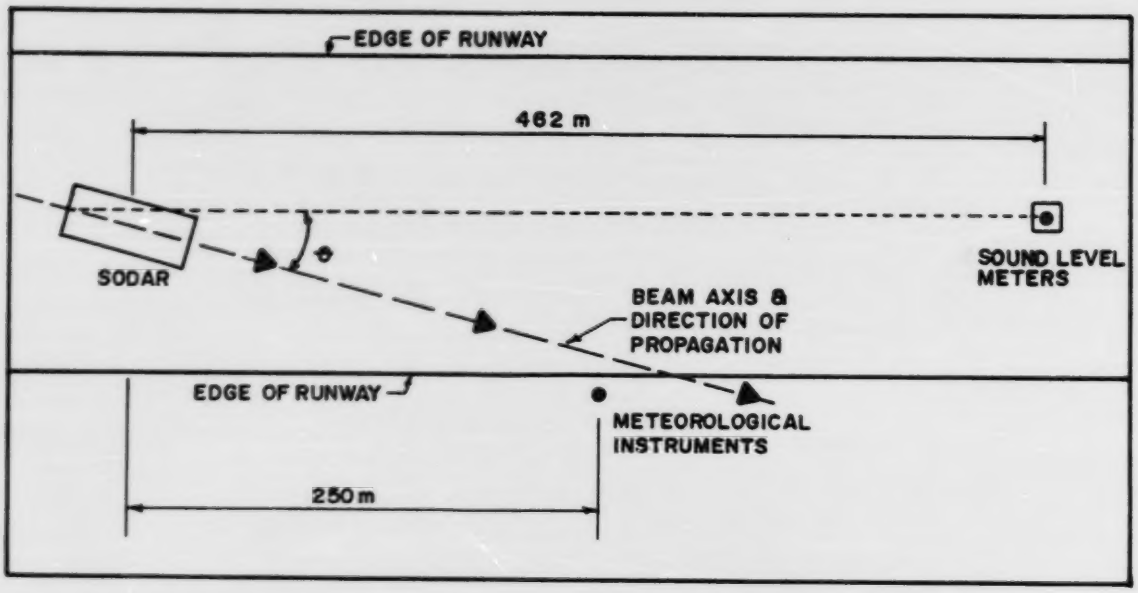

Figure 3-4: Plan view of experimental configurations used for beam pattern measurement at Boundary Bay Airport site, June 6, 1986.

Repeat measurements of the average values at each angular setting over the 3-hour, June 6 measurement period yielded consistency within approximately 2 dB. The average sound pressure levels as a function of θ are plotted in Figure 3-6 and in the more familiar polar form in Figure 3-7. The latter Figure includes the results of a much more detailed set of beam pattern measurements made by Hall and Wescott[10] for 2 kHz transmissions from a transducer mounted close to the focus of a 1.5 m diameter paraboloidal searchlight reflector. Data points are also included for a smaller set of angular measurements made on June 5 in which the directionality of the Sodar antenna was held fixed and data gathered for off-axis angles $\theta \leq 4.1°$ by moving the meter perpendicularly to the beam for distances up to half of the 72 m width of the airport runway.

The results from the June 6 measurements are suggestive of a 3 dB to 3 dB beamwidth somewhat larger (12°) than the nominal 7° value quoted for the antenna by the manufacturer. Additionally, the fall off in SPL at large angles was considerably smaller than that obtained by Hall and Wescott[10] with a smaller amount of acoustical shielding.

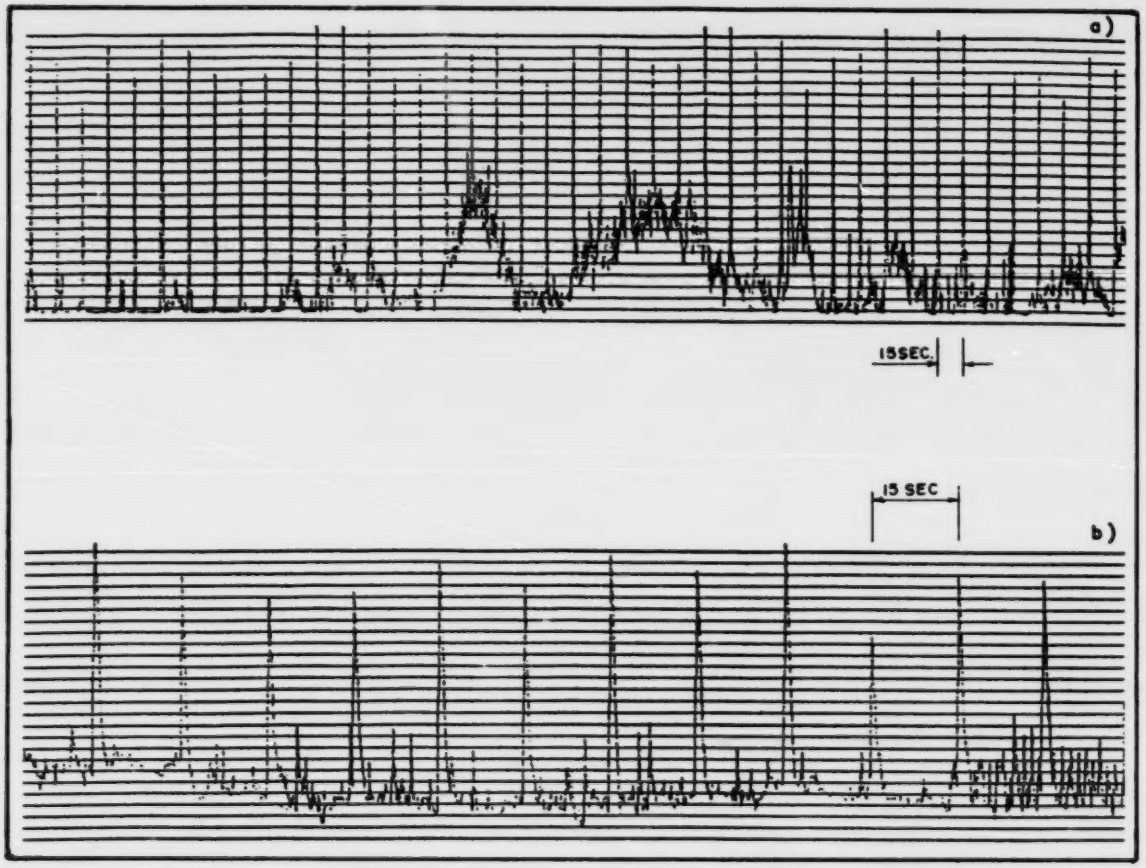

Figure 3-5: Sound level meter recorder output as recorded at the: a) Boundary Bay Airport site on June 6, 1986 and b) at the Oak Bay site May 30, 1986.

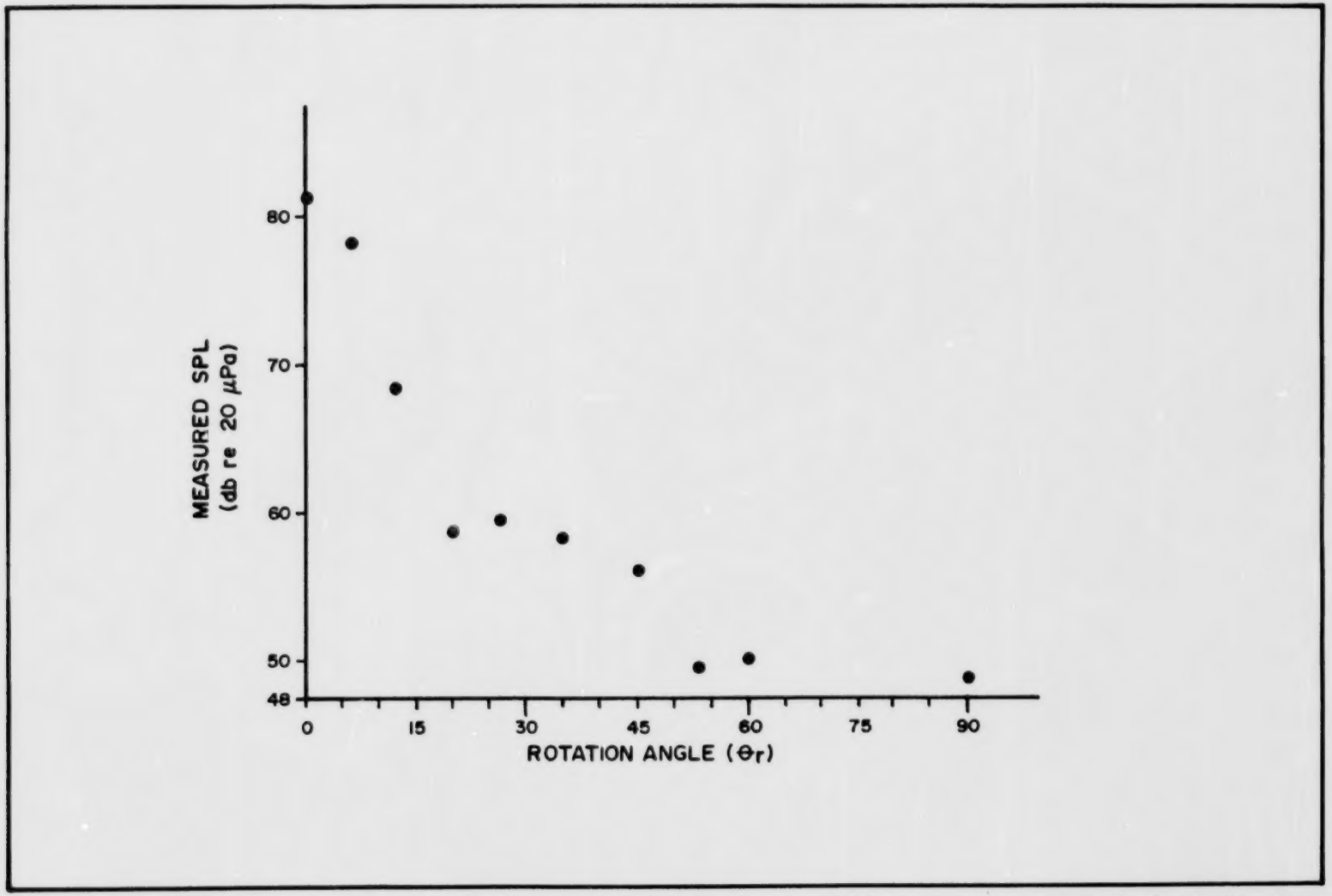

Figure 3-6: Average sound pressure level as function of antenna rotation angle as measured at the Boundary Bay Airport site, June 6, 1986.

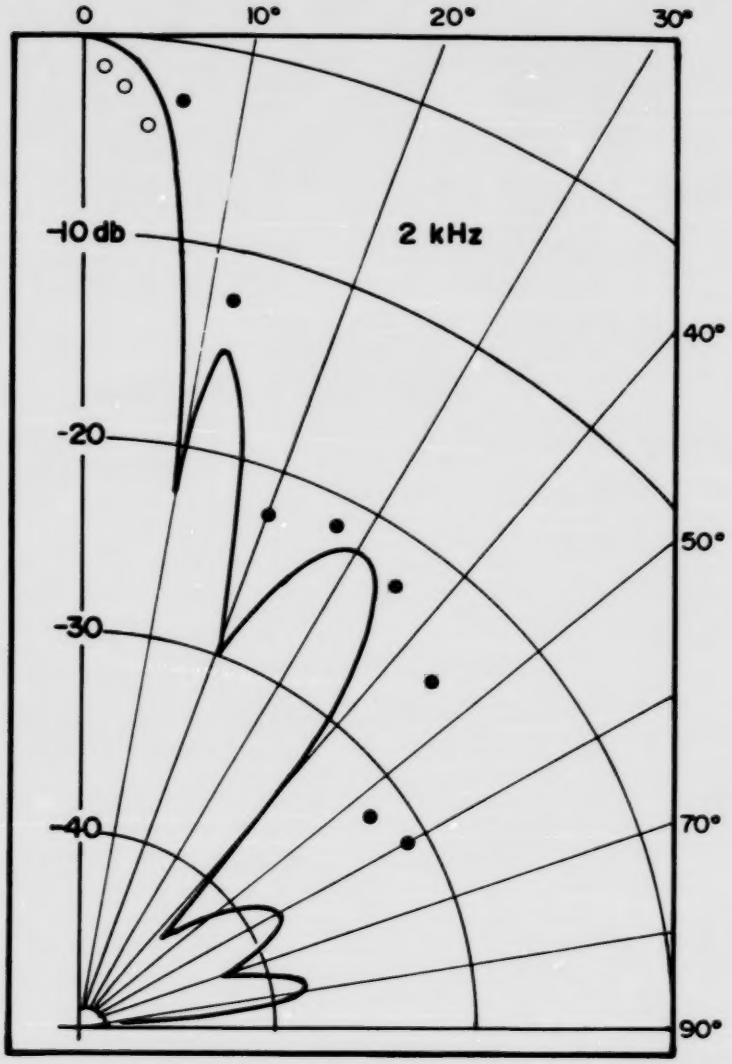

Figure 3-7: Polar diagram of beam pattern. Solid (•) and open (o) circle data prints were recorded on June 5 and June 6, 1986 respectively. The solid curve was reproduced from the f = 2000 Hz results of Hall and Westcott[18].

The latter result was most likely attributable to the warping of the Sodar reflector shield unit produced by its use in a horizontal position. The extent of warping was such as to create direct in-air acoustical paths several centimetres in total cross-section between the reflector interior and the outside environment. The resulting leakage, in particular, would have raised sound pressure levels in directions nearly perpendicular to the beam axis. This difficulty did not seriously interfere with the testing program other than perhaps to increase sensitivity to peripheral noise sources.

The much more limited set of angular dependence data recorded on June 5 (included in Figure 3-7) suggested a stronger angular falloff in transmitted intensity than either observed during the June 6 measurements or as specified by the manufacturer. In part, this result could be an artifact of the two different measurement techniques but is, more than likely, attributable to changes in propagation conditions. Thus, for example, the broader beam pattern observed on June 6 could be associated with higher levels of turbulence[8]. Some evidence for this hypothesis can be found in the sound level pressure (SPL) versus range results plotted for the two dates and for June 26 in Figure 3-8. If one ignores, for the moment, the June 26 (21:08) SPL reading, the June 5 and 26th levels can be seen to have had comparable magnitudes and were consistent with the $1/R^2$ range dependence (indicated by the broken line). The roughly 10 dB reduction from these values noted on June 6 could be interpreted as excess attentuation associated with the increased turbulence hypothesized on the basis of the beam broadening.

Further interpretations of these data are given in subsection 3.5 in terms of the limited meteorological data available for the two dates (Vancouver Airport hourly winds and temperatures after 16:00 PDT June 6) and on the basis of other information on the characteristics of the surface boundary layer.

The June 26 measurements were conducted specifically to include the transition from upward to downward refraction which normally occurs under low wind conditions [T. Priestly, pers.comm.] roughly one hour before sundown during the summer months. As indicated in Figure 3-8, the earliest transmission level recorded on this date (at 20:25 PDT and R = 435 m) was nearly identical to that recorded on June 5 averaging 91 dB (1/3 octave value) with the highest recorded individual return level equal to 98 dB re 20 μPa. Measurements of winds and temperature 25 m to the rear of the target at 2 m and 8 m heights were consistent with the continued presence of upward refraction throughout the surface boundary layer.

Results obtained at R = 715 m over the interval 20:56 to 21:00 were obtained during a period of steady weakening in the upward refractive 2 m to 8 m temperature gradient but yet were consistent with the earlier (20:25 PDT) SPL value and the R^{-2} geometric range dependence.

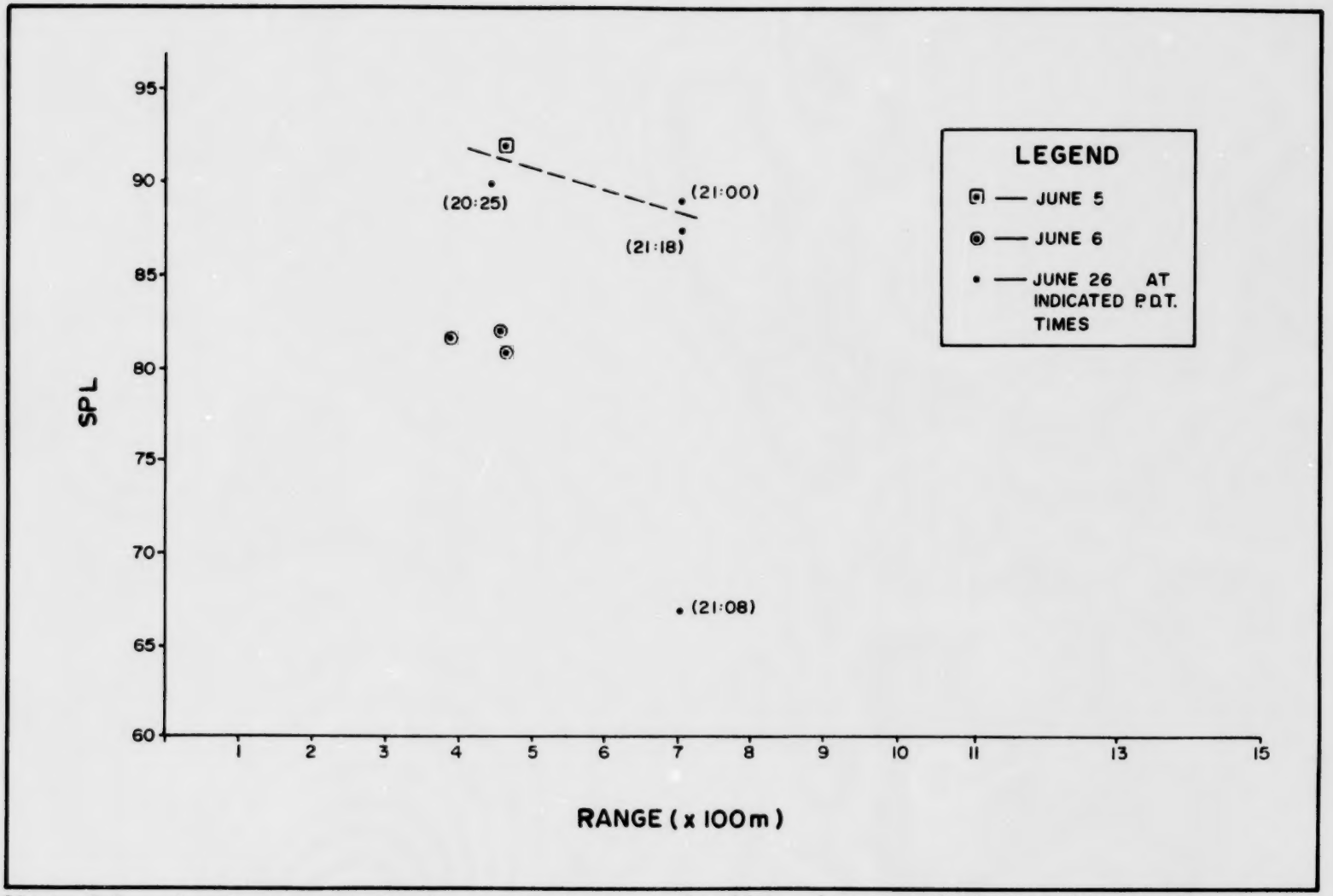

Figure 3-8 Sound pressure levels measured as a function of range at the target at the Boundary Bay Airport site June 5, 6 and 26, 1986. The broken straightline is indicative of the theoretically expected range dependence.

The 20 dB lowering of the sound pressure levels over the following 21:03 to 21:14 SPL measurement interval (labelled 21:08 in Figure 3-8) did not coincide with dramatic change in the recorded 2 m and 8 m temperature or wind readings. A distinct warming noted by the observer coincided with the level reduction suggested a causative mechanism associated with change in the 2 m thick surface layer. Evidence for such changes will be presented in the following subsection 3.3 and in the general interpretations of subsection 3.5.

Angular data were also recorded at the Oak Bay Marina site in the form of a small number of SPL measurements at locations up to 13° off the estimated direction of the Sodar transmission axis. The results were approximately in agreement with the June 5 results plotted in Figure 3-6 (i.e. at θ = 13° SPL values were 15 dB below on-axis levels). Range dependence data in Figure 3-9, taken at various times during the May 30, June 24 and June 30 measurements show considerable variance associated with changing refractive conditions. Moreover, it should be noted that the maximum recorded values are 6 to 7 dB below the values which would have been expected at the same ranges on the basis of measurements made over the Boundary Bay runway during the strong propagation periods of June 5 and 26.

Such differences are not unexpected due to the different geometries of the Boundary Bay Airport and the Oak Bay experiments. The antenna heights in the latter case are 4 to 5 m higher than the Boundary Bay value, although in both cases the sound level pressure measurements were made at 1 m elevation above the reflecting surface. Additional contributions to differences in the two experimental data sets are expected to be associated with the different acoustic impedance and scattering roughness of the cement runway relative to the wave-disturbed sea surface. The additional wave induced scattering, transmissions across the air-water interface and phase changes upon reflection at this boundary all would tend to reduce the amplitude of the marine-detected measured SPL values. Some compensation in this respect would be expected from the greater antenna elevation.

A final set of transmitted power measurements made at the Oak Bay site on May 30, 1986, explored the dependence of the SPL upon the inclination (angular deviation from the horizontal) of the Sodar antenna axis. Results for the two largest positive (elevation) and negative (depression) angles are plotted in Figure 3-10 along with the contemporary 0° inclination values. The solid curve represents the expected SPL-range relationship assuming an 80 dB SPL at R=590 m, the existence of a $1/R^2$ falloff in transmitted power, and an atmospheric attenuation of $2.5 \cdot 10^{-3}$ dB/m as calculated[1] from the results of Bass et al.[11]. The results indicate that the $1/R^2$ propagation law does appear to hold under the inferred weakly downward refraction conditions prevailing on a warm, relatively windless, day (May 30, 1986). Additionally, there is little evidence of a strong effect of beam inclination at ranges less than 1 km. Measurements at greater ranges (1.625 km) were less accurate because of

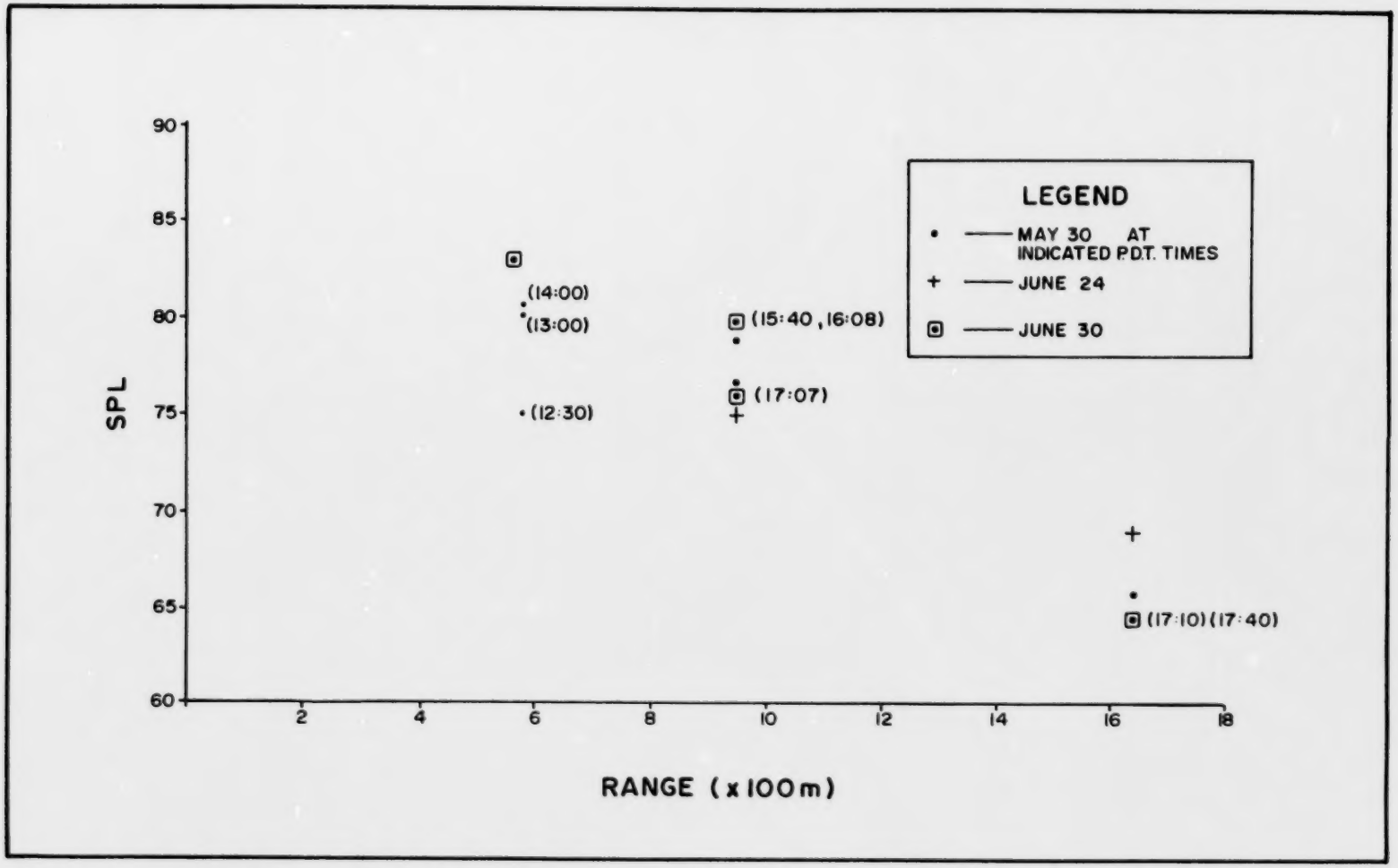

Figure 3-9 Sound pressure levels measured as a function of range 1 m off the water surface at the Oak Bay site at the indicated dates and times.

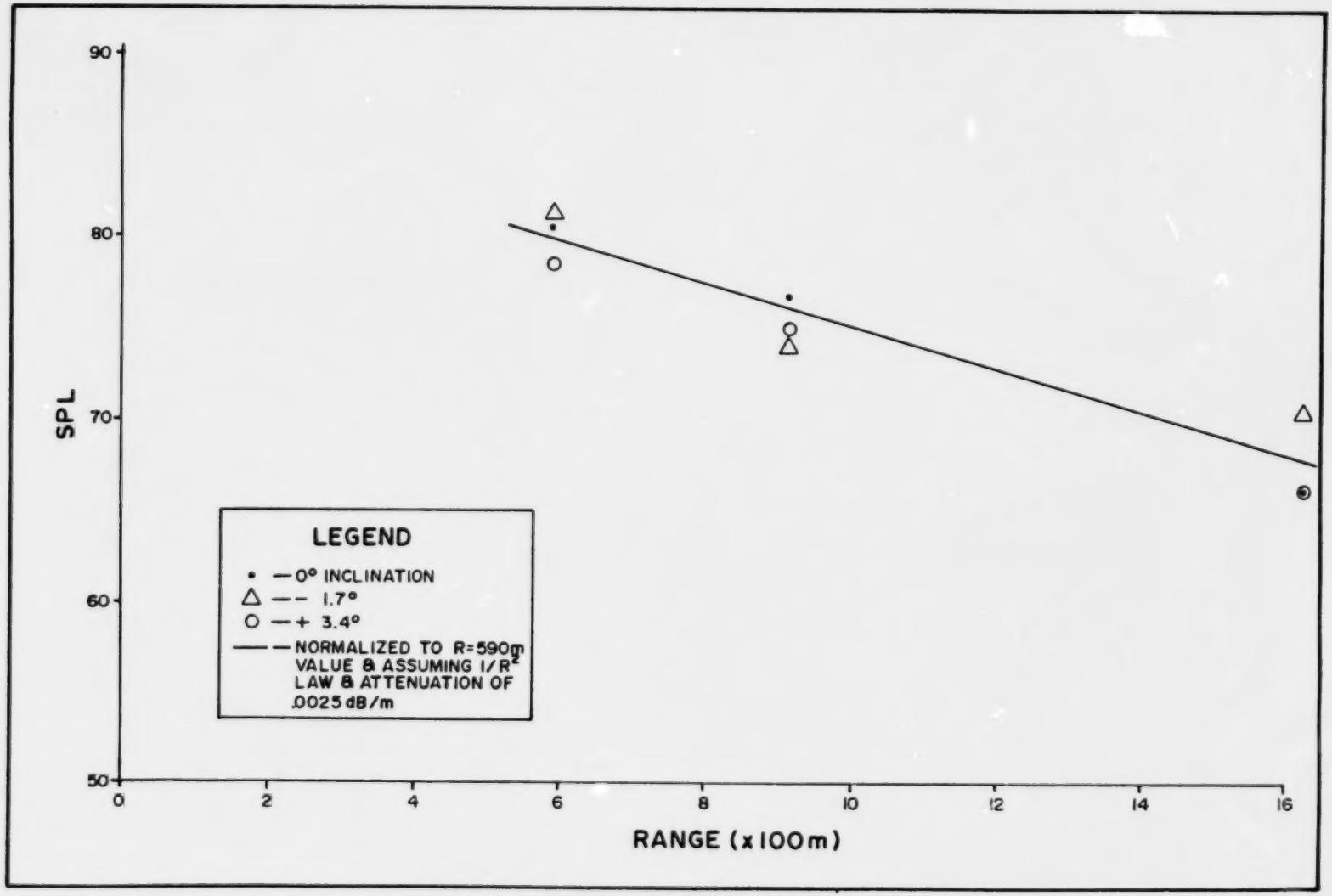

Figure 3-18 Sound pressure levels measured as a function of range at the Oak Bay site for horizontal, and slightly inclined Sodar antenna settings. The solid line was included to allow comparisons with the dependence expected from the standard $1/R^2$ propagation loss factor and the estimated 20°C atmospheric attenuation.

drifting and orientation problems but there appeared to be greater sensitivity to deviations from horizontal propagation.

3.3 RETURN SIGNAL RECEPTION

3.3.1 BACKGROUND

The SPL levels associated with reflections of the transmitted sound beam by a target are theoretically describable by the two-way sonar equation (2.1). This equation expresses these levels as the sum of the source level and target strength minus the transmission losses along the outward (TL_1) and return (TL_2) paths. The quantity TL_1 experimentally studied in the previous section and the target strength TS is related to the target cross-section and reflected acoustic intensities by Eqs. 2.2 through 2.4.

In general, the estimation of a backscattering cross-section involves detailed consideration of not only the size and orientation of the target surface relative to the incident sound beam, but as well quantitative representation of the surface 'texture' usually in terms of the statistical distribution of elevations relative to the mean surface plane. Texture was introduced into the theoretical evaluations[1] by using the expressions derived by Horton and Muir[12] and Horton, Mitchell and Barnard[13] for rough surfaces (surface elevation deviation equal to or greater than ~$\lambda/8$) assuming a Gaussian bivariate probability distribution of elevations for the reflecting surface. More recently, Greene and Stokes[14] have had considerable success in explaining measurements of underwater backscattering strength as a function of grazing angle carried out by Brown and Milne[15] underneath pack ice. Their treatment accounted for the non-Gaussian nature of the distribution of the slopes of the longer spatial wavelength components in the variability of surface elevation. In effect, by accounting for the concentration of surface roughness on the small fraction (10%) of the ice-covered plane occupied by ice ridges (and their underlying keels), Greene and Stokes managed to reproduce the experimental angular distribution which indicated an anomalously low falloff in cross-section at low grazing angles. This approach was also consistent with the previously sited[1] side-scan sonar data[16] which suggested that the acoustic returns from the under-surface of an ice cover are dominated by the presence of the high inclination surfaces associated with the keels of ice ridges. Little return was received from intervening flat regions because of shadowing produced by the ridges and the falloff of the scattering cross-section at small angles of incidence.

The sonar results have much in common with Figure 3-1 which displays a Sodar signal return which is composed of a finite number of discrete pulses superimposed upon an exponential-like decay from a high initial value. The discrete pulses are associated with reflections from highly localized objects of large inclination (i.e. telephone poles and the cement buildings), while the short-lived broad signal component is associated with the cumulative effects of scattering by the strongly irradiated surfaces in the immediate foreground of the transmitting/receiving antenna.

Although the latter component of the signal in Figure 3-1 is usually negligible for ranges R≥450 m, its magnitude, in general, is a function of antenna height, foreground roughness and meteorological conditions. In some cases measurements of this magnitude can give important indications of changes in the properties of the surface or of the atmospheric boundary layer. Although an important example of the usefulness of this component will be presented in the following subsection (3.3.2), our primary interests in this report are in the behaviour of those discrete bursts of reflected sound which can be associated with individual localized objects containing surfaces of sufficient inclination and appropriate orientation (in the horizontal plane) for specular reflection (angle of incidence equals the angle of reflection) into the receiving beam of the Sodar antenna. Since the primary effect of surface roughness is to broaden the angular dependence expected from a smooth planar 'mean' surface, our field studies tended wherever possible to utilize smooth well-characterized targets. Results obtained in such cases gave measure of the variability introduced by the critical transmission loss terms TL_1 and TL_2 of Eq. 2.1. The temporal and spatial aspects of variability in the total reflected signal strength will be documented and discussed in the following subsection (3.3.2). Interpretation in terms of simple propagation models will be presented in subsection 3.5.

3.3.2 ACOUSTIC RADAR RETURN SIGNAL VARIABILITY

3.3.2.1 MARINE DATA

Of the four locations used in our study of sound reflection off fixed targets, by far the largest amount of data on the extent and characteristics of return signal variability was collected at the Oak Bay Marina site. This location offered the advantage of several <u>in situ</u> targets, conveniently aligned and having comparable sizes and shapes at ranges within the 2.15 km maximum limit imposed by our chosen sampling and pulse repetition rates. Moreover, the Marina site was usually subject to significant and generally progressive changes in meteorological conditions over the course of each day which had noticeable effects on the acoustic radar return signals. The primary disadvantage of this site was associated with the inherent difficulties of obtaining representative measurements of the vertical air-temperature- and wind-gradients. Measurements at two vertical levels at a nearby shore station were judged to have little validity because of the measurement site's great separation from most sections of the 2 km long beam path and because of solar heating of the terrestrial surface beneath the weather station. Eventually, in the last two experiments of the series, the remote recording weather station was erected (each day) on a small, rocky islet, Harris Island, adjacent to the marker #2 target (Appendix B). These data still contained evidence of heating of the underlying terrestrial surface and full data return was not achieved from all sensors due to shorting and/or cable cutting on the barnacle-encrusted rocks. Nevertheless, the obtained records at least provided direct indications of meteorological changes which had immediate effects on the amplitude of the target-reflected acoustic signals.

A second difficulty arose from the presence of multipath propagation associated with reflections off the nearby shoreline, buildings and vehicles. The extent of interference produced by these alternative sound paths was dependent upon meteorological conditions and, while affecting the clarity of some returns, did not seriously interfere with the testing program.

In fact, the Sodar return signals recorded at the Oak Bay site provided the best illustration of the characteristic variability of both the absolute and relative levels of sound reflections originating near-simultaneously from targets at different ranges. Time changes in the relative strength of target returns were most easily followed from logarithmically normalized displays of the 128 digital voltage samples extracted from the signal return as a function of time after successive pulsed transmission. The plotted logarithmic intensities were corrected for the expected $1/R^4$ geometric range dependence of reflected signals in order to provide an instantaneous representation of the relative reflection strength of each interrogated range cell during the periods following each transmission pulse. Such plots (see Figures 3-11a, b and 3-12a, b) were used throughout the study to provide a quick overview of the results of each set of experiments and to allow the elimination of returns contaminated by extraordinary noise (i.e. low flying aircraft or nearby automobile engine noise).

The data plotted in Figures 3-11 and 3-12 correspond to the echo returns obtained from Sodar transmissions along a sight-line which either includes or is adjacent to three major reflecting targets indicated in the map of Figure B-1. More specifically, the beam is directed at a cement navigational marker at a range R=590 m. Two other similar markers at R=935 m and 1645 m are, respectively, +3.5° and +4.5° off the Sodar transmission axis, thus receiving, in principle, incident acoustic power levels about 3 dB lower than would be expected from the level measured at the near marker after accounting for the geometric and attenuation losses associated with the additional range.

The surface areas of markers 1 and 3 directed perpendicularly to the antenna axis were on the order of 6 m^2. Although marker 2 has a comparable surface area an 8° misalignment of part of the target with the antenna axis reduced the strength of its reflections in our experimental configuration. This reduction was however, in part, compensated by the presence of weak reflections from the low, rocky islet of Harris Island which augmented and broadened (in time) the marker 2 returns. The June 24 data of Figure 3-11a, obtained at 11:30 PDST, show strong returns from all three targets, together with the initial decay associated with foreground scattering. The marker 1 and 2 returns also show an unusual precursive (toward earlier arrival times) broadening adjacent to the two shorter range targets. More typical widths, equal (in time) to the 200 ms duration of the transmission pulses, were evident later in the day at 18:40 PST (Figure 3-11b) after the earlier easterly 3 m/s winds were augmented (to approximately 4.5 m/s) and nearly reversed in direction (from antiparallel to parallel to the propagation direction of the transmitted pulse).

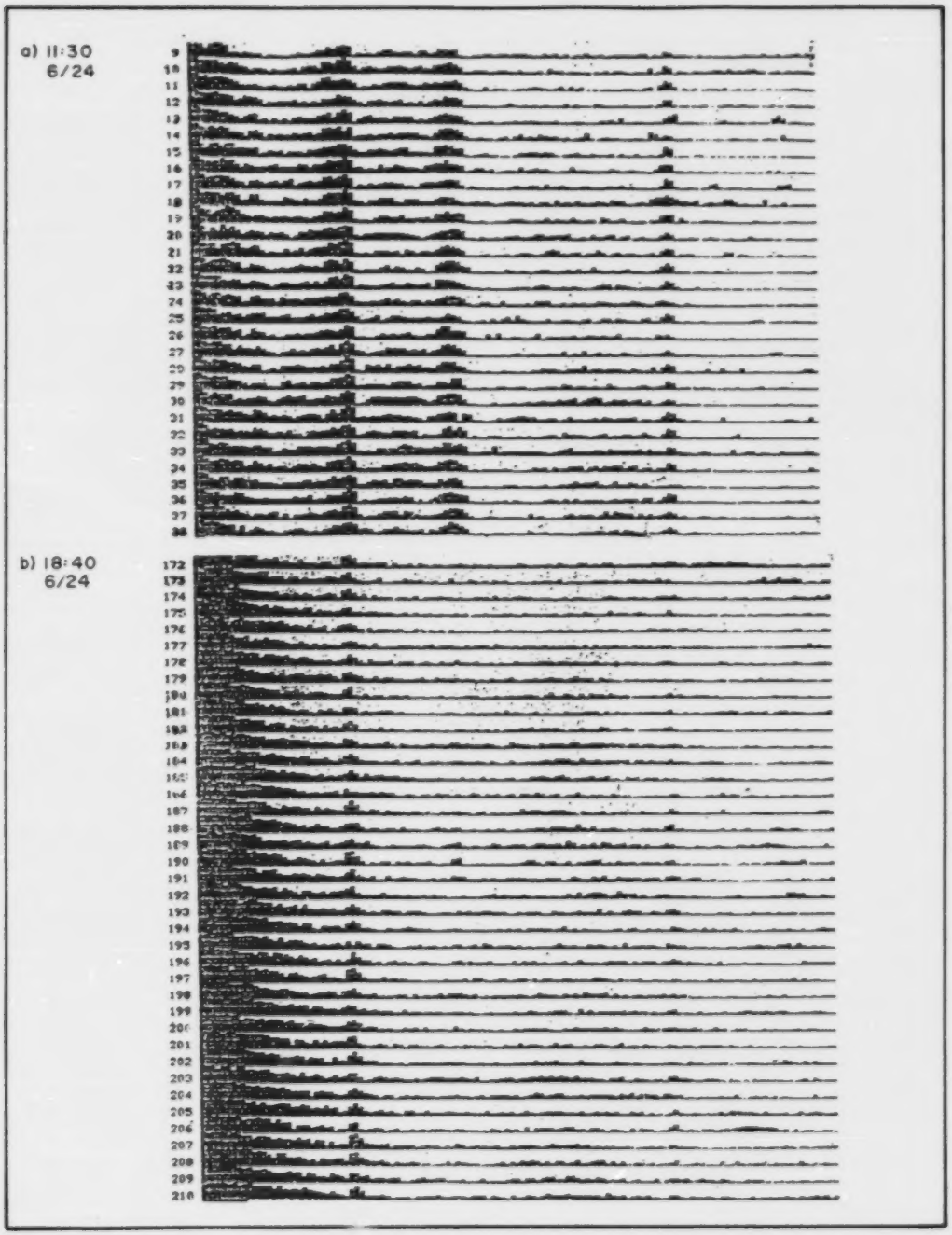

Figure 3-11: Distance converted logarithmic intensities of reflected signal returns as a function of range/time (i.e. in the limits of the horizontal axis corresponds to reflections ranges of 18 m and 2.178 km or from 100 μsec to 12.9 sec after the end of the 200 μsec transmission sound pulse). The axis of the transmitter/receiver was directed at the nearest marker #1 (Appendix B Figure B-5). The displayed sequences represent successive repetitions at 15 second intervals beginning a) 11:30 PDT and b) 18:40 PDT June 24.

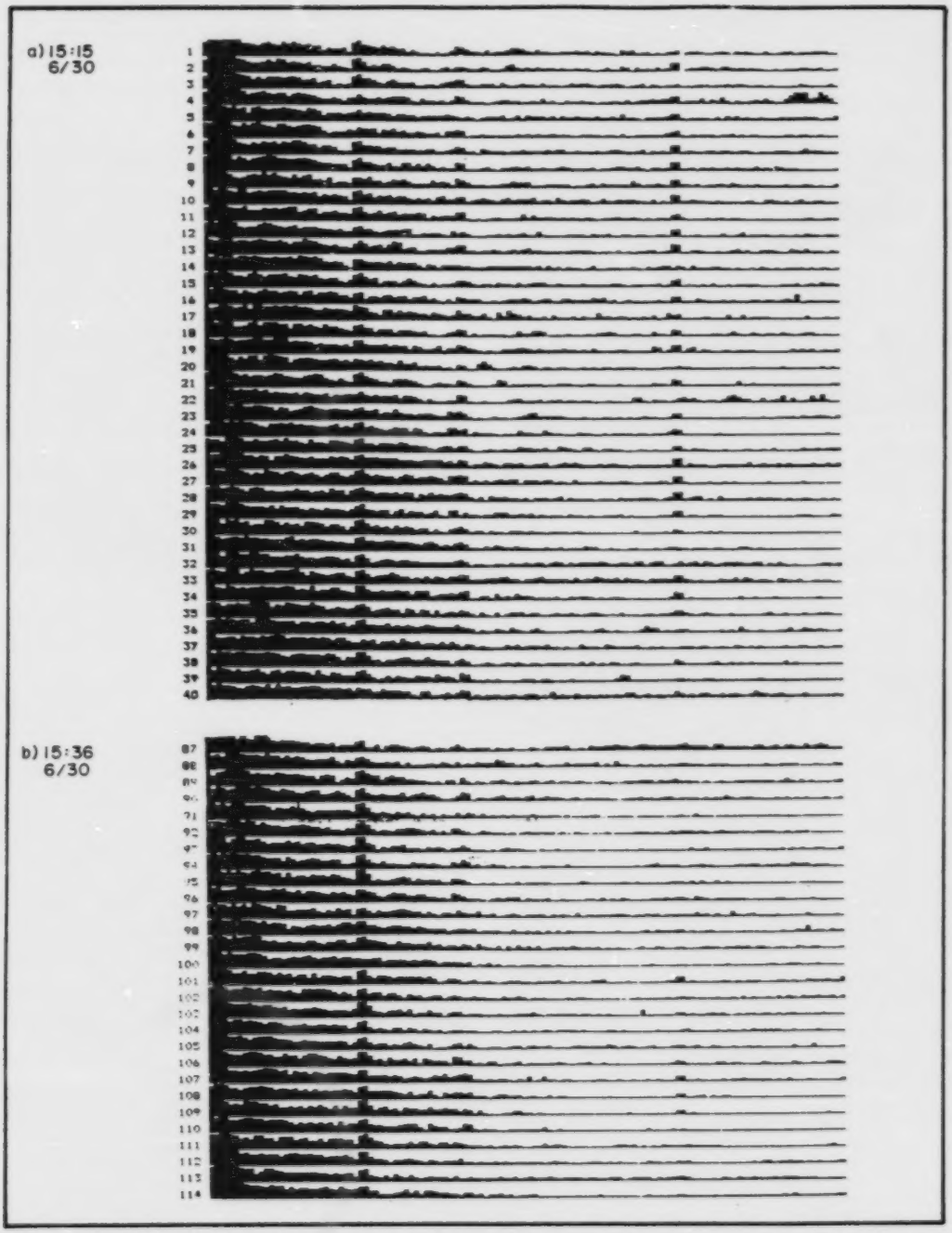

Figure 3-12: Distance converted logarithmic intensities of reflected signal returns as a function of range/time (i.e. in the limits of the horizontal axis corresponds to reflections ranges of 18 m and 2.178 km or from 100 μsec to 12.9 sec after the end of the 200 μsec transmission sound pulse). The axis of the transmitter/receiver was directed at the nearest marker #1 (Appendix B Figure B-5). The displayed sequences represent successive repetitions at 15 second intervals beginning a)15:15 PDT and b)15:36 PDT, June 24, 1986.

However, an overall weakening of the returns was noted relative to the noise background and the echo from the second marker virtually disappeared.

Data obtained 6 days later (Figure 3-12a,b) showed an even more rapid transition (in 20 minutes) from a situation in which comparable returns were received from all three targets to conditions in which the marker 2 return was noticeably weakened and only occasional marginally detectable signals (on a single pulse basis) were received from the third marker. The records of Figure 3-12a also show the Sodar's capability for following the progress of small boat traffic through the beam at ranges as large as 1.5 km in the form of the linearly aligned local peaks in the adjacent returns of pings 19-25 and 33-39.

Although displays such as those presented in Figures 3-11 and 3-12 readily allow visual averaging and detection of the fluctuating individual ping returns, more compact representations of changing signal characteristics are possible using either the interval averaged display such as that previously presented (subsection 3.1) for data obtained at the Glamorgan Road and Institute of Ocean Sciences test sites (Figures 3-1 and 3-2)) or in other displays (see below) which quantify the detectability (signal level elevation relative to noise) of specific targets.

In the former case, the basic trends observed during the six Oak Bay Marina test sequences can be illustrated by the interval averages reproduced in Figures 3-13 to 3-18. In each sequence, returns are displayed as averaged over the indicated numbers of pulses at the specified times (corresponding to the start time of the averaging interval). With the exception of the May 16 data and the two earliest May 21 averages, data were recorded for a 15 second pulse repetition interval and with a 10 Hz sampling rate. [Earlier data, obtained with 10 second PRI and 20 Hz sampling were less useful because of the restriction of detection to targets at ranges less than 1.15 km and their contamination by returns from earlier pulses (see Figure 3-13)]. With the exception of the June 30 data of Figure 3-24 and the May 16 transmissions of Figure 3-13a, all results were obtained from transmitted pulses directed at marker 1. The June 30 data were obtained with a 3.5° change in directionality corresponding to alignment on the second marker.

The main features of the interval-averaged data were:

(1) the consistent visibility of returns from the nearest marker at a range of R=590 m. Interval average return signal magnitudes expressed in terms of sound pressure levels (SPL) ranged from +42.6 dB re 20 μPa on May 21 to 53.2 re 20 μPa in the late morning hours of June 24; and

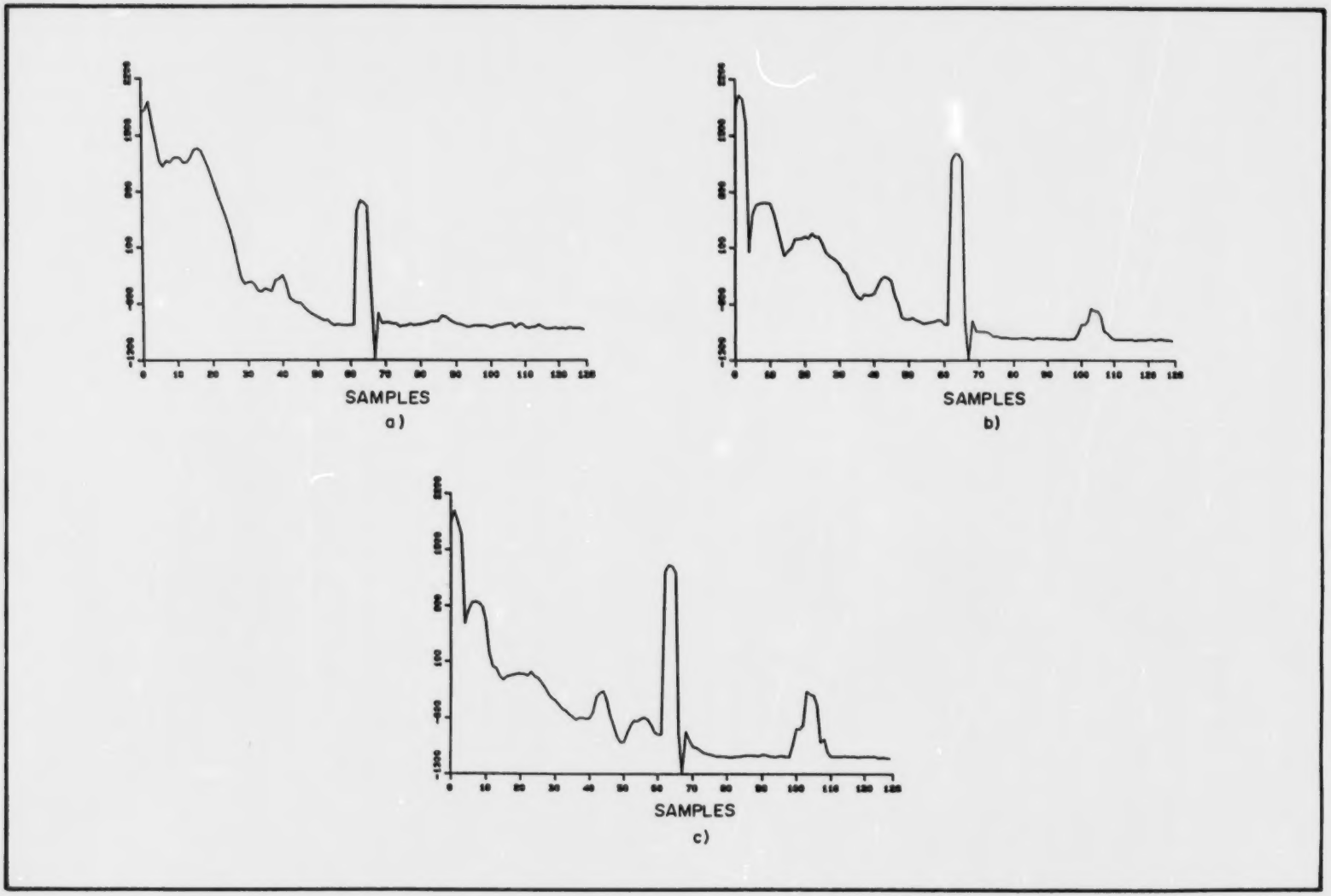

Figure 3-13: Interval averaged signals recorded for: a)11:44-12:19 PDT, b)18:00-18:19 PDT, and c)18:20-18:35 PDT on May 16, 1986. Traces were obtained with the Sodar transmission axis directed at Marker #2 (a) and Marker #1 (b and c). Arrows are included to indicate return feature associated with returns from ranges beyond the R>1.15 km limit of the 20 Hz sampling, 10 sec pulse repetition interval parameters of the second measurement.

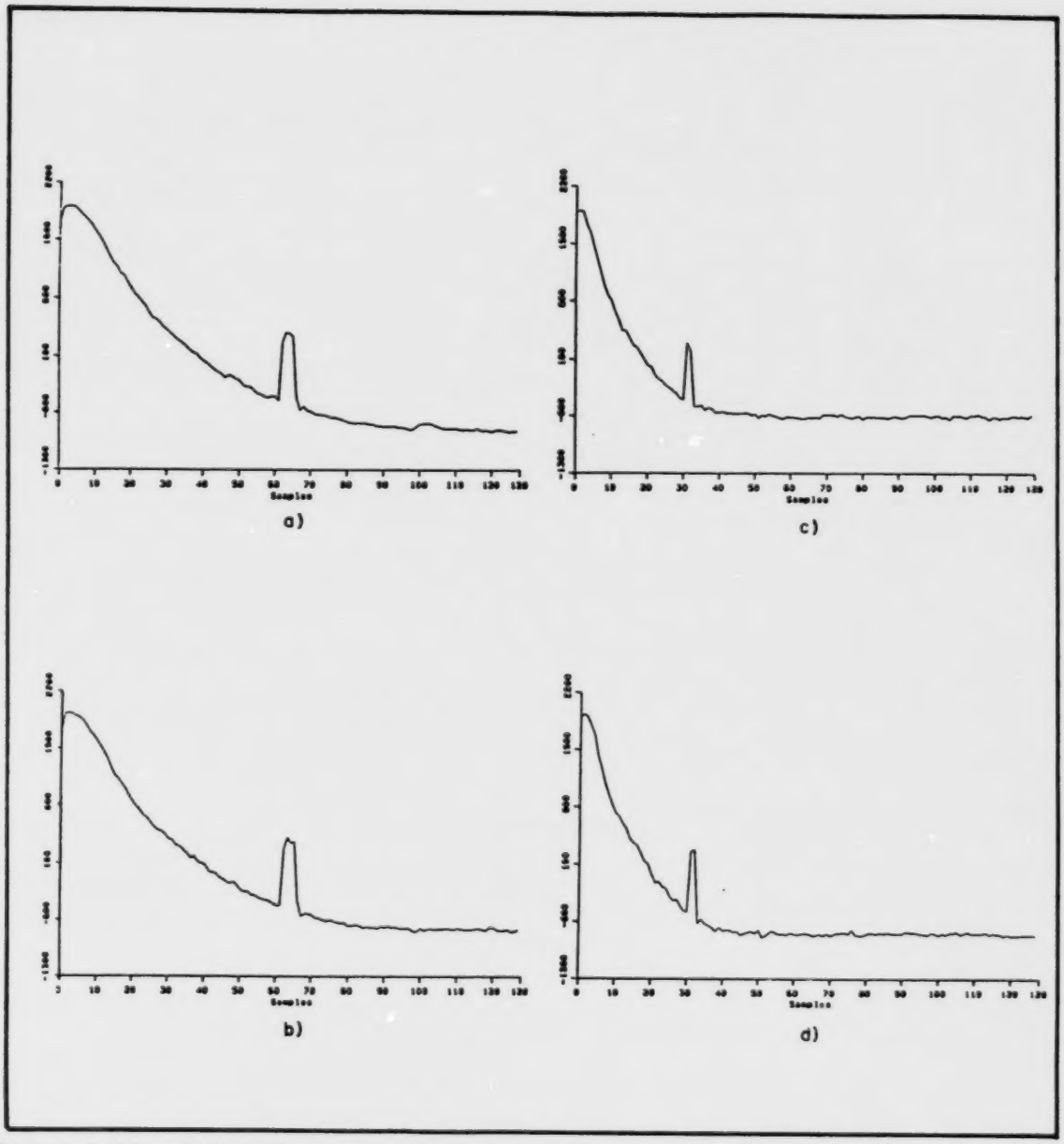

Figure 3-14: Interval average signals for the periods a)11:26-11:56, b)11:59-12:19, c)15:05-15:24 and d)15:51-16:09 May 21, 1986. The Sodar axis was directed at marker #1 except in d) where it was directed at marker #2.

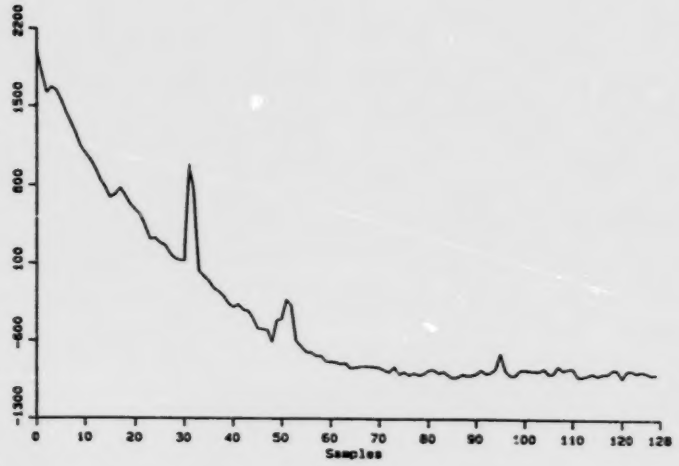

a)

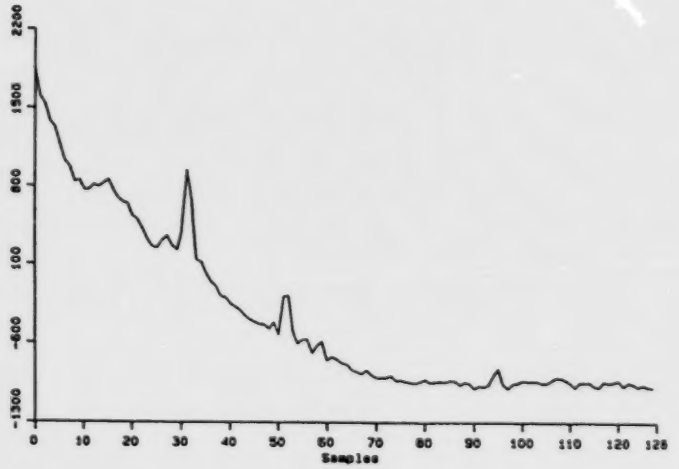

b)

Figure 3-15: Interval average signals for the periods a)13:27-13:44 and b)15:21-15:31, May 23, 1988. In each case the Sodar axis was directed at marker 1.

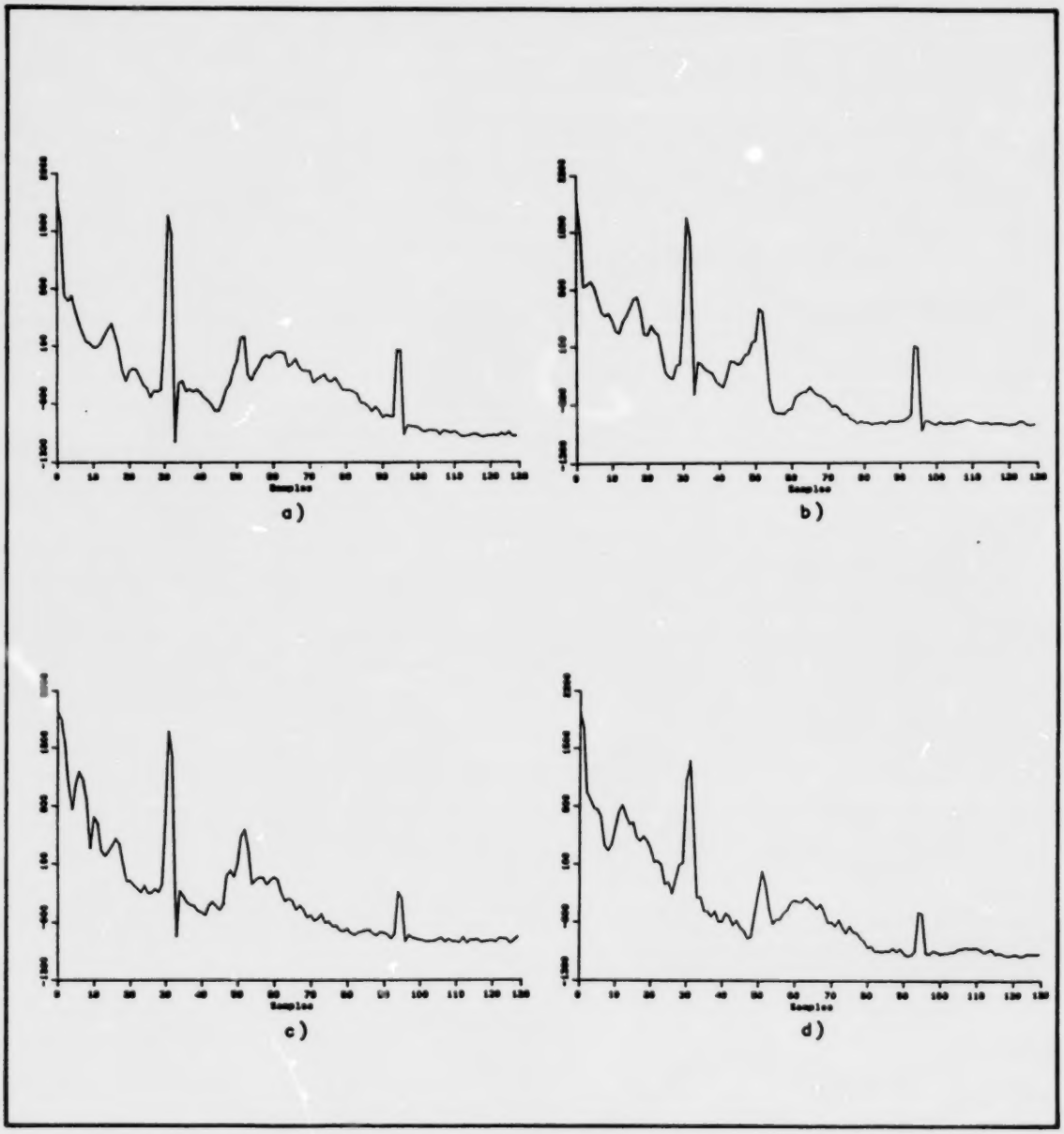

Figure 3-16: Interval average signals for the periods a)11:03-11:15, b)12:49-13:12, c)15:03-15:11 and d)16:45-16:52 PDT May 30, 1986. In each case the Sodar axis was directed at marker #1.

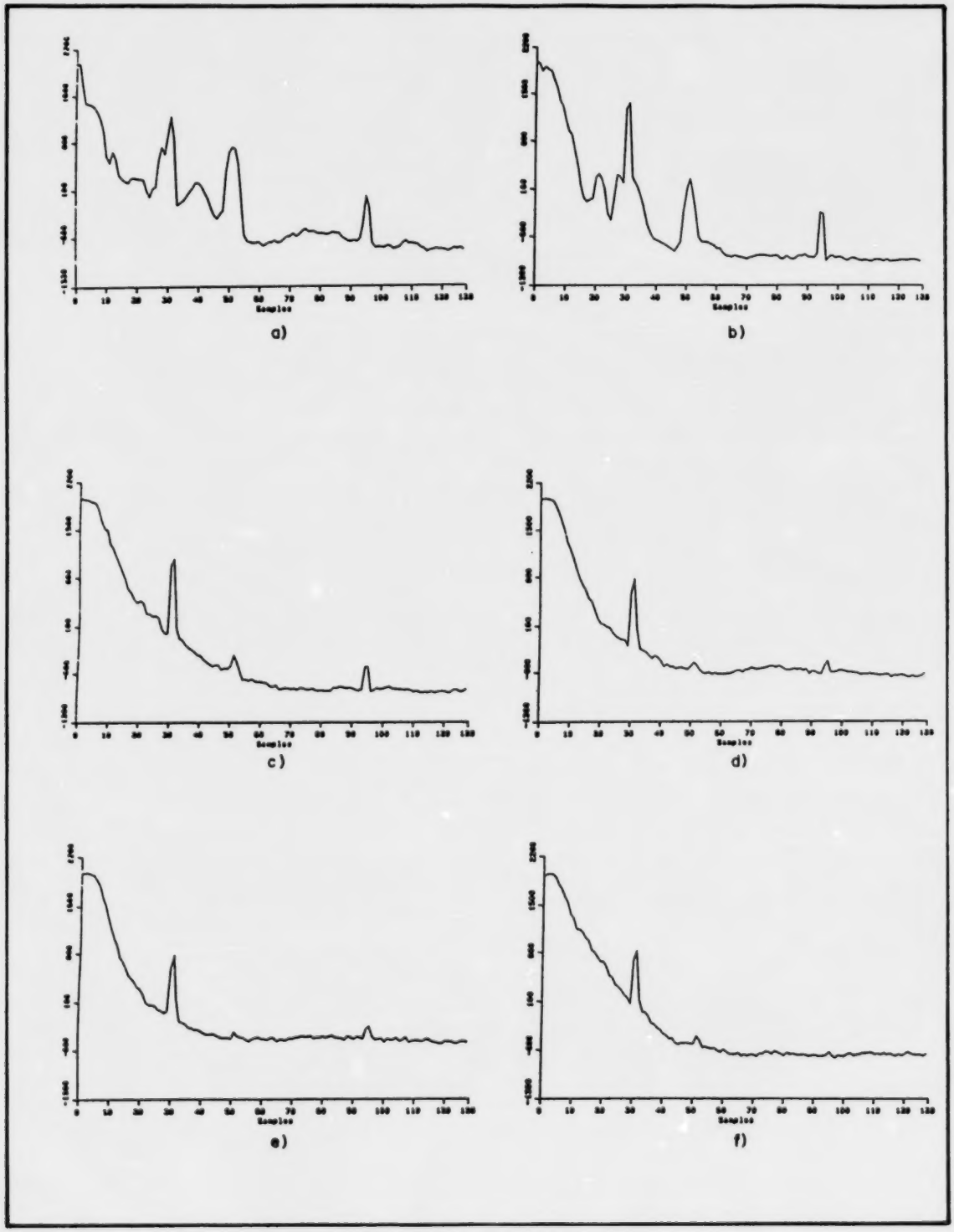

Figure 3-17: Interval average signals for the periods a)11:26-11:45, b)13:41-14:00, c)15:51-16:12, d)17:14-17:32, e)17:50-18:09, f)18:59-19:17 PDT, June 24, 1986. In each case the Sodar axis was directed at marker #1.

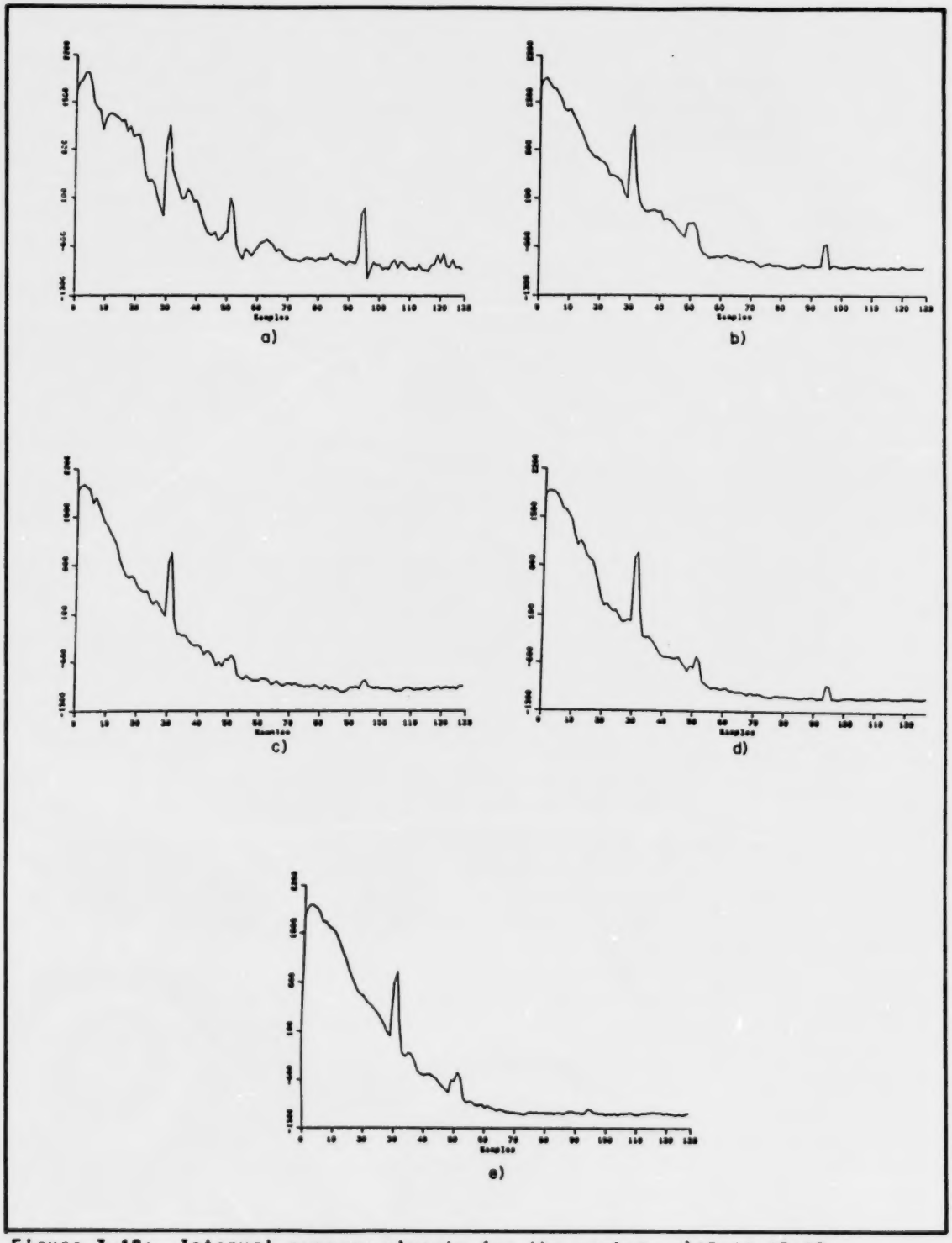

Figure 3-18: Interval average signals for the periods a)15:11-15:18, b)15:29-15:47, c)16:07-16:17, d)16:56-17:22, e)17:38-18:10 PDT, June 30, 1986. In each case the Sodar axis as directed at marker #1.

(2) decreasing SPL values associated with reflections from all markers during the progress of the day from the late morning to the early evening. The more distant target returns (i.e. from markers 2 and 3) were particularly sensitive to this effect. The May 21 results were the exception to this behaviour. Returns on this date were weak throughout the measurement period but showed little change with time in the only easily visible return (from marker 1).

Sound pressure level data corresponding to reflected signals received at the Sodar are listed in Table 3-1 for each of the 3 markers as recorded during representative time intervals in Table 3-1. The decrease in the marker 2 and 3 levels relative to contemporary marker 1 values are given in brackets adjacent to the corresponding listings. Missing data points were due to:

(a) weak signal returns (May 21);

(b) the use of a 10 second PRI in the 15:46 to 16:17 PDT interval of May 23, precluding the observation of marker 3 reflection; and

(c) distortions from strong and anomalous broadening of the reflections on May 30.

With the exception of the very weak May 21 returns, the data suggests a relatively narrow range of reflection, 46.9 to 54.8 dB re 20 μPa, from the near marker relative to the 31.5 to 47.7 dB and 21.5 to 41.6 dB ranges of levels recorded for markers 2 and 3 respectively. Reductions relative to contemporary marker 1 values were 4.5 to 16.6 dB for marker 2 and 11.6 to 26.3 for marker 3. Levels of return from marker 2 exceeded those from its more distant neighbour by 4 to 8 dB except on June 24 when, during at least three intervals, stronger returns were received from the more distant target. In general, however, the fluctuation in the levels of the more distant markers tended to follow the trend of the near marker results.

Additional measurements of the interval averages were made as a function of the angular deviation in the horizontal plane of the transmission axis relative to the imaginary line connecting the antenna and marker 1. The data taken during the stable signal conditions of May 21 showed a much weaker angular dependence (Table 3-2) than would have been expected from the sound pressure levels measured at the targets on other days (May 30, June 24 and 26). Unfortunately, because of the rough seas, no sound pressure level data were taken in the vicinity of the targets during the May 21 experiments. The apparent broadening of the transmitting and/or receiving beams implied by these data would be consistent with the presence of a large amount of air turbulence which would have accompanied the observed high wind speeds and sea states. Other evidence for the attenuating and beam-broadening effects of such turbulence have been discussed in subsection 3.2 with reference to the work of Brown and Clifford[8].

Table 3-1: Sound pressure levels measured at Sodar receiver (Oak Bay Marina site data).

Date	Time (PDT)	Target 1 (590 m)	Target 2 (935 m)	Target 3 (1145 m)
May 21	15:05-15:23	42.6		
May 21	15:51-16:09		trace	
May 23	13:27-13:44	49.3	36.7(12.6)	30.5(18.8)
May 23	15:21-15:31	47.2	36.2(11)	28.2(19)
May 23	15:46-16:17	48.8	34.3(14.5)	
May 30	11:02-11:14	54.8	distorted	40.5(14.3)
May 30	13:12-13:34	54.0	42.8(11.2)	39.4(14.6)
May 30	15:02-15:10	54.8	distorted	37.6(17.2)
May 30	15:33-15:33	53.2	43.9(9.3)	39.7(13.5)
May 30	16:43-16:52	51.6	39.5(12.1)	35.0(16.6)
June 24	11:26-11:42	52.2	47.7(4.5)	41.6(11.6)
June 24	13:41-14:00	52.0	41.9(10.1)	37.6(14.4)
June 24	15:02-15:11	50.4	41.2(9.2)	39.9(10.5)
June 24	15:50-16:01	49.3	35.0(14.3)	36.2(13.1)
June 24	16:01-16:11	49.4	32.8(16.6)	30.6(18.8)
June 24	17:21-17:31	46.9	31.5(15.4)	33.7(13.2)
June 24	18:29-18:39	48.0	33.5(16.5)	36.2(11.8)
June 24	18:59-19:09	46.3	31.5(15.3)	25.8(20.5)
June 30	15:28-15:46	49.8	35.1(14.7)	32.6(17.2)
June 30	16:07-16:17	48.0	33.1(14.9)	26.2(21.8)
June 30	17:38-18:11	47.8	33.7(14.1)	21.5(26.3)

Table 3-2: Reduction of the May 21, 1986 marker 1 reflected signal as a function of the angular deviation of the Sodar antenna axis from direct alignment on the marker.

θ	Signal Decrease (dB)
6	1
10	2.4
15	3.6

The shorter term detectabilities of returns from the three markers are displayed in Figures 3-19 to 3-24 for representative, usually late afternoon periods of May 23, May 30, June 26 and June 30. As used here, the term detectability is defined as the elevation (in millivolts, 1000 mv = 8 dB re 20 μPa in SPL) above background of the average of two adjoining voltage samples corresponding to the range cell centered on each target. The background in this case was established for each ping and target by calculating the average of the two second and two third closest (in time) voltage samples to those associated with the target return.

Examination of these data show that marine detection capability generally decreased over the usual late-morning to early-evening experimental period with poorest performance usually coinciding with the late-afternoon strengthening of thermally-driven westerly winds over the nearby Strait of Juan de Fuca. In general, the data suggest that under such unfavourable conditions, only returns from the shortest range R=590 m marker were normally detectable on the basis of a single transmission (ping) and reception. More specifically the return signal from this marker rarely dropped below the 300 mv level which corresponded to roughly the 5% exceedance value for the amplitude of the fluctuations in the background return signal levels.

Although the detectability of returns from the two more distant targets did, at times, reach levels comparable to those recorded for marker 1 (see Figures 3-20b,c; 3-21b,c; 3-22b,c), in general these signals were more subject to fading associated with refraction-induced scintillation and other system-related effects (subsection 3.5) which produced fluctuation amplitudes comparable to or greater than the mean detectability level. In such cases, positive identification of these targets on the basis of a single ping was not feasible. However, statistical averaging over as few as four consecutive pulses (equivalent, with our pulse repetition interval, to a 1 minute interrogation) allowed detection of even very weak signals with a reasonable degree of confidence (see Figure 3-25 for comparison with its single pulse version, Figure 3-23b).

The connection between the strength of target returns and the component of the wind along the beam axis is also worth further exploration in the data sets. The existence of such a relationship, expected on the basis of the theory[11] is certainly consistent with the best quality sets of simultaneous wind and reflected signal level data. This correspondence is evident in the common plot of the marker 1 return signal strength and the along beam component of the wind velocity as a functions of time in Figure 3-26. The wind components plotted in these Figures were obtained from the hourly readings recorded at the nearby Gonzales Observatory until 14:30 and 16:00 PDT on June 24 and 30, respectively. At later times, the plotted values were taken from the 8 m elevation wind sensors located on Harris Island adjacent to marker 2. In each case, reductions in return signal strength accompany increases in the wind component parallel to the outgoing acoustic beam. The inverse proportionality between beam-parallel wind velocity and return signal strength is readily apparent in the larger

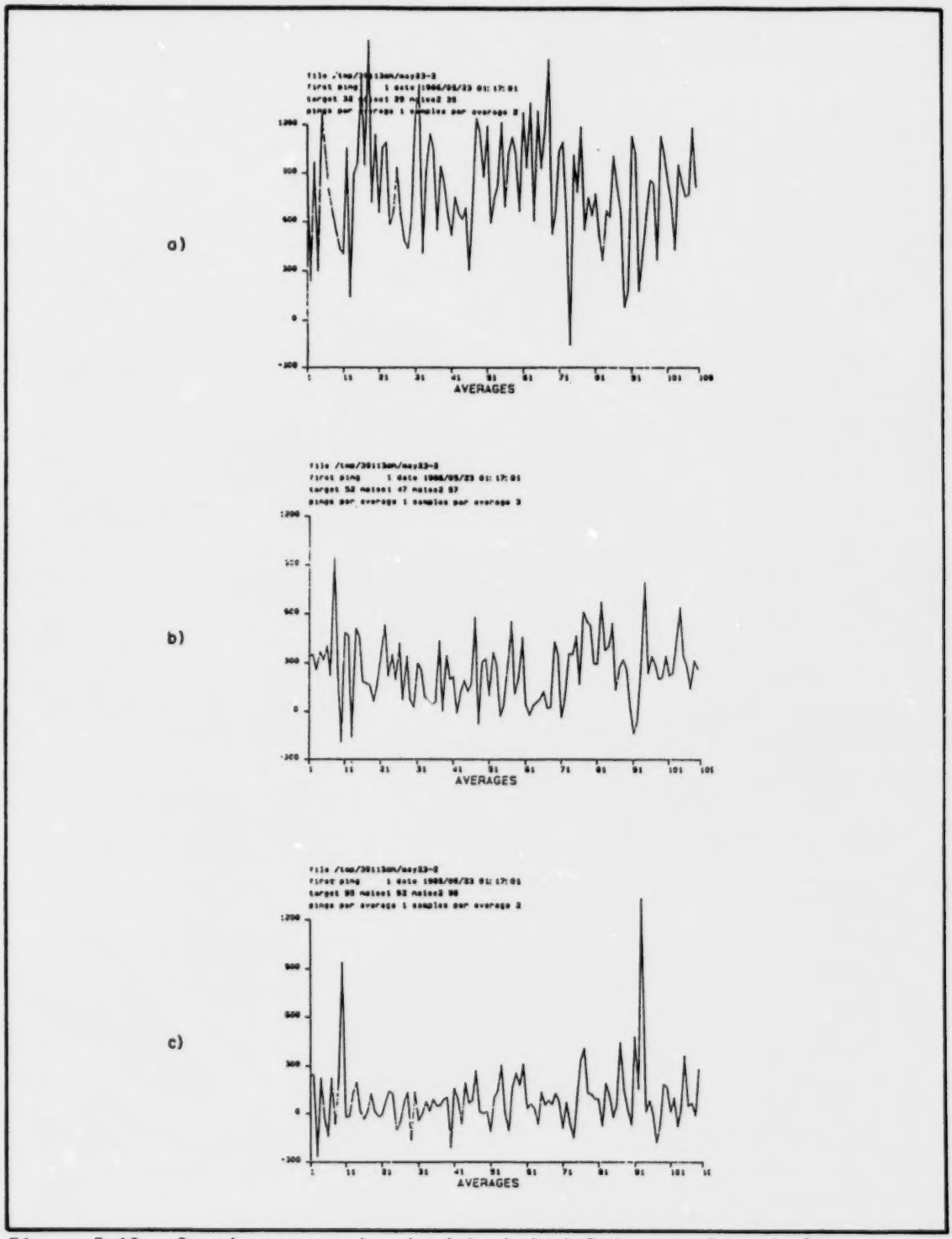

Figure 3-19: Sound pressure levels detected at Sodar receiver during representative daily periods as recorded at the Oak Bay Marina. The detectability (elevation above background) of signals associated with reflectors from markers 1(a), 2(b) and 3(c) for the periods 13:17-13:34 May 23, 1988. In each case the Sodar axis was directed at marker #1.

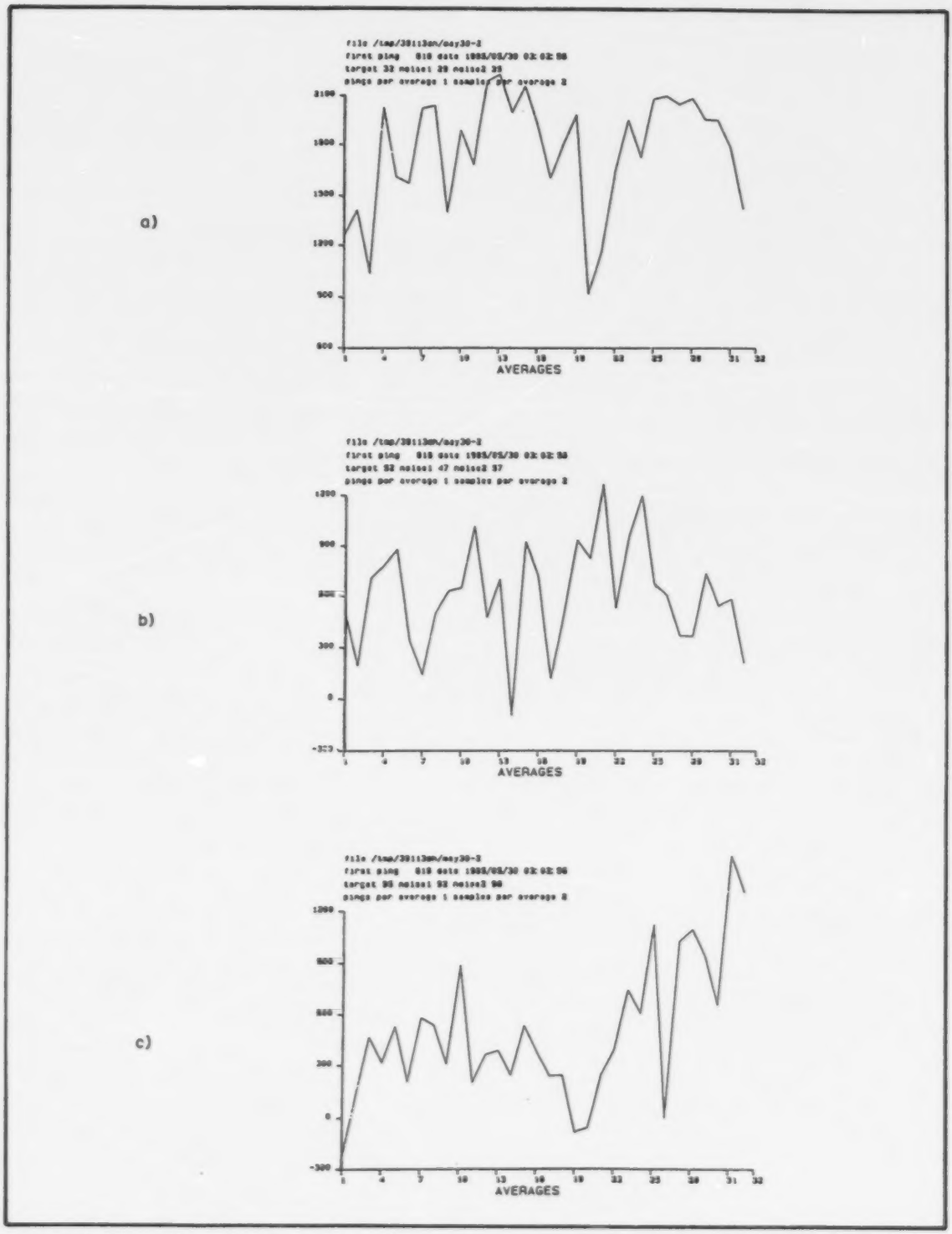

Figure 3-28: The detectability (elevation above background) of signals associated with reflectors from markers 1(a), 2(b) and 3(c) for the period 15:03-15:11 May 30, 1986. In each case the Sodar axis was directed at marker #1.

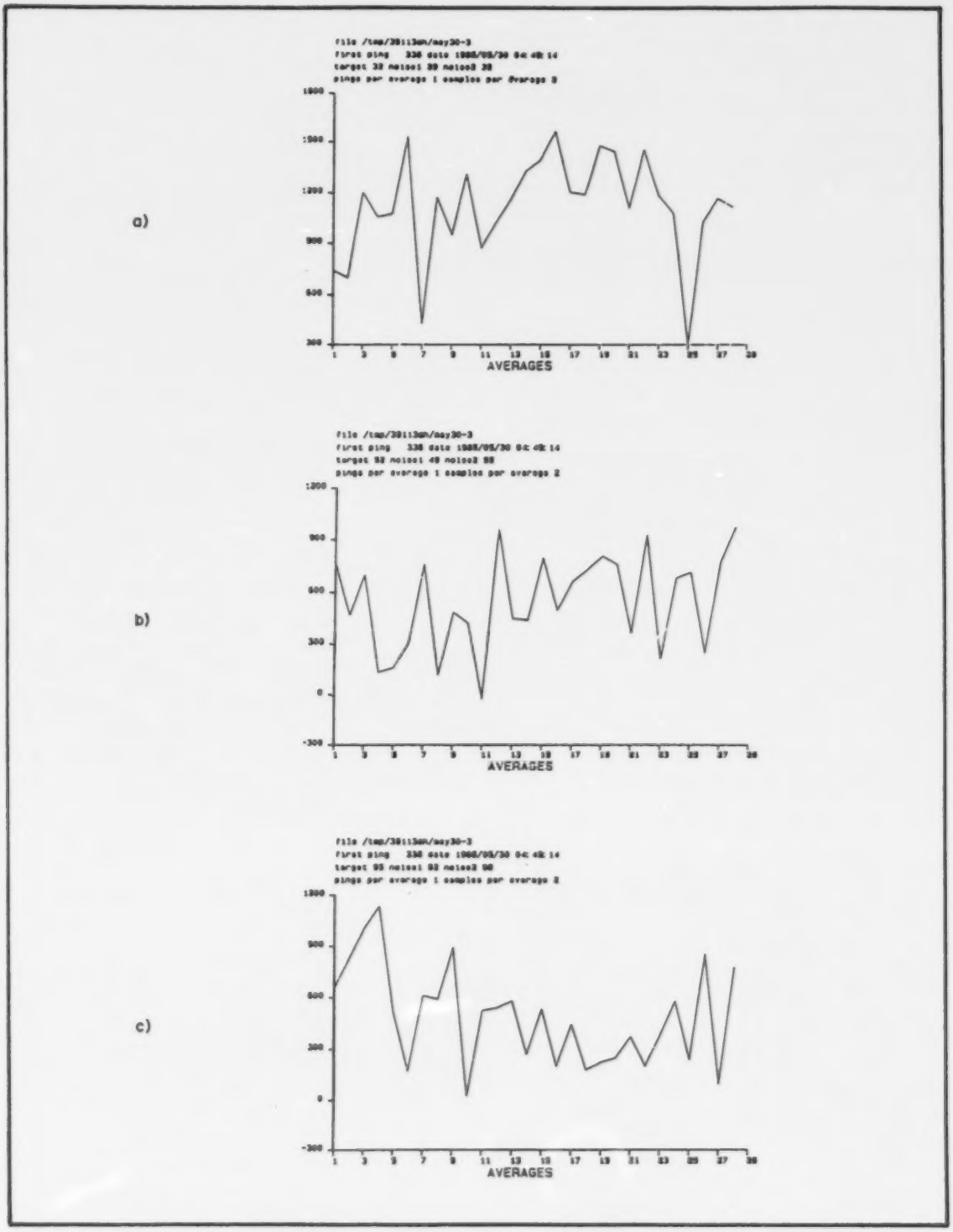

Figure 3-21: The detectability (elevation above background) of signals associated with reflectors from markers 1(a), 2(b) and 3(c) for the period 16:45-16:52 May 30, 1986. In each case the Sodar axis was directed at marker #1.

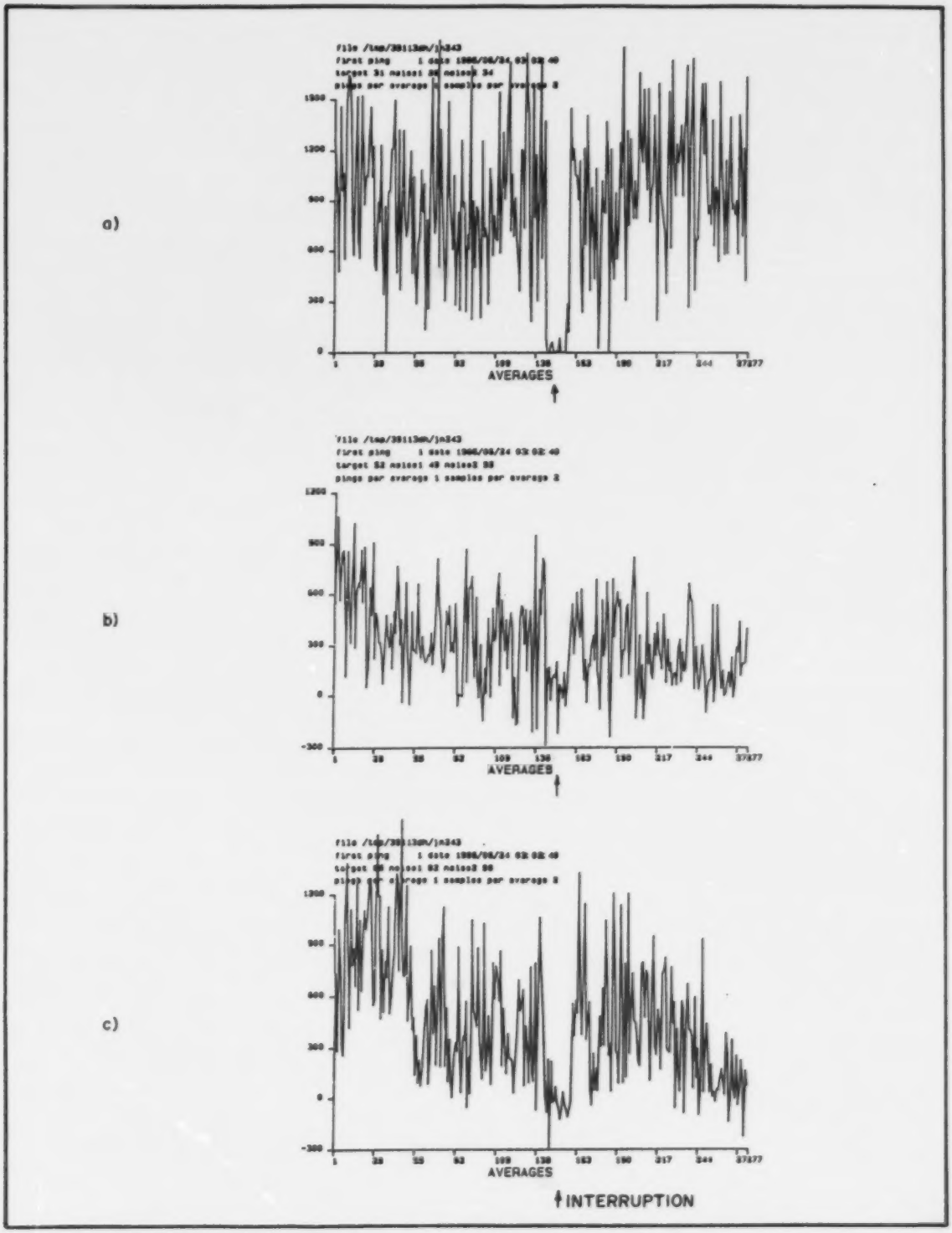

Figure 3-22: The detectability (elevation above background) of signals associated with reflectors from markers 1(a), 2(b) and 3(c) for the period 15:02-16:11 June 24, 1986. In each case the Sodar axis was directed at marker #1.

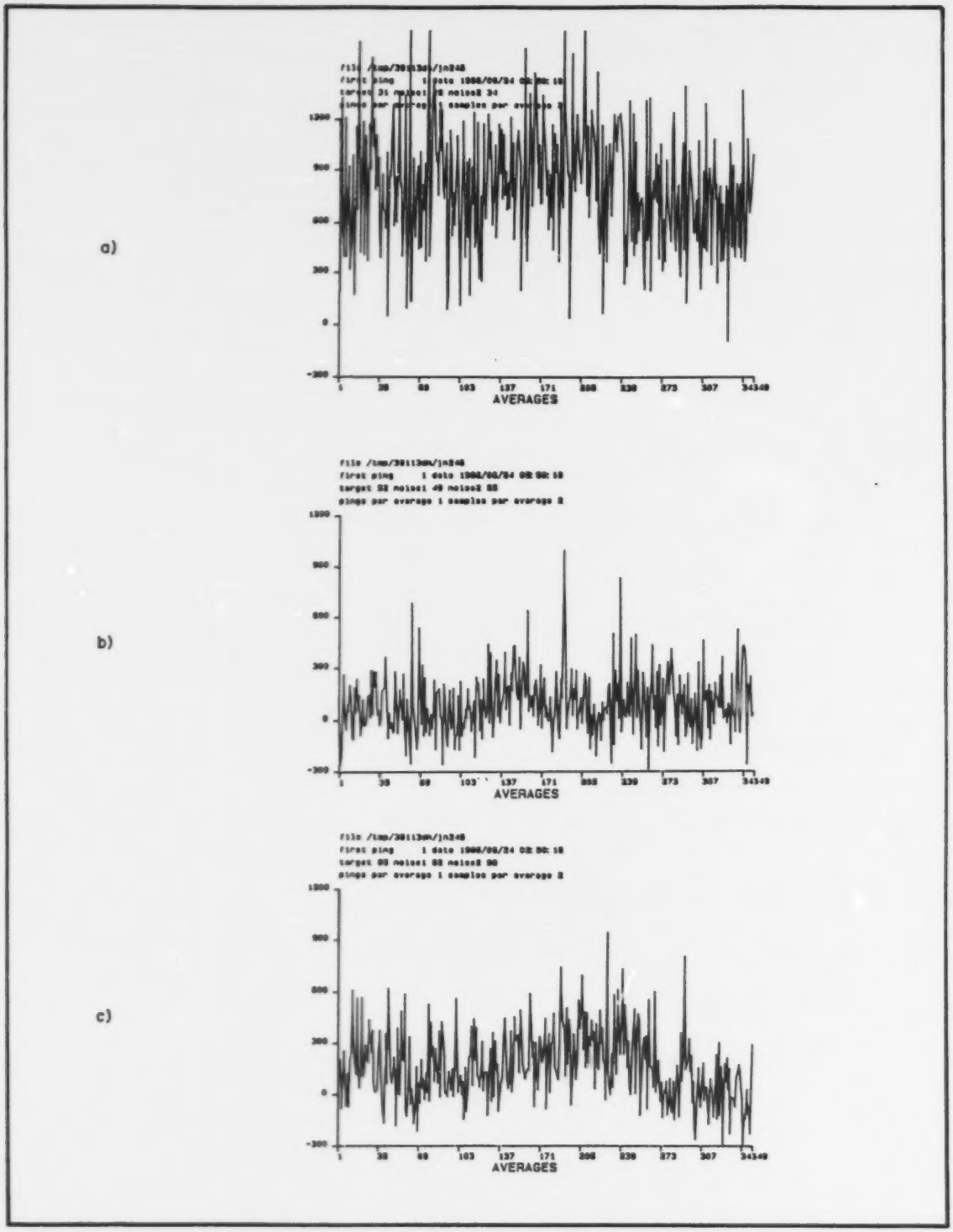

Figure 3-23: The detectability (elevation above background) of signals associated with reflectors from markers 1(a), 2(b) and 3(c) for the period 17:50-19:17 June 24, 1986. In each case the Sodar axis was directed at marker #1.

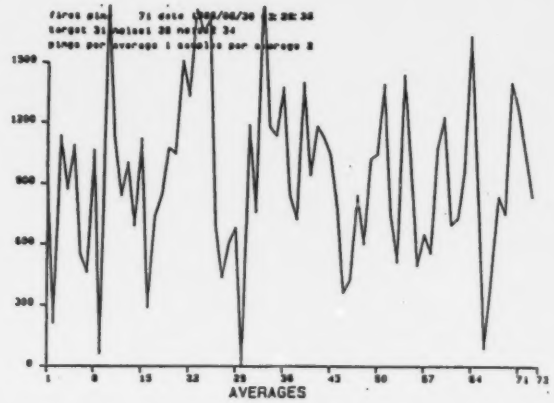

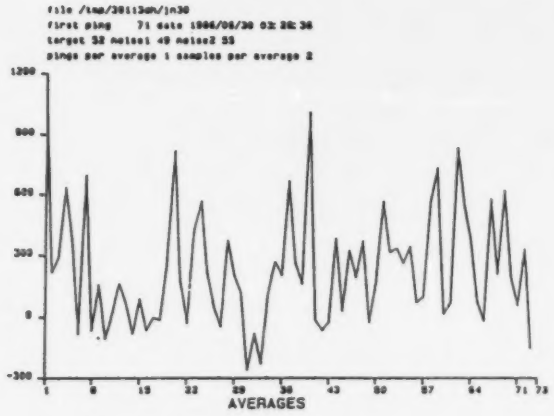

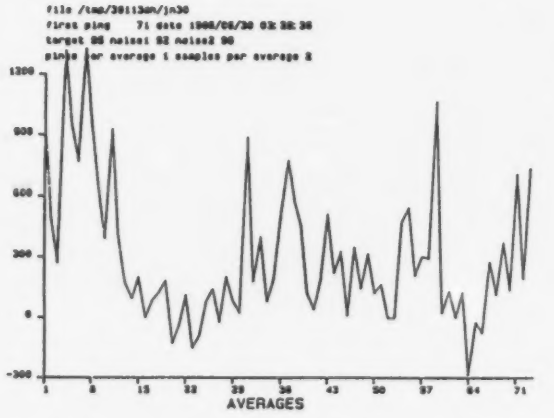

Figure 3-24: The detectability (elevation above background) of signals associated with reflectors from markers 1(a), 2(b) and 3(c) for the period 15:28-15:46, June 30, 1986. In each case the Sodar axis was directed at marker #2.

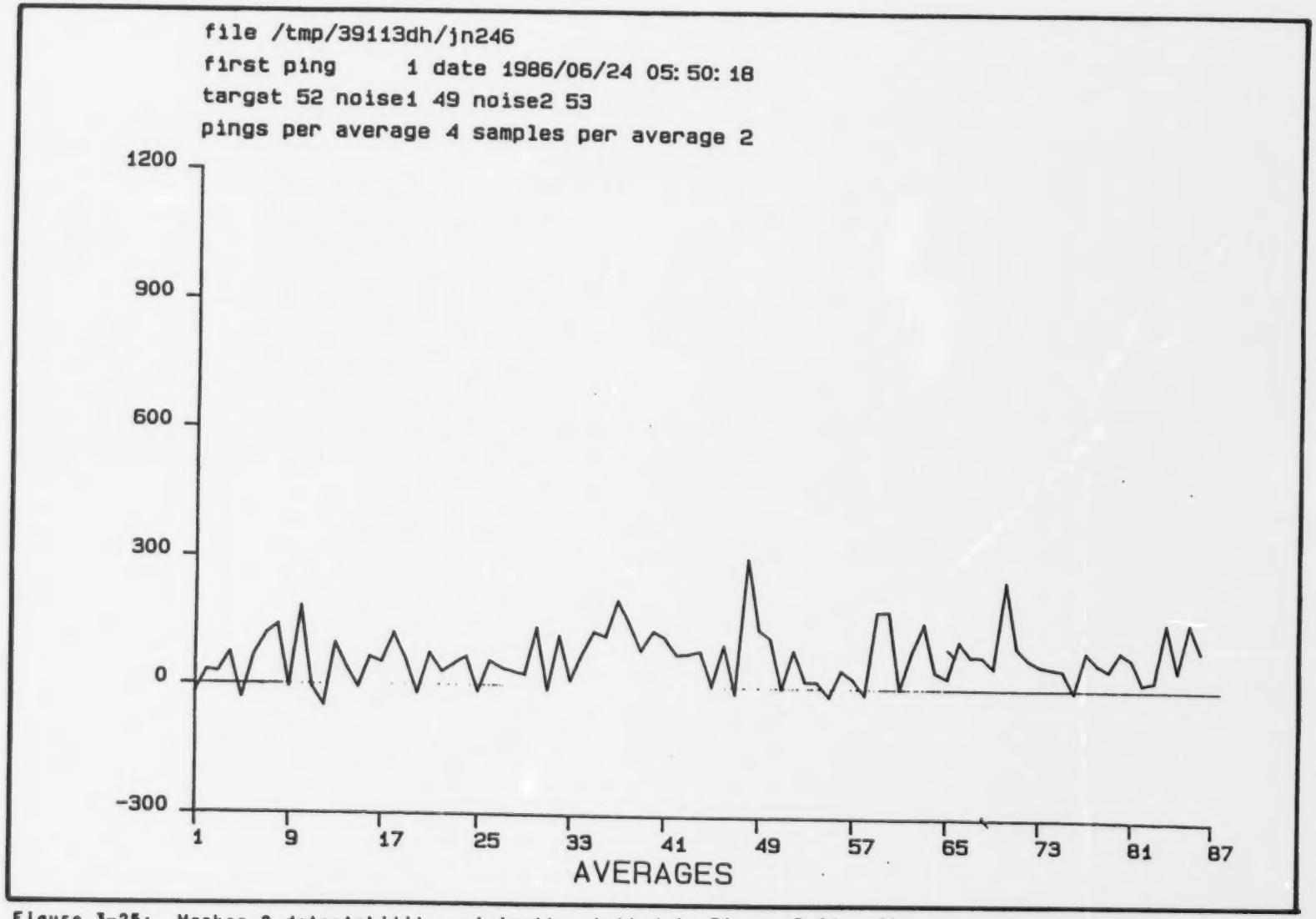

Figure 3-25: Marker 2 detectability originally plotted in Figure 3-24, after averaging over groups of 4 consecutive voltage samples. The small number of negative values obtained confirms the effectiveness of even short term (1 minute) interval averaging of return data.

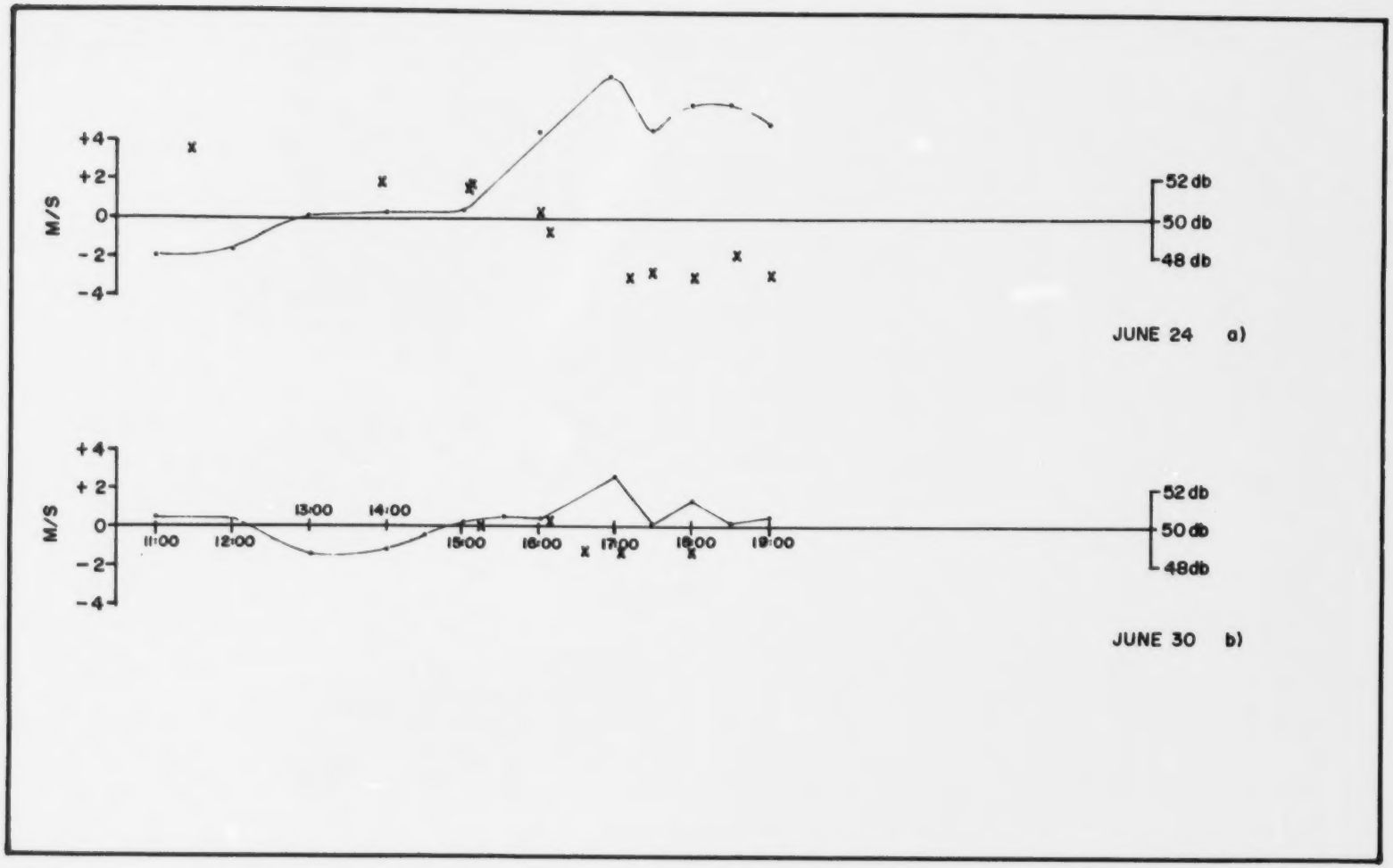

Figure 3-26: Plots of near-simultaneous SPL values associated with reflected returns from marker 1 (x) and windspeed component along Sodar Antenna axis (.). Positive and negative wind component values correspond to winds parallel and anti-parallel to the propagation axis of the transmission pulse. Data are plotted for June 24 (a) and June 30 (b).

set of data from May 21 through June 30 plotted in Figure 3-27a. The experimental relationship for antiparallel wind components (i.e. data points located on the left-hand side of the ordinate axis in Figure 3-27a) is less clear cut with increasing wind component magnitudes, actually, in the case of May 30, appearing to enhance signal strength. Corresponding plots for markers 2 and 3 (Figure 3-27b,c) were much more erratic and indicated no particular relationship to the beam parallel wind.

Finally, comment should be made on the fact that both the interval average and detectability data suggest that on time scales as short as 15 seconds and as long as several minutes the size of the fluctuations in return signal strength are significantly smaller than corresponding fluctuations in the SPL as measured at the target. In general, the extent of the latter variability was on the order of 20 dB at all measured ranges. The magnitude of the variability in the corresponding return signals was observed to decrease with range (see Figure 3-23) from a 12 to 14 dB value at the R=590 m nearest marker to 7.5 and 6 dB at the R=935 and 1645 m markers. Data on the spectral content of these fluctuations would have been of use in analyzing the sources of variability. Unfortunately, the presence of sampled signal frequency components as high as 10 Hz made it impossible to carry out spectral analyses.

3.3.2.2 TERRESTRIAL DATA

The terrestrial experiments carried out at the Boundary Bay Airport were enhanced by the availability of easy access to all portions of the site. This access simplified the effort needed to obtain useful meteorological data and allowed some flexibility in the placement and configuration of the single target used in our studies of reflected signal variability. The target, used previously in the preliminary raft-based experiments at the Institute of Ocean Sciences (Figure 3-2) consisted of a 4' x 6" x 1/8" steel sheet reflector mounted at any one of four angles (45°, 60°, 80° and 90°) relative to the horizontal base of a wooden support platform.

Average returns for several representative time intervals during the June 5 and June 6, 1986 experiments are presented in Figures 3-28 and 3-29, respectively. The returns in these cases were obtained with the target positioned on the beam axis at a range of R=462 m. Comparisons of returns from targets at fixed range and inclination over periods of time as large as 5 hours suggest a greater degree of stability of received signal levels relative to the marine data. This stability was also evident in the relatively small changes noted (equivalent to an SPL range of ~4 dB) in the mean levels of fluctuating target detectabilities plotted in Figure 3-30a,b for early afternoon and late afternoon-early evening periods, respectively.

It should be noted here that in making the latter comparisons on the basis of data obtained with, in one case, the target platform on the ground (Figure 3-30a) and, in the other, at 2 m elevations (Figure 3-30b) we have

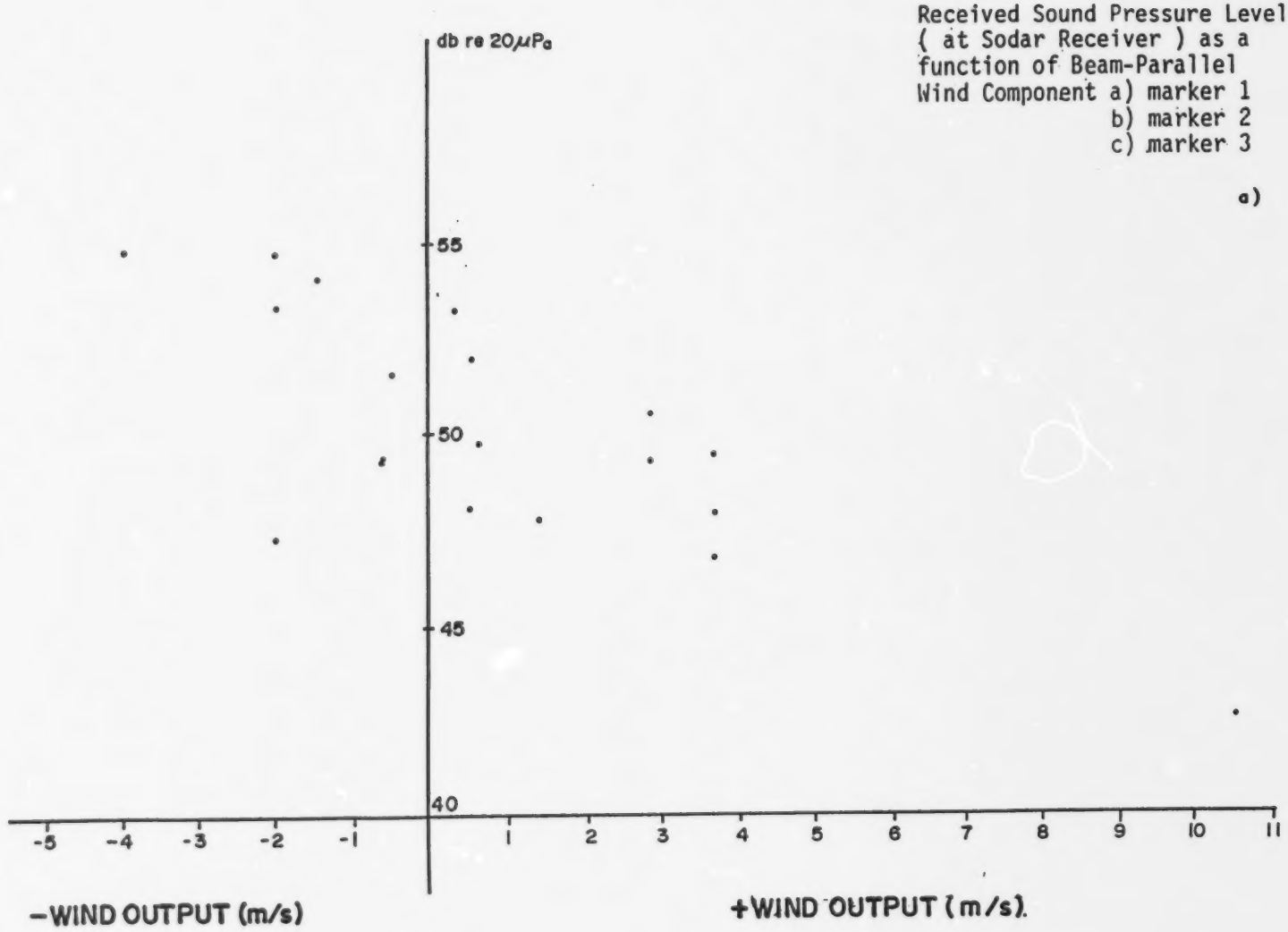

Figure 3-27: Plots of Sodar-received SPL values for markers 1(a), 2(b) and 3(c) as a function of wind component parallel to the transmitting antenna axis.

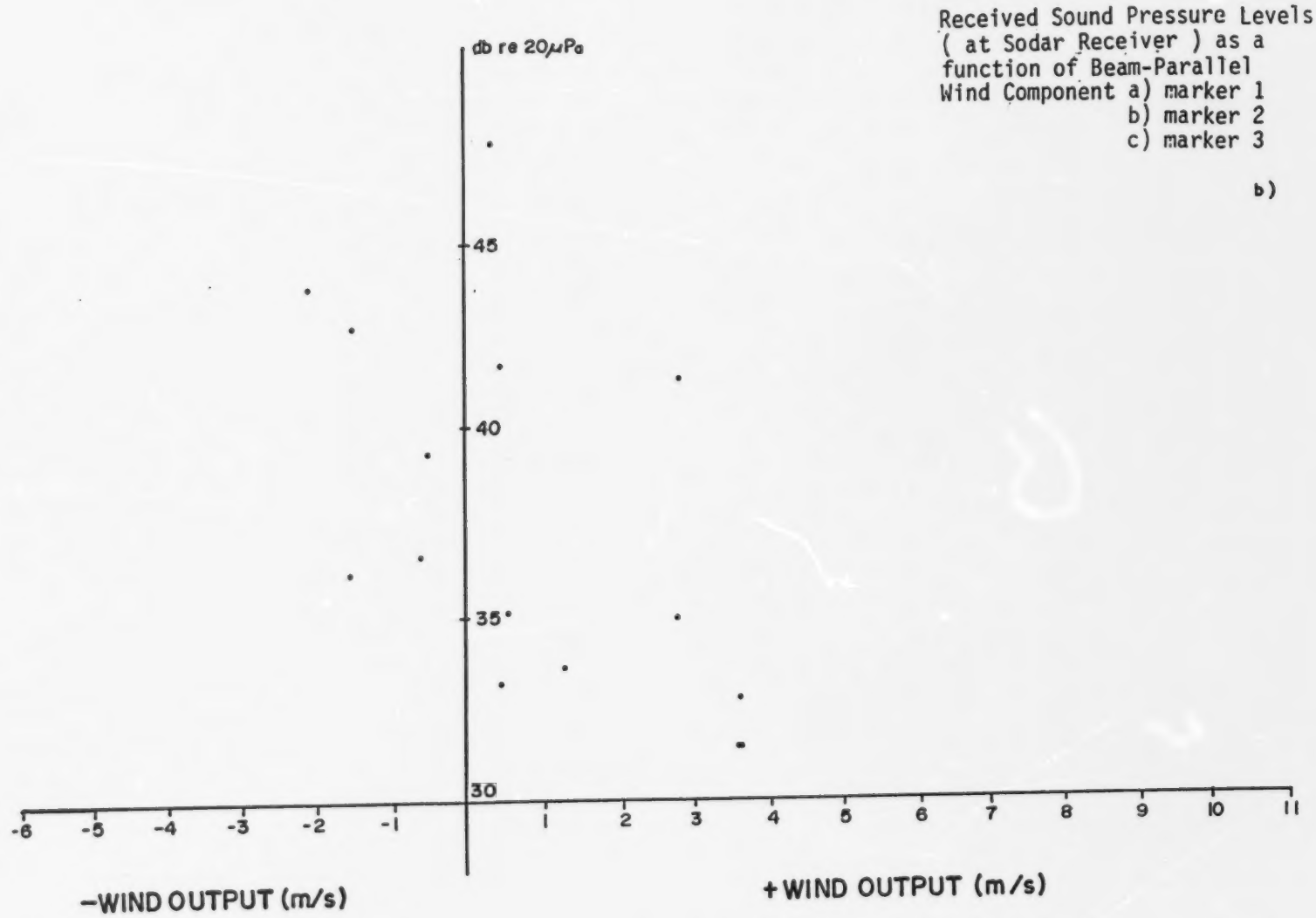

Figure 3-27: Plots of Sodar-received SPL values for markers 1(a), 2(b) and 3(c) as a function of wind component parallel to the transmitting antenna axis.

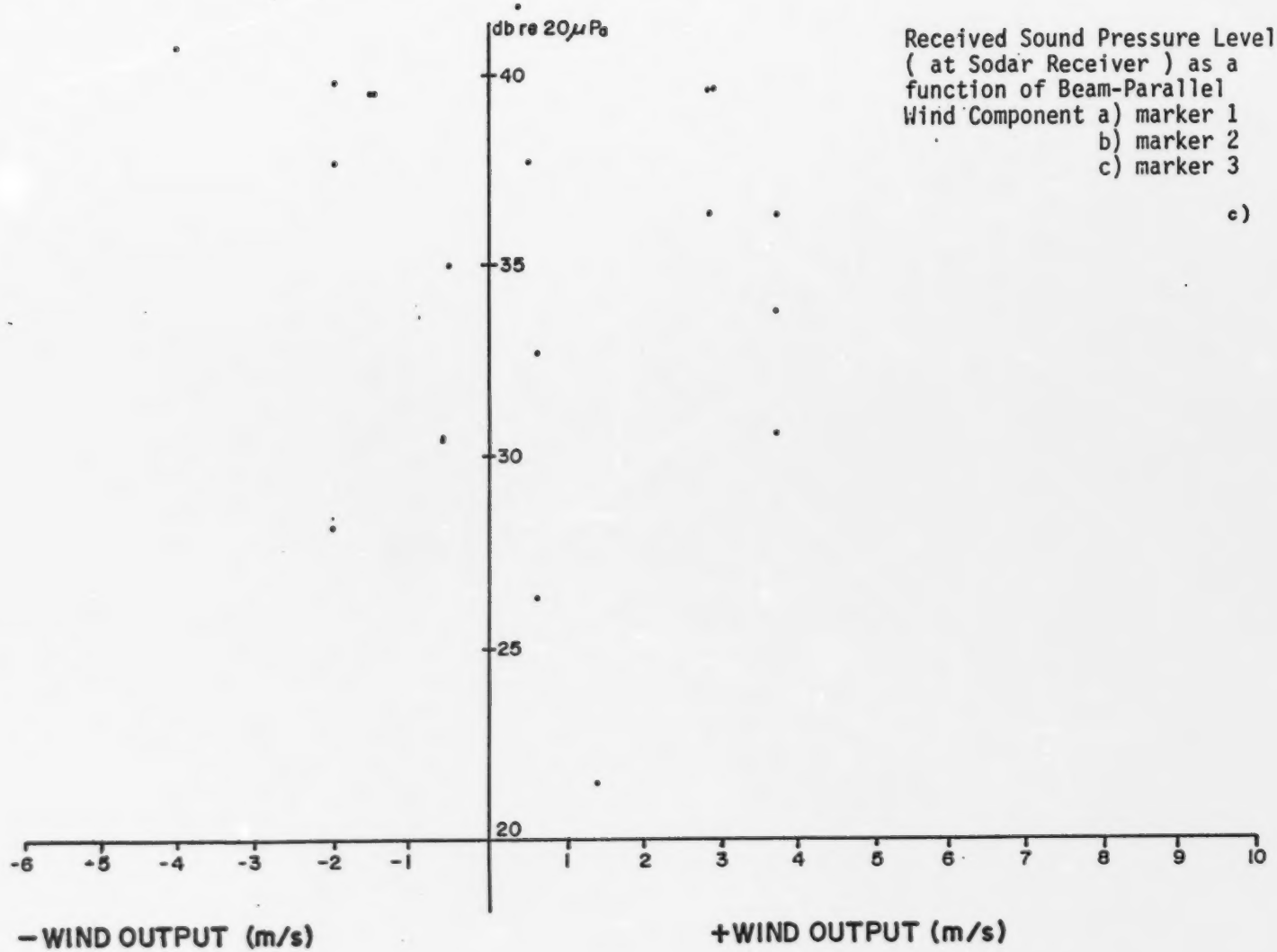

Figure 3-27: Plots of Sodar-received SPL values for markers 1(a), 2(b) and 3(c) as a function of wind component parallel to the transmitting antenna axis.

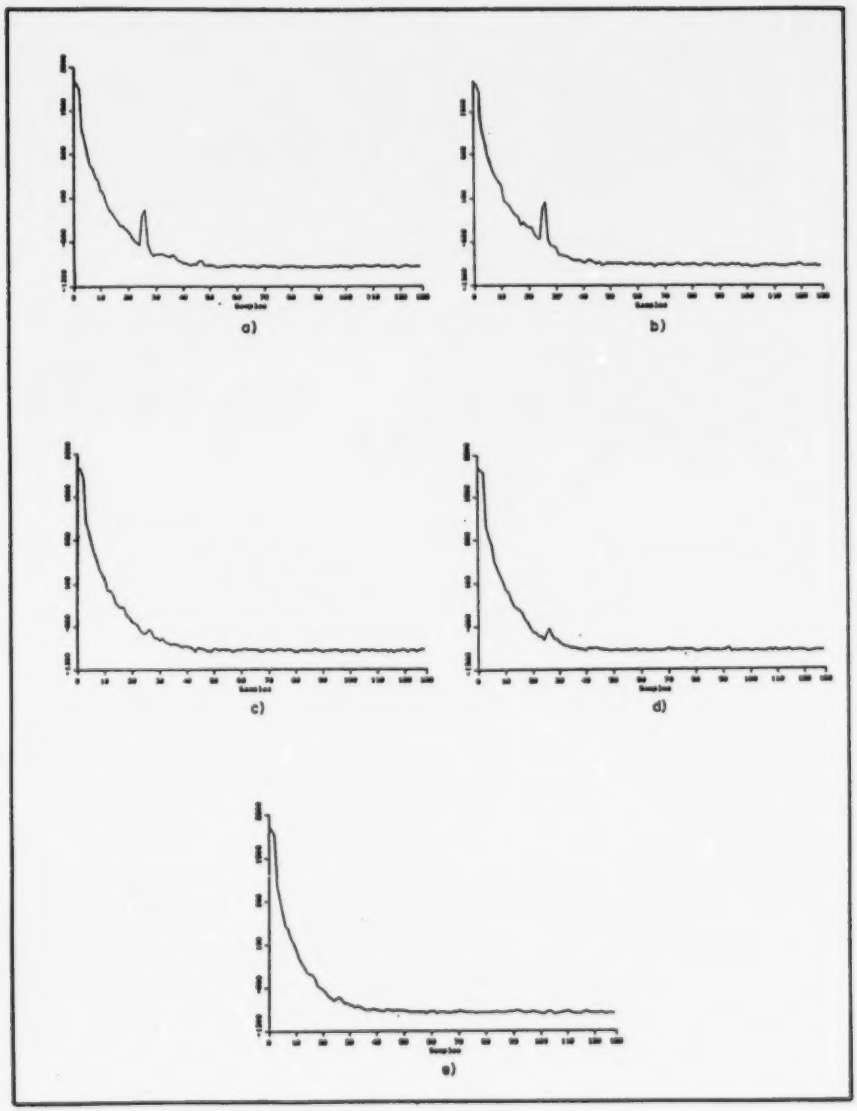

Figure 3-28: Interval average signal returns obtained with a horizontal beam at height 1.2 m directed at a 2.25 m^2 steel plate target mounted at ground level on airport runway. Timer and orientations on June 5, 1986 are: a)14:44-14:57 PDT, 90° inclination, plate perpendicular to beam axis, b)15:50-15:58 PDT, 90° inclination, plate perpendicular to beam axis, c)15:59-16:07 PDT, 80° inclination, plate perpendicular to beam axis, d)17:27-17:38 PDT, 90° inclination, plate normal rotated 9° from beam axis, e)17:40-17:58 PDT, 90° inclination, plate perpendicular to beam axis.

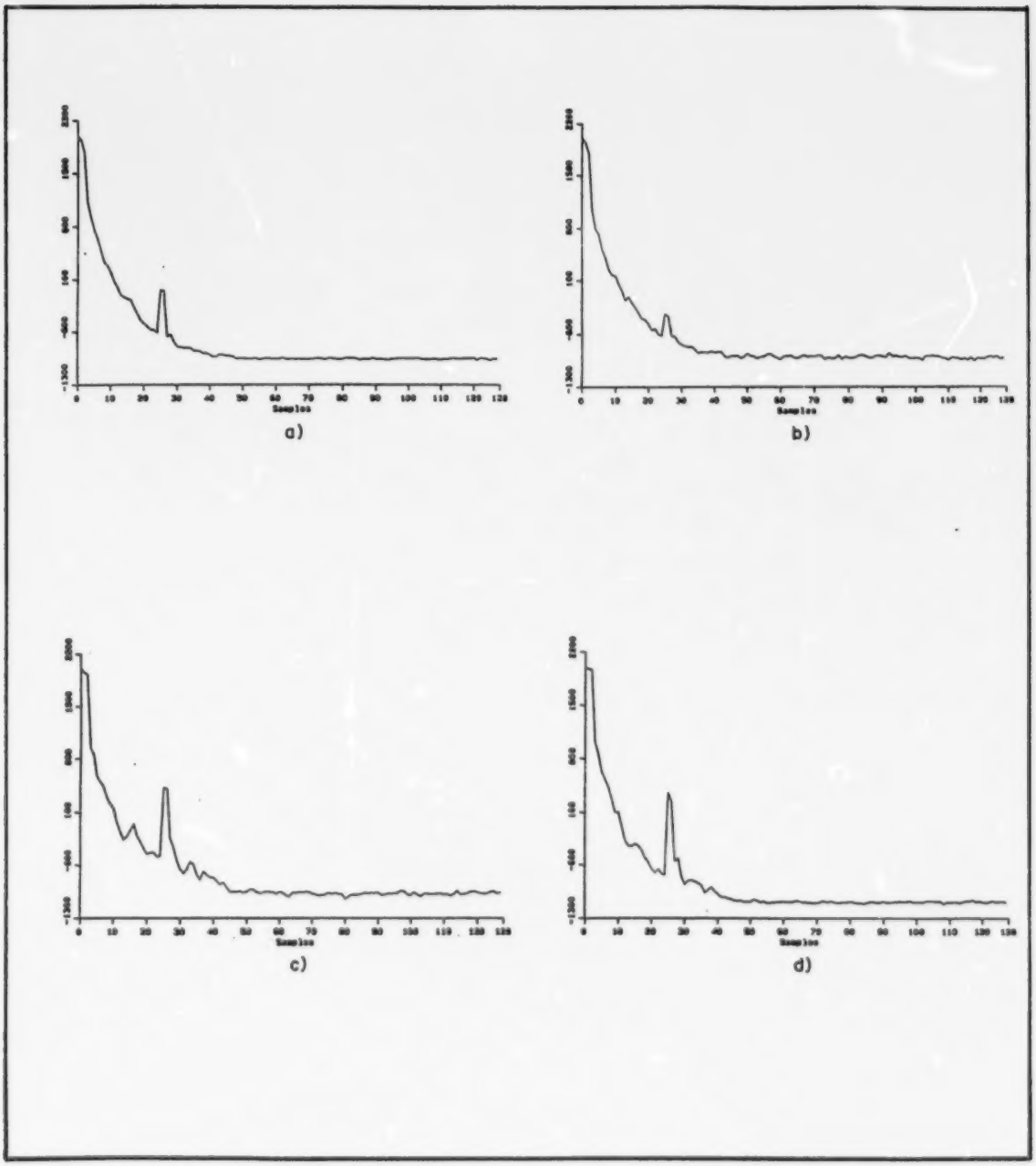

Figure 3-29: Interval average signal returns from horizontal beam at height 1.2 m directed at 2.25 m^2 steel plate mounted at ground level on airport runway. Timer and orientations on June 6, 1986 are: a)12:50-13:26 PDT, 90° inclination, plate perpendicular to beam axis, b)13:43-13:51 PDT, 90° inclination, and beam axis rotated 6° horizontally from plate normal, c)16:19-16:28 PDT, 90° inclination, plate perpendicular to beam axis, d)17:18-17:31 PDT, with the 2.25 m^2 plate mounted on a scaffold 2 m above the airport runway with 90° inclination and the plate perpendicular to the beam axis.

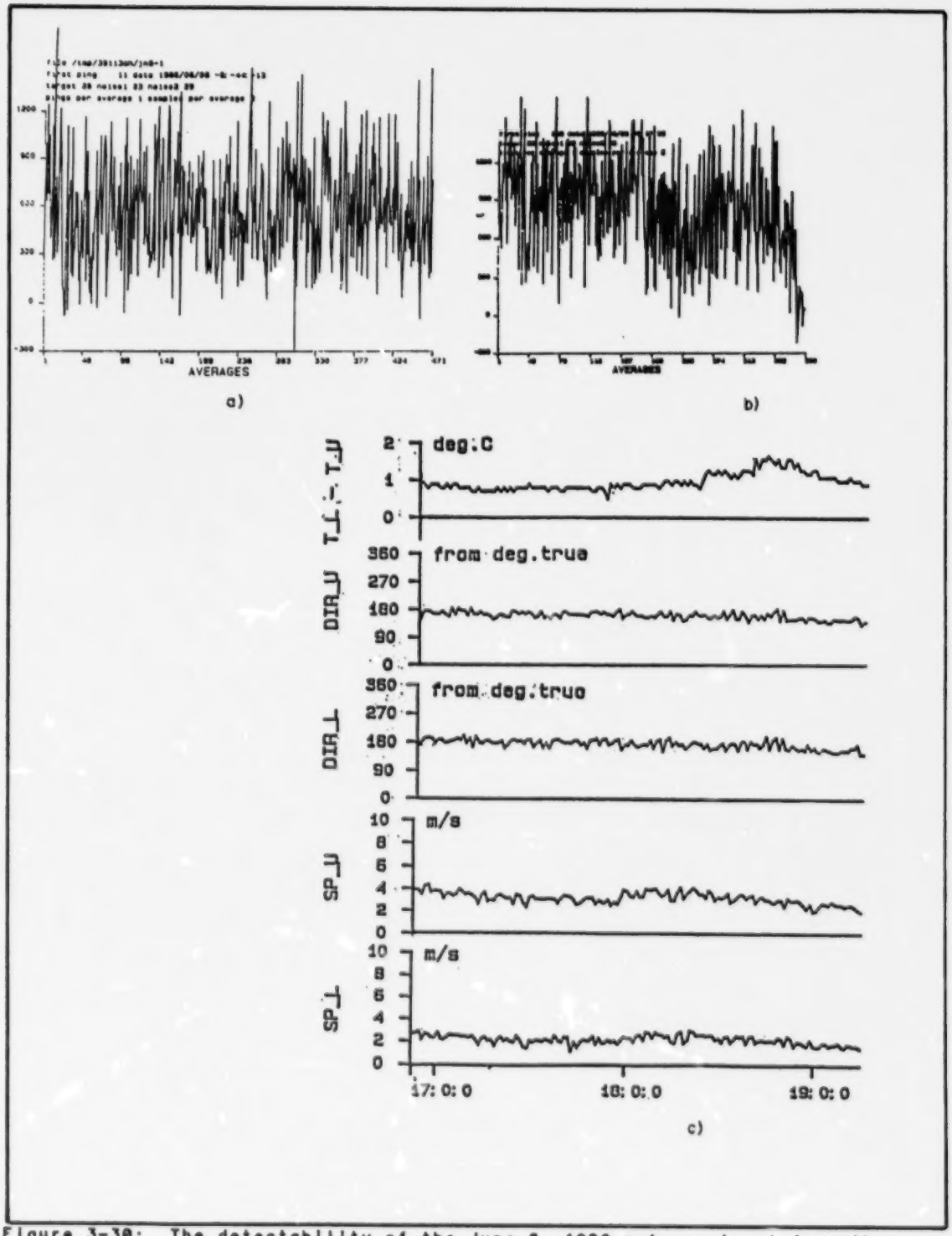

Figure 3-30: The detectability of the June 6, 1986 return signal from the 2.25 m^2 target included at 90° at a range R=462 m: a) target on airport runway with base at ground level 11:28-13:26 PDT; b) target relocated 1.5 m above airport runway 17:20-18:52 PDT. A section of the local meteorological data record is positioned to allow direct comparisons of events in the wind, temperature and detectability records.

assumed the negligible effect of such elevation changes as implied by the nearly identical interval average returns of Figures 3-29c,d. The inclusions of common timescale wind-speed, -direction and 2-level temperature difference records in Figure 3-30c facilitates the interpretations of the time varying signal levels. Comparisons show the close correspondence of wind-and/or temperature-(or temperature difference-) changes with shifts in the elevation of the reflected sound level above background. In particular, the sudden rise in both the 2 m and 9 m wind speeds (and the vertical wind gradient) at ~ 18:00 PDT reduced the detectable signal levels. A sharp increase in the $T_L - T_\mu$ temperature difference at 18:20 PDT subsequently raised the mean detectability close to its earlier level before a common decrease in $T_L - T_\mu$ and the lower and upper wind speeds produced a pronounced signal falloff at the end of the interval.

Target orientation dependence taken from the plots of Figure 3-28 and 3-29 indicate that a 10° reduction in the target inclination produced a 700 mv or 5.6 dB drop in the return signal. Likewise, rotation of the 90° inclined target normal by 9° and 21° in the horizontal plane lowered the averaged return signal strength by 5.6 and 6.5 dB respectively (Figures 3-28d,e). Signal returns received from the target at an inclination of 60° were barely detectable above the noise background.

These results are reasonably consistent with the transmission pulse parameters reported in subsection 3.2 and confirm the expectation, expressed in the theoretical study[1], that negligible returns may be expected (in the absence of roughening) from surfaces with normals deviating by more than 25° or 30° from the instantaneous direction of the beam axis. Direct comparisons of mean signal levels during two periods of SPL measurement at the R=462 m target (Figure 3-8) show that the observed 2.4 dB rise in average power level between roughly 16:20 and 17:20, June 6 and produced a somewhat smaller, 1.7 dB, elevation in received signal level.

As noted in subsection 3.2, data were recorded on June 26 with the intention of probing the simpler propagation conditions which were anticipated to exist at times coincident with the cross-over from daytime upward refractive to evening downward refractive propagation conditions. The complexities noted in the sound pressure levels measured at the target had their counterparts in the reflected signal receptions. This difference was readily apparent even in the earlier portions of the measurement period roughly 40 to 50 minutes prior to the apparent gradient cross-over period. Thus although data recorded during this period were complicated by the presence of two other reflectors, an automobile and the weather station, in the immediate vicinity of the target at R=435 m, the appearance of the interval average return as a function of time differed qualitatively from observations on June 5 and 6. This difference is illustrated in the traces of Figure 3-31 relative to the composite smooth decay plus localized peak forms observed on the earlier dates. The June 26 interval averages show significant increases with time in the strength and duration of the broad

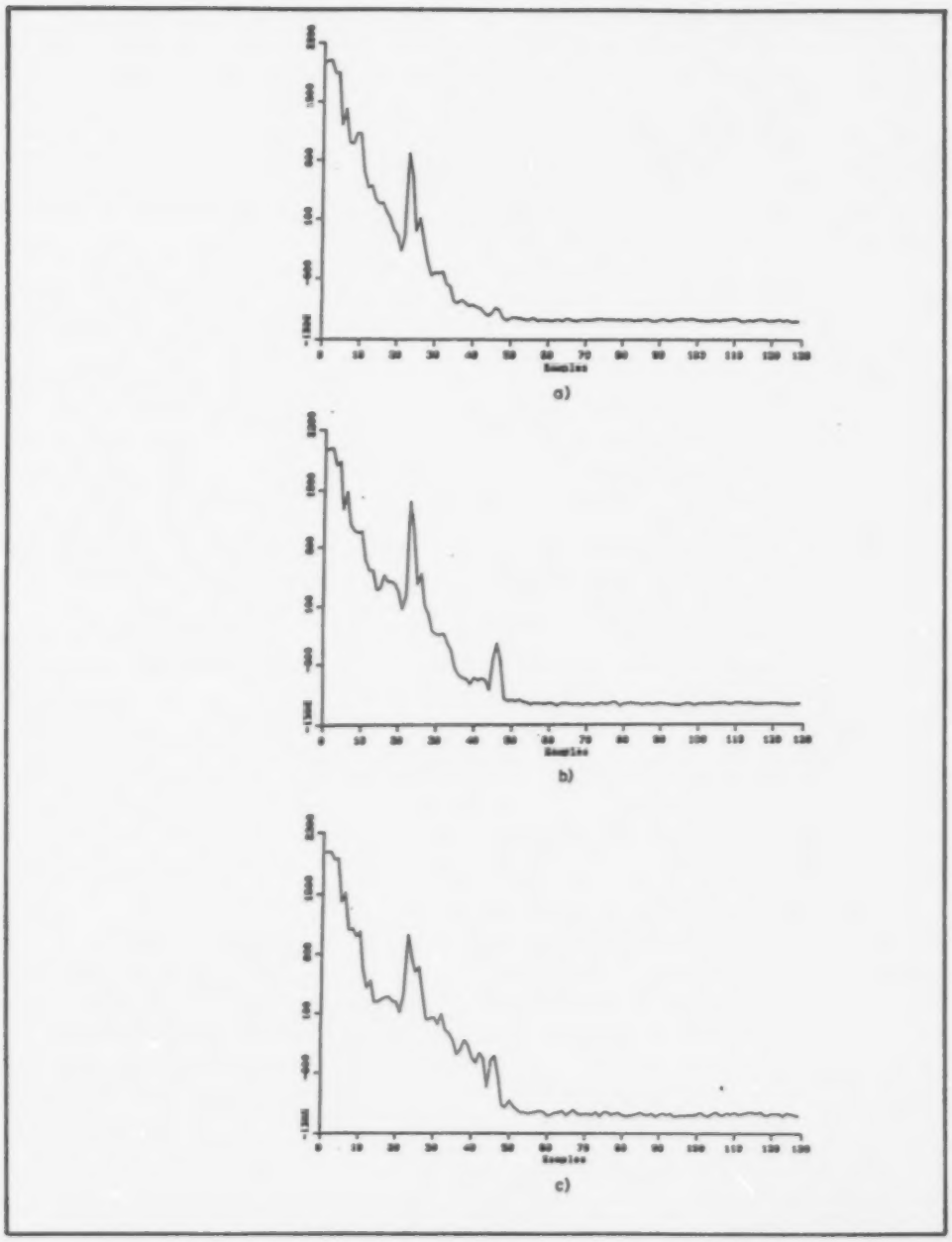

Figure 3-31: Interval average signal returns obtained on June 21, 1986 with the 2.25 m^2 target mounted at ground level on the airport runway: a) 19:59-20:10 PDT when the target is at zero inclination (flat on the ground) R=435 m elevation, an automobile at R=438 m and a weather station at R=470m (all objects on the beam axis); b) as in a but with target at 90° inclination 20:11-20:22 PDT; c) as in b but for the interval 20:22-20:26 PDT during which sound pressure level measurements were made at the target.

decay following the transmission pulse. This decay contains multiple bumps and dips and at least two distinguishable, localized lines near voltage samples n=10 and n=46 which were not associated with the target, weather station or automobile. The n=46 line apparently corresponded to a long, low hedgerow located about 410 m behind the R=435 target, oriented perpendicularly to the runway axis. No obvious object was recorded as being present in the R = 185 m range cell which would normally be identified with the n = 10 peak in the return voltage trace. Possible explanations for the peak include:

(a) anomalously strong returns from one of the several plastic traffic control marker which were scattered about the runway in front of the Sodar antenna; and
(b) reflected returns of the previous pulse (i.e. at a time separation greater than one pulse repetition interval) by a 2 to 3 m high super highway embankment 2.7 km from the antenna.

Difficulties exist with both interpretations since the strength of the mysterious return (= 11 dB greater than that produced by our target) is difficult to reconcile with the maximum possible sizes of the postulated reflectors and a $1/R^4$ range dependence of the reflected signals.

The additional structures in the returns are also accompanied by a pronounced strengthening of the R=435 m target returns relative to those obtained previously (June 5 and 6) with the same target at a similar range (R=462 m). This effect is evident from either a comparison of Figures 3-28, 3-29 and 3-31 or from the listing of Table 3-3. These data show that the observed target returns exceed the values recorded during the early and mid-afternoon periods of June 5 and 6 by 8 to 10 dB and are 3.0 to 4.8 dB larger than the maximum value recorded for the R=462 m target on the latter two dates.

Moving the target to R=715 m coincided with the period 20:36-20:51 PDT when the 2 m to 8 m temperature difference was equal to zero within the accuracy of our measurements. The strength of the target-related return during the period 20:45 - 20:57 PDT, when the temperature difference clearly became less than zero (i.e. downward refractive) was 12.3 dB lower than the peak value recorded at 435 m. This reduction was 2.5 dB larger than expectations in terms of the $1/R^4$ dependence and the additional attenuation expected in terms of the active (two-way) sonar equation. Inspection of Figures 3-32, 3-33 and the data in Table 3-3 show that the signal strength rose to 38.9 dB (approximately the range-reduced value of the peak level recorded at R = 435 m) before dropping again to the lowest recorded levels during the 21:04-21:10 PDT interval. Target related returns then increased to 43 and 49.3 dB in the 21:10-21:13 and the 21:14-21:19 PDT intervals, respectively. The dramatic drop of the 21:04-21:10 interval and the subsequent increases were accompanied by further qualitative changes in the interval average sampled voltages.

Table 3-3: SPL values corresponding to target reflected signals, June 5, 6 and 26, 1986

Date	Time (PDT)	Target Range	SPL (re 20μPa)	Elevation	Remarks
June 5	14:44-14:57	462m	39.2	0	
June 5	15:02-15:19	462m	38.9	0	
June 5	15:20-15:28	462m	39.7	0	
June 5	15:38-15:50	462m	37.8	0	
June 5	15:50-15:58	462m	40.1	0	
June 6	11:25-12:00	462m	37.4	0	1.5 to 2 minutes before SPL measurement at target
June 6	12:01-12:26	462m	38.9	0	
June 6	16:19-16:28	462m	43.3	0	during SPL measurement at target
June 6	17:18-17:31	462m	43.0	2	
June 6	17:31-17:43	462m	44.0	2	
June 6	18:34-18:47	462m	44.0	2	
June 6	19:20-19:33	R=350m	44.7	0	
June 6	19:33-19:46	R=350m	45.0	0	during SPL measurement at target
June 26	20:11-20:22	435m	49.8	0	
June 26	20:22-20:26	435m	48.0	0	during SPL measurements at target
June 26	20:45-20:57	715m	37.5	0	
June 26	20:57-21:02	715m	38.9	0	
June 26	21:04-21:10	715m	31.7	0	
June 26	21:10-21:13	715m	43.0	0	
June 26	21:14-21:19	715m	49.3	0	

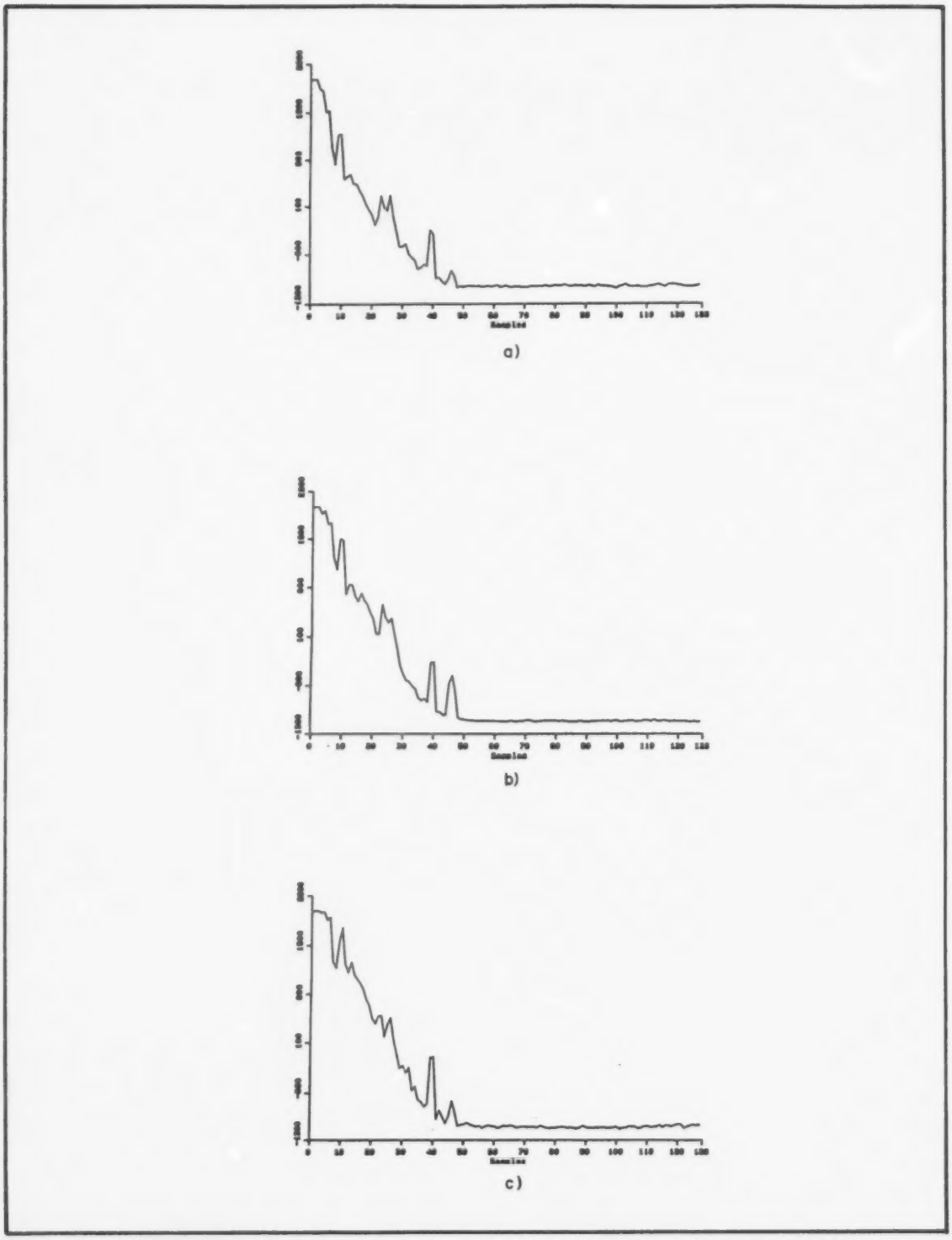

Figure 3-32: Interval average signal returns obtained on June 26, 1986 from the 2.25 m^2 target mounted at ground level on the runway at R=715 m: a) 20:35-20:45 PDT target inclination 90°; b) 20:45-20:57 PDT target inclination at 90°; and c) 20:57-21:02 PDT target inclination at 90°. In all cases a car and the weather station were located near R=430 and 470 m respectively.

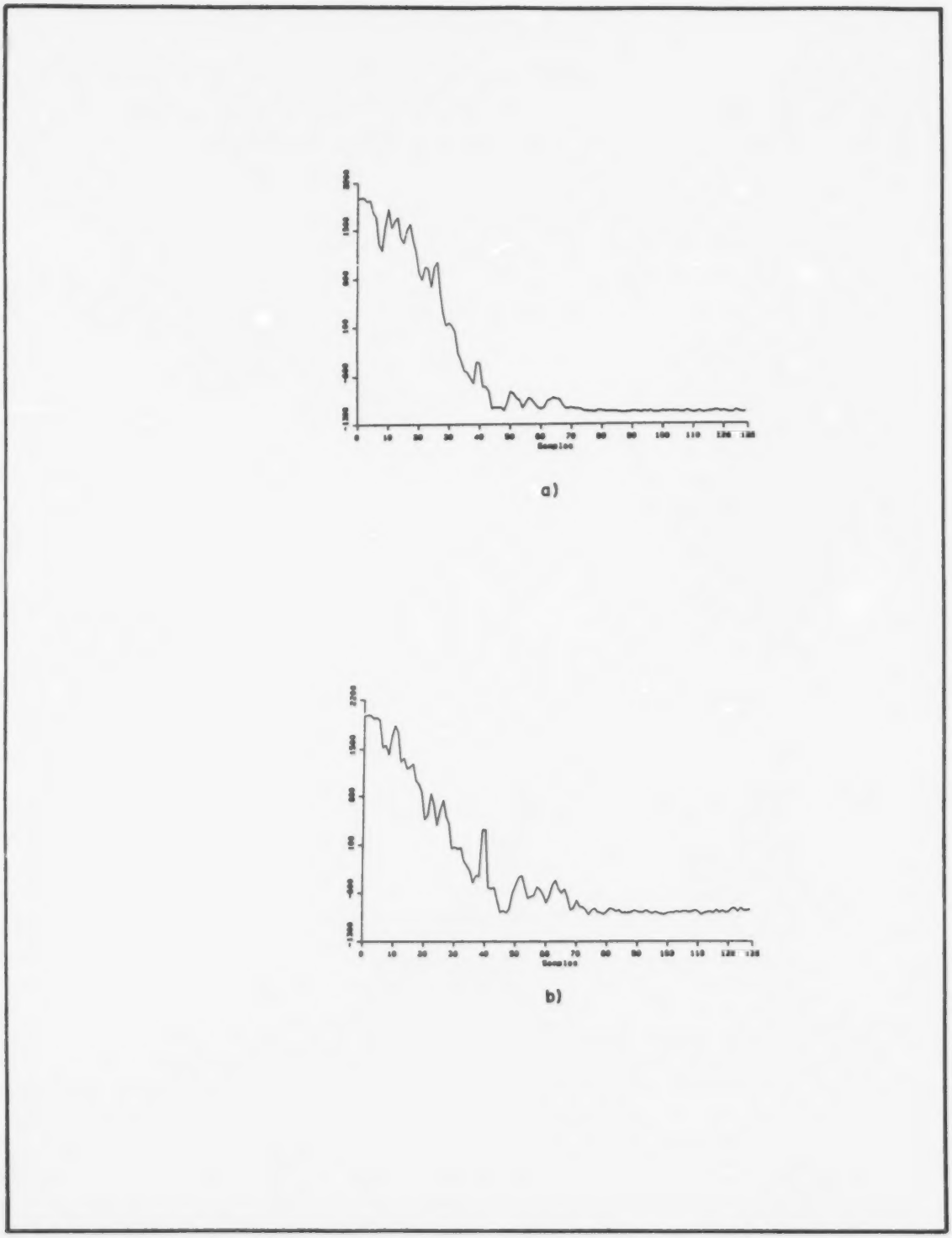

Figure 3-33: Interval average signal returns obtains on June 26, 1986 from the 2.25 m^2 target mounted at ground level on the runway at R=715 m: a) 21:03-21:10 PDT; b) 21:10-21:14 PDT. In all cases the inclination of the target was 90°.

These changes are first apparent in Figure 3-33a,b with:

(1) the disappearance of the anomalous local peak near n=46;
(2) the appearance of 3 or more broader lines between voltage samples n=50 and n=65;
(3) a 260 mv (or 2.1 dB) rise in the baseline noise (in the 21:10 - 21:14 PDT interval).

The presence of the n=50 to n=65 structure continued on through the last two interval average segments displayed in Figure 3-34a,b for the periods 21:14-21:19 and 21:19-20:21 PDT. These two segments show not only the elevated target return level noted in Table 3-3 but, as well, the higher baseline noise which first appeared between 21:10 and 21:13 PDT. It is also significant that a pronounced further broadening of the initial decay was apparent during these intervals.

Thus although readily distinguishable returns from the R=715 m target continued to be seen throughout the entire observation interval, the significant changes in the character of the returns observed during the crossover and negative temperature gradient periods poses a considerable challenge to interpretation. Some clarification in this regard may be possible by breaking the observed signal returns into four distinct components:

(1) The R=715 m target return as defined by the detectability (elevated above local background) of the target return at n=40-41.

(2) The return appearing at voltage samples n=50 through 65. (Practical monitoring of this component was carried out by measuring the voltage elevation at n=50 relative to the baseline at n=110 through 120.)

(3) The broad initial decay, whose intensity as a function of time (after each successive transmission pulse), is measured by monitoring the n=16 voltage sample which corresponded to a point in the initial decay which was free of distinct localized structure.

(4) The noise baseline, the behaviour of which as a function of time is represented by the n=120 voltage sample values.

The magnitudes of each of these component quantities are plotted in Figure 3-35 together with the corresponding 2 m - 8 m temperature difference, $T_L - T_U$, for the common 20:33 to 21:21 PDT interval. Inspection of the plots shows that a steady growth occurred in the strength of the broad initial layer contribution (Figure 3-35c) throughout the

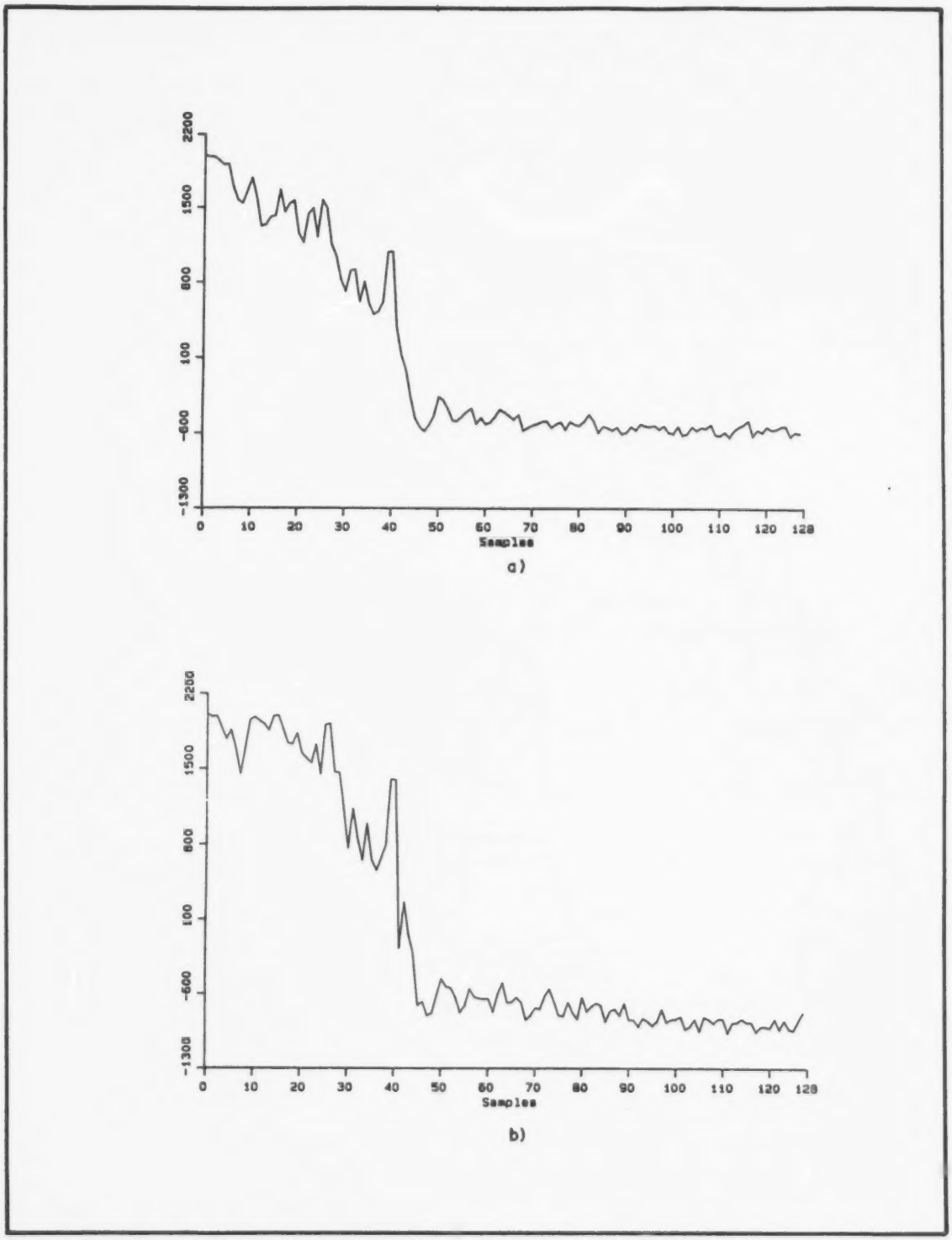

Figure 3-34: Interval average signal returns obtained on June 26, 1986 from the 2.25 m^2 target mounted at ground level on the runway at R=715 m: a) 21:14-21:19 PDT; b) 21:19-2 : PDT. In all cases the inclination of the target was 98°.

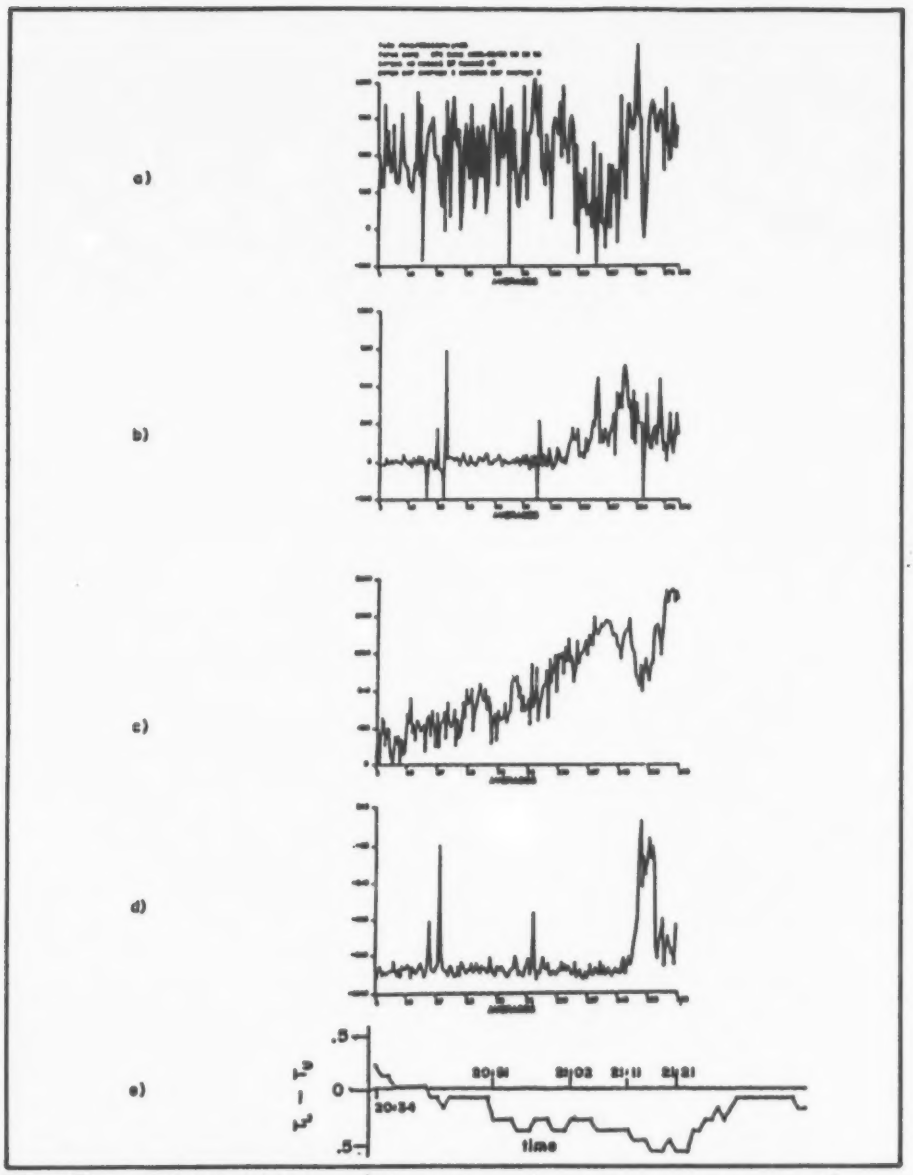

Figure 3-35: The detectability (elevation above local background) associated with signals recorded at 20:34-21:21 PDT June 26, 1986 with the 2.25 m^2 target mounted on the runway surface at R=715 m with an inclination of 90°. The detectability plotted in a) corresponds to returns from the target (voltage sample n=40 and 41); while b) represents returns associated with the anomalous "mystery" structure appearing over the voltage samples range n=50 through 67. The detectability of the broad background component (c) is defined by the elevation of the n=16 and n=17 voltage samples above the long range part of the return (voltage samples 110 through 126). The corresponding changes in the noise baseline are plotted in (d) in the form of the values of n=120 voltage samples recorded following successive transmission pulses. Finally, the temperature differences between the lower and upper (2 m and 8 m above ground respectively) thermometers are plotted in (e).

interval which was associated with near-zero or negative (downward refractive) values of the 2 m - 8 m temperature difference. The approximately 550 mv ($\simeq$ 4.4 dB) drop in target signal detectability which occurred over the 21:02 to 21:10 interval (Figure 3-35a) coincided with a sharp rise in the detectability of the n=50 to n=65 structure (Figure 3-35b). The only sustained jump in the noise background was observed (Figure 3-35d) during the 21:13 to 21:19 PDT interval when target detectability returned to its former high level and the strength of the n=50 to n=65 structure weakened. Its should also be noted that the strength of the broad initial decay component decreased during the high noise period.

Any serious attempt to interpret such a complicated sequence of changes in the return signal should recognize that the steady growth of the broad initial decay coincided with the transition from upward to downward refraction in the 2 m to 9 m atmospheric layer. Since this component is associated with foreground scattering, such behaviour is not surprising during a period when the transmitted beam was increasingly refracted downward toward the runway surface. (It should be noted that the strength of the initial decay, even during the nominally upward refractive [in the 2 to 8 m layer] 20:21 period was considerably in excess of the levels attained during the afternoon hours of June 5 and 6 under more strongly upward refractive conditions.) Nevertheless, in the absence of meteorological data at more than one point along the beam path and in particular at heights within the 0 to 2 m layer, full explanation of our observations is unlikely. Some further discussions of the particulars of this complex period are given in subsection 3.5 but for the moment it is sufficient to note that the enhanced foreground scattering, the appearance of mysterious reflections without any immediately apparent real world counterpart and the anomalous noise level increases are all consistent with the onset of downward refractive conditions conducive to detection of noise and reflection from very distant objects. Thus for example the timing of the reception of the n=50 to n=65 structure is coincident with previous pulse reflection from a line of huge power-line pylons oriented roughly perpendicular to the runway axis at a range of approximately 3.5 km. The presence of such distant returns is not surprising in view of the marine data obtained under generally downward refractive conditions. It is important to note for our purposes, however, that with the exception of the anomalous 21:04 - 21:10 fading, the transition from upward to downward refractive conditions resulted in a 2 to 2.5 dB (300 mv) increase in the detectability of the R=715 target returns.

3.4 NOISE

3.4.1 BACKGROUND

In addition to obtaining representative data on the propagation of an insonifying beam and its reflection and detection, our evaluation requires information on the levels of noise or extraneous (unrelated to target reflections) sound incident on the receiving antenna. Contributions to noise, beyond the inherent level imposed by the shot noise of the transducer resistance and subsequent system noise factors, are to be expected from:

(a) Avoidable (in principal) sources such as heavy street traffic, low flying aircraft, boat motors or, in some of our experiments, the electrical generator used to provide system power.

(b) Unavoidable natural sources associated with vortex production or Aoelian generation at the boundary of physical objects close to or coinciding with the receiving antenna and transducer. These sources were associated with the violent external environment which typically includes air turbulence, waves, on the open-sea surface and blowing snow on a surrounding sea-ice cover.

(c) Unavoidable man-made sources such as would be present in a shipboard detection application Relevant examples include airborne transmissions from vessel engines, cooling fans, icebreaking, and wave impact. Additional contributions from these sources also appear through structure-transmitted vibrations.

(d) Noise sources associated with the acoustic detection process. Such sources include the reflection of the transmitted sound beam by atmospheric turbulence and in particular by the foreground ice- or water-covered surface. These sources all contribute to the broad initial decay which dominates the early portion of each received return signal. To the extent that such sources are unrelated to the presence of the sought after hazard targets, these contributions limit target detectability.

Three sources of data were cited in our earlier theoretical evaluation[1] of the effect of noise on acoustic iceberg detectability. Two bodies of work by Mandics and Hall[17] and Ottersten et al.[18], provided data on noise levels on the upper portions of ocean-going vessels moving in open water (Figures 3-36 and 3-37). The third source of data[19] was measured directly in the interior of an icebreaker hull at the water line. The latter data would tend to over estimate the level of noise which would have been detected at a deck- or mast-mounted receiver. Nevertheless, these data (Figure 3-38) represent the most detailed documentation of the dependence of noise levels on acoustic frequency, ship speed, and the nature of the surrounding environment (i.e. the presence of

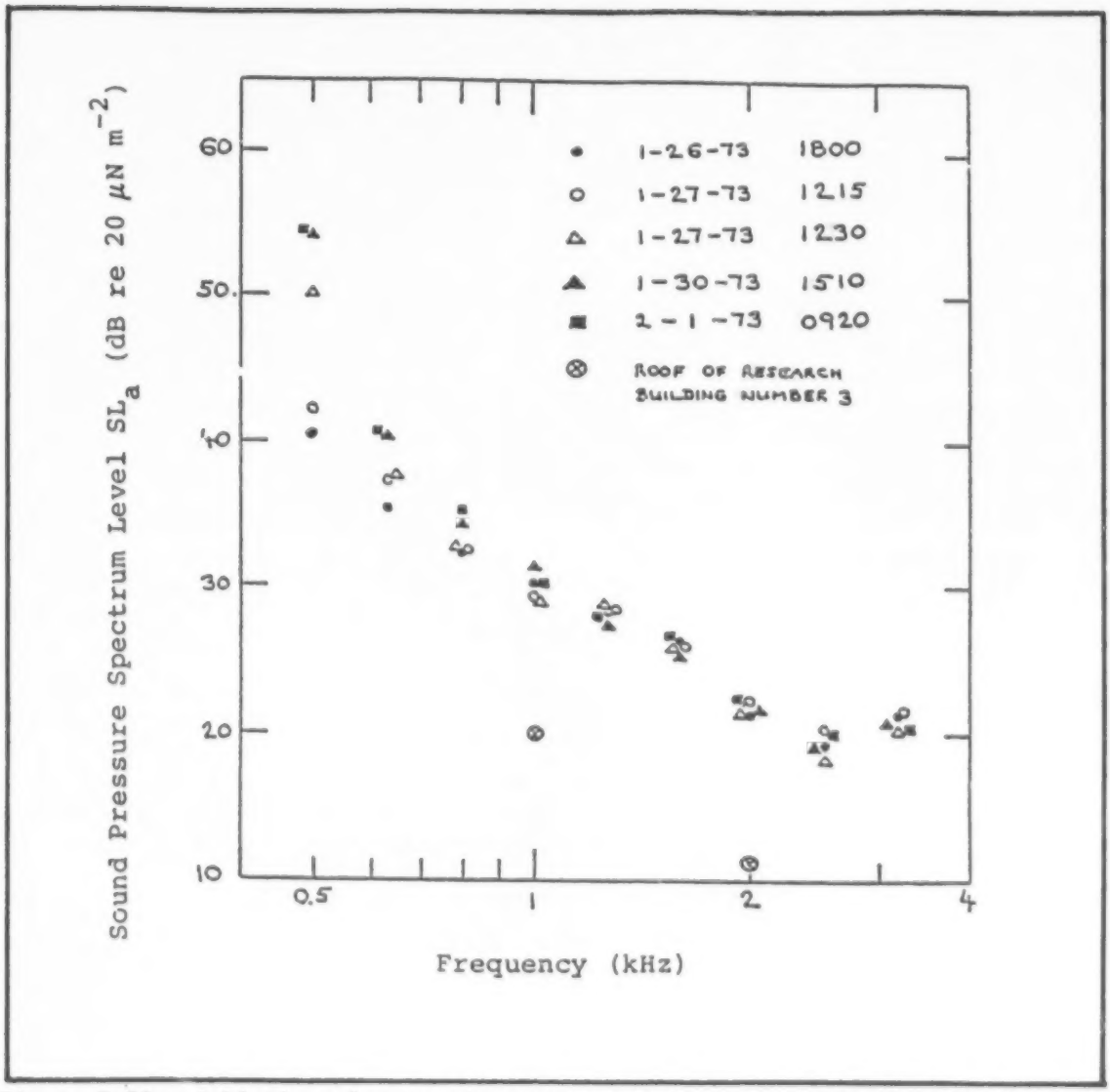

Figure 3-36: Ambient noise sound pressure spectrum levels measured by Mandics and Hall[17] on various dates on the forward superstructure of The Oceanographer. For comparison, values measured on the roof of research building number 3 at the University of Colorado, Boulder, CO, are also included.

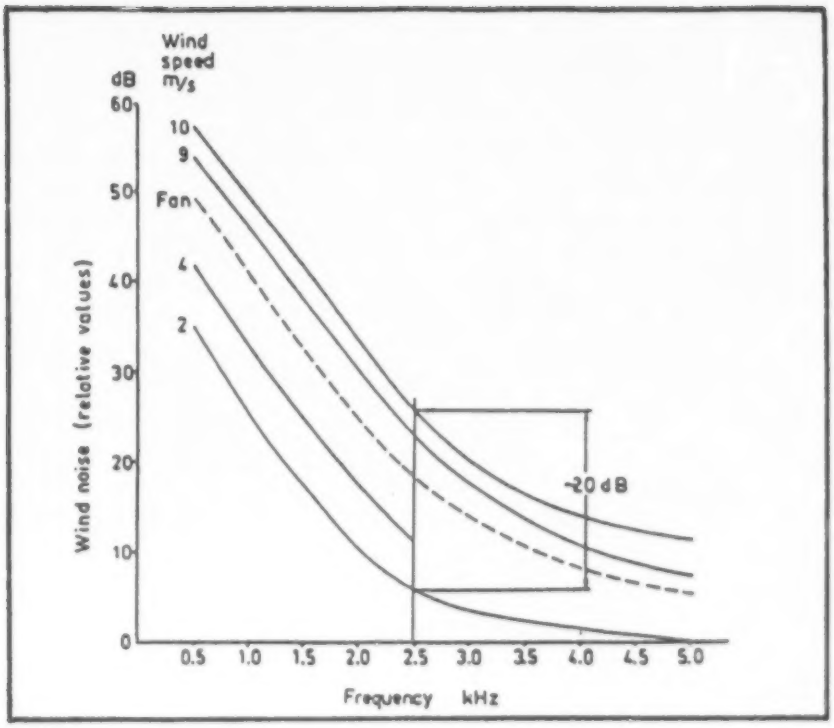

Figure 3-37: Wind-generated noise measured[18] within a 100 Hz bandwidth in the Sodar receiver on board the Planet, in the North Sea, Sept. 1973. By using the rear fan only, the limit for Sodar operation was set by the wind-generated noise. The noise level with two fans in operation, measured when winds were low, is indicated by the dashed line.

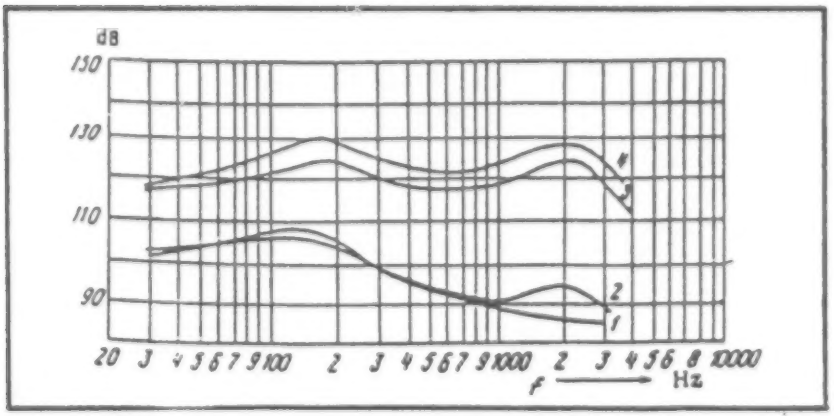

Figure 3-38: Spectral characteristics measured[19]: 1) during motion of an icebreaker in clear water (0 to 1 point on the sea-height scale) at a speed of 15 knots; 2) during motion in water covered with nilas (grey crust ice) at 15 knots; 3) during motion in external ice fields at 4 knots; 4) during motion in annual ice fields at 12 knots.

open water, nilas, first year (annual) or multi-year (external) ice fields).

Unfortunately, quantitative differences in these data sets have introduced some confusion into present understanding of shipboard noise levels. One particular difficulty is the remaining uncertainty as to the dependence of noise level on frequency. Thus, for example, Mandics and Hall[17] and Bogorodski and Gavrilo[19] data suggest that noise levels at 1 kHz exceed those at 3 kHz by 10 and 4 dB respectively. On the other hand, Ottersen et al.[18] data indicate that this decrease is on the order of 34 dB (Figure 3-37).

Likewise, the very strong increase in noise level with wind speed reported by Ottersten et al.[18] does not appear to have a counterpart in the Mandics and Hall[17] results (Figure 3-36) which show little variation among the sound pressure levels recorded at different times, under significantly different wind conditions (wind speeds as large as 12 m/s).

Since noise level estimation is essential to establishing the operational limits of the acoustic iceberg detection process, some resolution of these discrepancies is necessary.

Assistance in this regard is available from the octave band sound level data recorded by Edwards et al.[20] (Figures 3-39 and 3-40) at various interior locations on board the Canadian Coast Guard icebreaker Radisson. Measurements were carried out both during level icebreaking and in passage through open water. Although the obtained values vary considerably with measurement location, the data suggest (except in the forward engine room) a generally monotonic decline in level with increasing frequency. In the open water and icebreaking cases, the 1 kHz - 3 kHz differences, adjusted to a common (1 Hz or 100 Hz) bandwidth, are about 15 dB. The change from open water to icebreaking modes of operation raised the 2 kHz noise levels by 20 to 25 dB. The first of these results is more or less consistent with the Mandics and Hall[17] frequency dependences while the additional noise generated by icebreaking is some 15 to 20 dB smaller than that measured by Bogorodski and Gavrilo[19]. The latter difference is not surprising considering the relatively lessened importance of icebreaking noise in the generally upper level interior locations tested by Edwards et al.[20] relative to the forward water line locations used in obtaining the Bogorodski and Gavrilo[19] data.

3.4.2 EXPERIMENTAL DATA

Information on the levels of noise (defined here as sound pressure level variations detected by the antenna transducer which are unrelated to reflections of previously transmitted acoustic pulses by a distinct target) were obtained during the course of this study from:

(a) direct measurements of sound pressure levels with the B & K instruments on board sea-going vessels; and

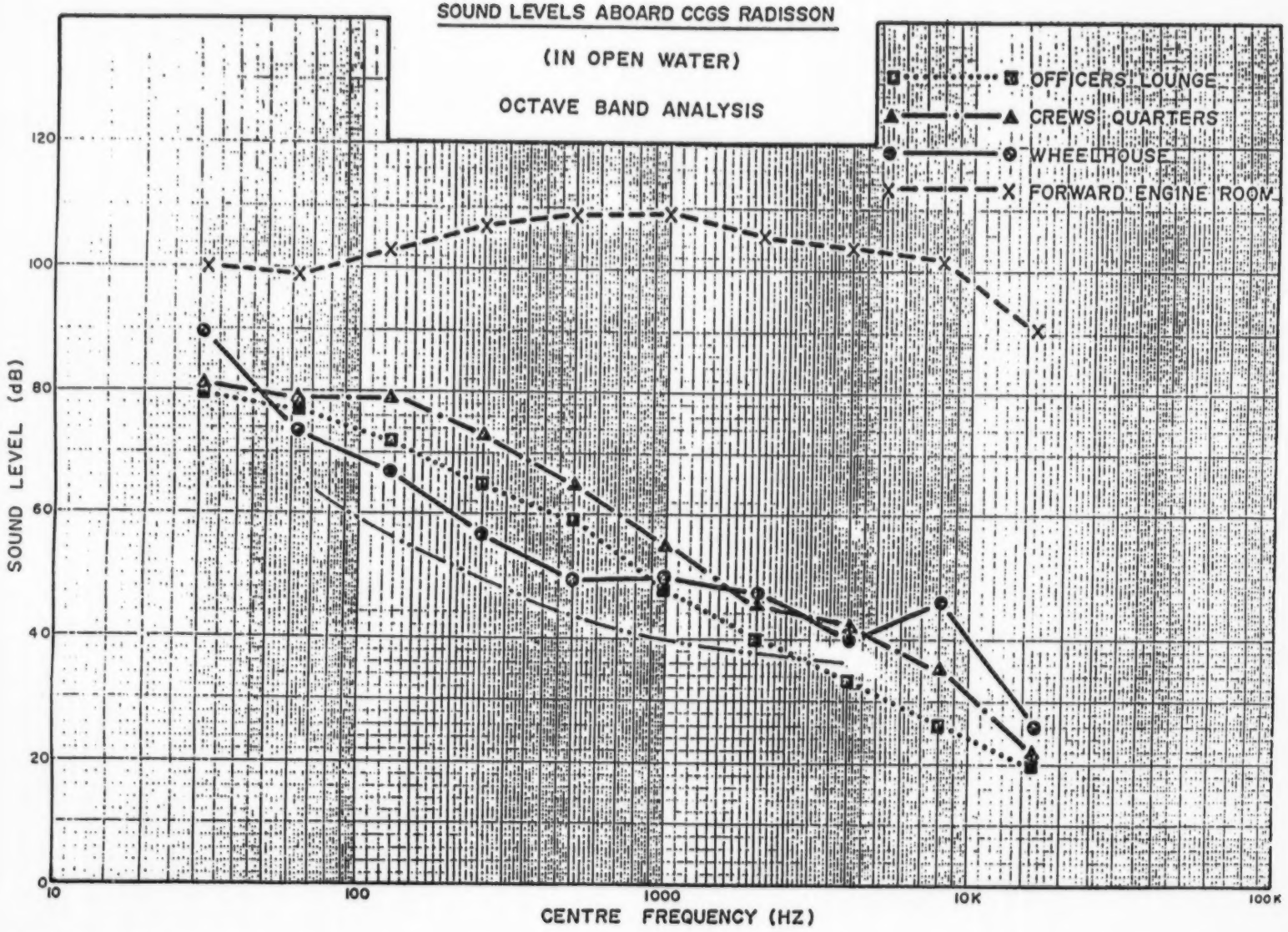

Figure 3:39: Octave band sound pressure levels as measured[20] on the CCGS Radisson in open water.

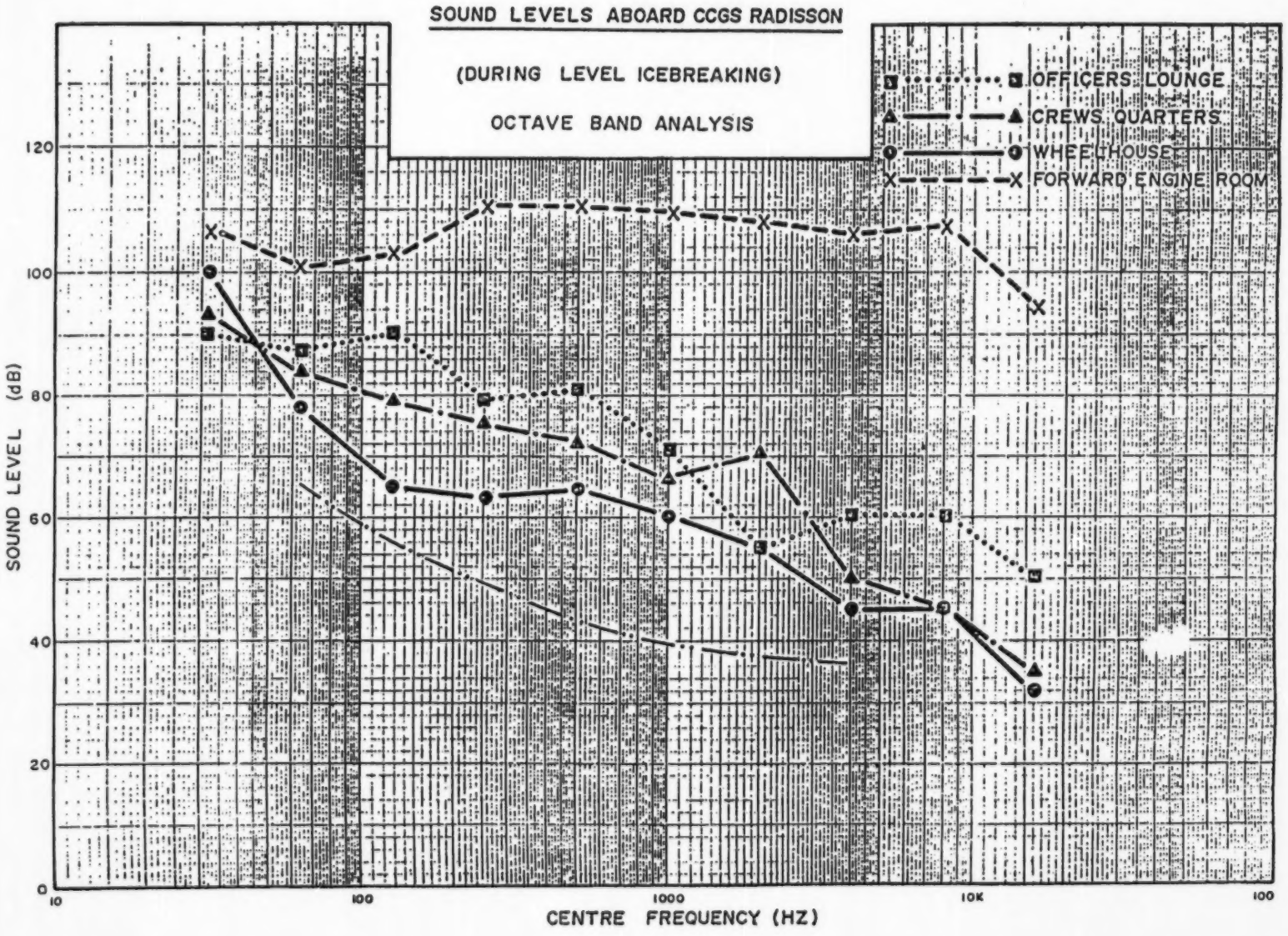

Figure 3-40: Octave band sound pressure levels as measured[20] on the CCGS Radisson when moving through level (first year) ice.

(b) measurements of Sodar system noise levels during the course of the general experimental program. Such measurements were made by either recording return "signals" following pulse transmissions with the gain of transmitter power amplifier reduced to its minimum value or alternatively, by monitoring signal levels corresponding to returns from distances greater than the ranges of all known targets.

In both cases conversion to equivalent noise pressure levels were made possible by repeated calibrations utilizing sound-pressure level measurements at the receiving/transmitting transducer. This additional step was necessary since the more directionally isotropic nature of noise allowed only use of the signal voltage - sound pressure level relationship derived in Appendix A for incident sounds directed approximately parallel to the antenna axis.

The shipboard measurements were intended to obtain additional data relevant to establishing the frequency dependence and magnitudes of noise generated during typical transits of open water and sea ice.

Good frequency dependence data were obtained from measurements made in an exposed location on the upper foredeck of the Queen of Sidney, a large coastal passenger and motor transport ferry making passages between Sidney and Tswassen B.C.

The resulting data plotted in Figure 3-41 in the form of sound pressure levels in a 1 Hz bandwidth were obtained in three separate sets of measurements made at roughly one hour time intervals with the ferry underway at 9 m/s (18 Kts) with 4.5 to 5 m/s winds perpendicular to the ship headings. The data agree quite closely with the results reported by Mandics and Hall[17] for similar environmental and speed conditions on board an oceanographic vessel. Importantly, however, the extension of our measurements to frequencies as high as 8 kHz suggests that the slight increase in noise reported by Mandics and Hall[17] between 2.5 and 3.1 kHz is not universally present and the slightly faster than $1/f^2$ falloff noted at lower frequencies was sustained to at least the upper 8 kHz frequency limit of our measurements.

It is important here to reiterate the earlier observation[1] that the insensitivity of the Mandics and Hall[17] data to wind speed and direction is indicative of the predominant influence of ship engine and fan noise in the reported sound levels.

In the case of their measurements and in our own ferry experiments, the noise was highly directional, originating from the central stack portion of the vessel. A forward-looking Sodar receiver mounted on the forward decks of such vessels would detect this noise after reduction by the 50 to 90 dB rejection figure appropriate to sounds incident from the rear half-space of the shielded receiver.

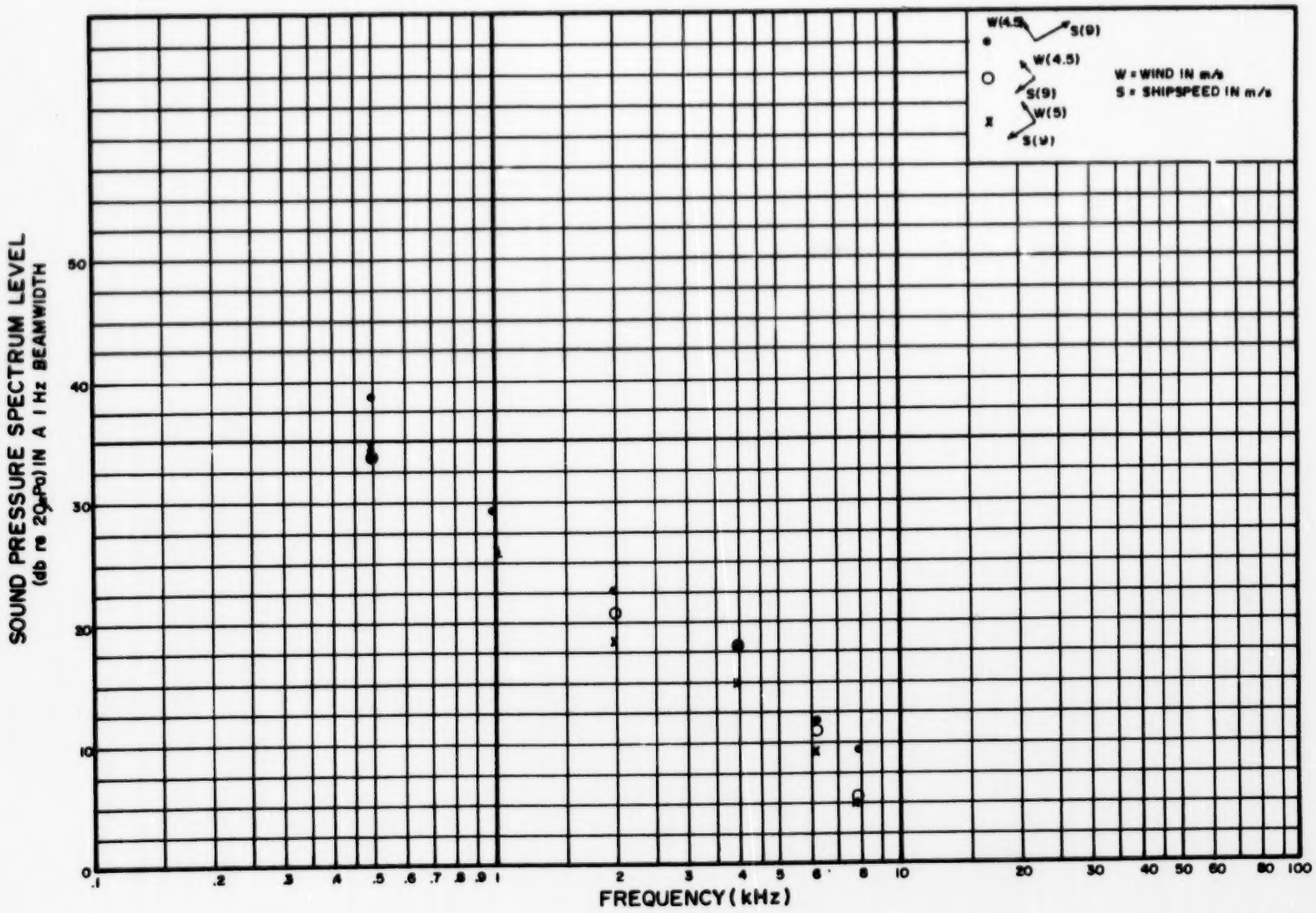

Figure 3-41: Sound pressure spectrum levels measured on the upper forward deck of the Queen of Sidney, July, 1986.

In most cases, this rejection will reduce noise levels close to those appropriate to the contributions from relative motion of the ship and lower atmosphere (i.e. Aoelian noise). The resulting noise levels are likely to be a strong function of the absolute wind speed and directionality (which determine the strength of turbulence generated noise sources in the atmosphere and on the ocean and/or ice surfaces in the forward half-space of the Sodar receiver).

The second set of shipboard noise measurements made aboard the Sir John Franklin on April 15-16, 1986 was much less satisfactory due to a combination of instrument difficulties and unusually light ice conditions over the Grand Banks to the east of our Botwood, Newfoundland port of embarkation. The instrument difficulties were associated with unexpectedly high levels of internal instrument noise generated by the active components of a 3% tunable filter. Measured environmental noise levels apparently never exceeded instrument levels and no significant noise data were obtained.

Nevertheless it is possible to derive a relatively consistent characterization of acoustic noise levels aboard an icebreaker moving through open water and/or annual ice from the collection of data sets cited above. Our approach assumes that noise levels measured on the foredeck of a large ferry moving at 18 kts in open water are a good approximation to those measured at a similar location on an icebreaker moving at similar speeds in ice-free waters. The approximate inverse square frequency dependence of such open-water noise was confirmed by three independent sets of measurements made by ourselves, Mandics and Hall[17] and by Edwards et al.[20]. The stronger and weaker open-water dependence reported, respectively, by Ottersten et al.[18] and Bogorodski and Gavrilo[19] can be safely assumed to be the result of measurement errors or unusual idiosyncrasies of the vessel or of the shipboard measurement location.

In this approach, consistency between the three "valid" open-water data sets (our own, Mandics and Hall[17] and Edwards et al.[20]) is easily achieved by assuming that the measurements inside the Radisson yielded values 5 dB lower than the corresponding on-deck values. If this attenuation is assumed to be representative of the degree of acoustic isolation characteristic of upper-level ship interior locations, on-deck icebreaking octave-band noise levels may be derived by the addition of 5 dB to the Radisson icebreaking data curves (Figure 3-40). This procedure provides a noise spectrum level versus frequency curve (Figure 3-42) which represents a generous value for the upper limit of the corresponding noise levels measured on the upper deck of an icebreaker during the icebreaking operational mode. Justification for this assessment is in the form of observations by numerous correspondents that noise levels on deck are distinctly lower than those obtained in the forward interior portions of such vessels. The open-water noise curve is derived by adding 5 dB to the spectrum levels derived from the Edwards[20] data.

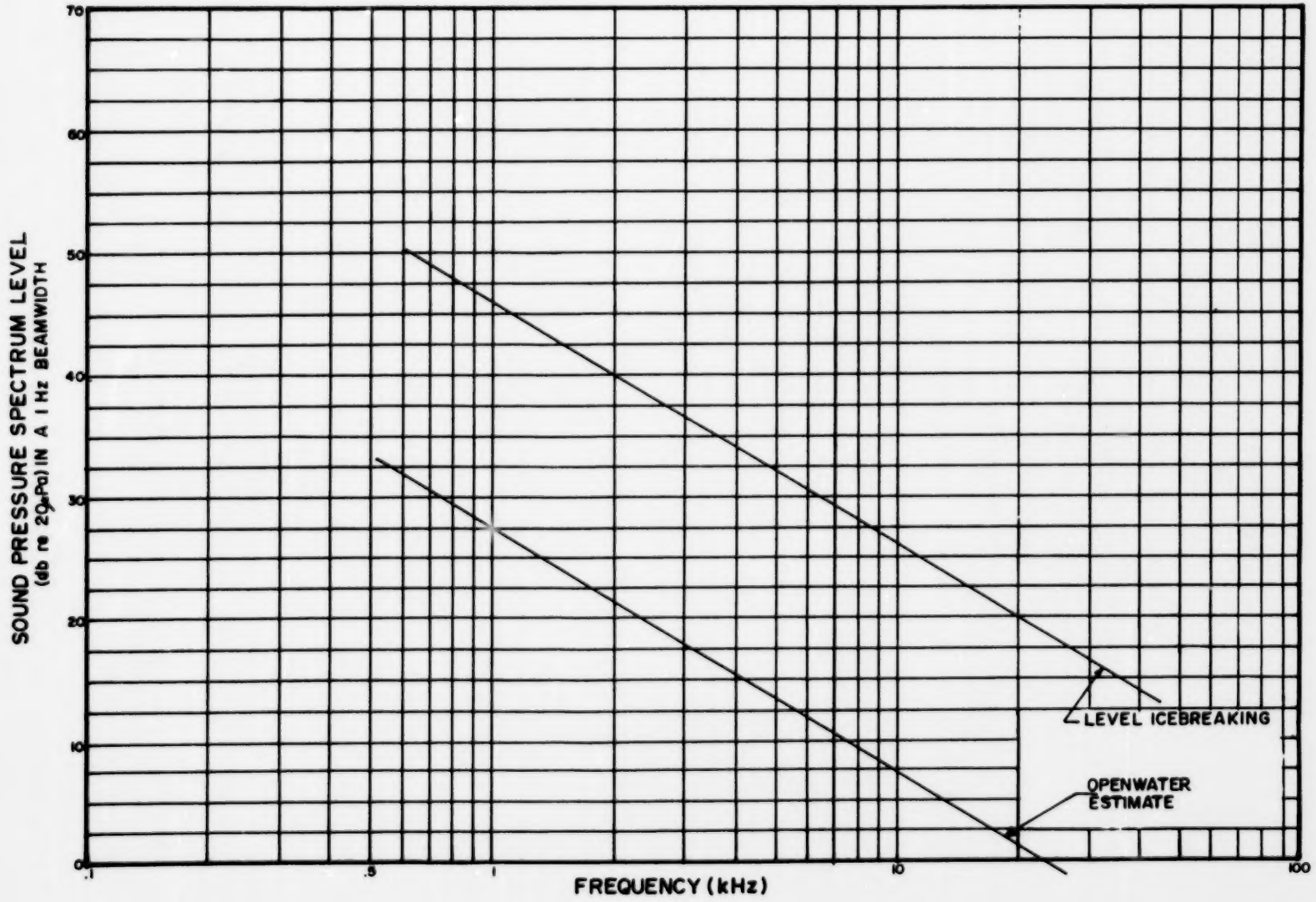

Figure 3-42: Estimated noise spectrum levels on a forward deck (i.e. fo'c'sle) for an icebreaker moving through level ice and open water.

Conversion of the above estimates of noise spectrum levels to actual levels detected by a Sodar instrument required detailed consideration of the directional properties of noise originating from collisions with the ice and/or ocean waves along the forward section of a vessel. Since in both cases the noise sources are close to or in the forward half-space of the antenna, rejection figures will be considerably reduced from those estimated above for rearward stack and fan noise. Antenna positioning and height relative to the ice and wave-breaking surfaces will be critical parameters in determining Sodar noise levels.

Conversion of these acoustical noise level characterizations into representative Sodar output noise levels required additional measurements which were carried out both at the Sheringham Lighthouse experimental site and during our other studies of beam propagation and signal return.

The advantages of the Sheringham Lighthouse site for noise studies were associated with its isolated location on an elevated promontory immediately adjacent to the rough waters of the Strait of Juan de Fuca. As a result, noise level measurements were relatively uncontaminated by contributions from automobile and aircraft traffic and from most other man-made sources. The resulting measurements allowed the best obtained characterizations of the relationship between the baseline noise measured with the Sodar receiver and influential environmental factors such as the ambient noise level and the atmospheric wind field. This relationship is needed to correctly estimate the limitations imposed by the operational environment on hazard detectability.

Sodar noise data were obtained by the power amplifier gain reduction method or, more frequently, from the interval averaged voltage readings obtained 11 to 12 seconds after the pulsed transmissions. Corresponding acoustic data were derived from the 1/3 octave sound pressure level values recorded with the microphone of the B&K 2230 instrument placed along the cylindrical sides of the antenna transducer (with the transmitter power amplifier gain reduced to zero). The resulting data (Figure 3-43) are representative of the Sodar response to acoustic noise generated by wind in the presence (in this case, the measurements were 13 and 23 m above highest high water) of a wind-affected sea surface. The plotted data show an approximately linear relationship (indicated by the broken line) between Sodar output noise levels and the sound pressure spectrum level (i.e. the sound pressure level in a 1 Hz bandwidth). Figure 3-43 also includes a representation of the linear relationship derived in Appendix A, between the simultaneous Sodar and sound level meter outputs upon reception of an acoustic pulse reflected by a localized planar target. (Note the sound pressure levels plotted here have also been reduced to 1 Hz bandwidth values in accord with the noise results.)

The Figure's apparent indication of a higher sensitivity of the Sodar signal to environmental noise as opposed to coherent sound waves back-reflected along the antenna axis is an artifact of the measurement technique in the presence of wind-related noise generation at the Sodar

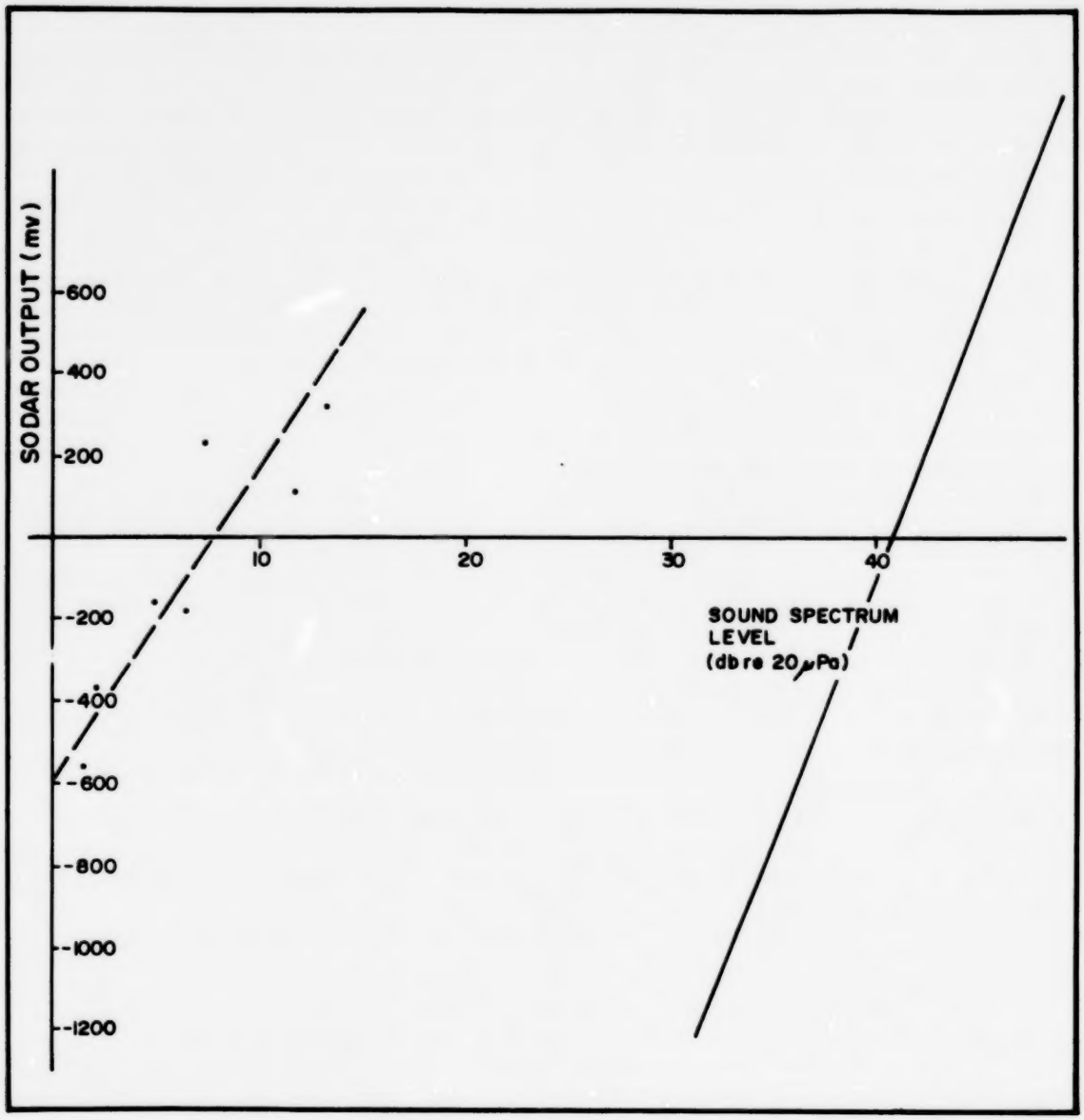

Figure 3-43: Experimental Sodar output values(clustered about broken line) obtained at the Sheringham Lighthouse site as a function of the noise spectrum levels measured adjacent to the cylindrical side of the detecting transducer. The solid line represents the corresponding relationships deduced between Sodar output and incident sound pressure spectrum levels.

transducer face (which was not protected by a windscreen). The unknown directional anisotropy of the marine noise field precluded the use of calibrations against the SL meter-measured third-octave SPL values similar to those used in connection with the reflected coherent returns (Appendix A). The spectrum levels plotted for the noise signal in Figure 3-43 were derived from measurements made with the wind-screened sound level meter located with its microphone head next to the cylindrical side surface of the Sodar transducer. The resulting measurements undoubtedly gave values which were considerably lower than those which would have been measured immediately adjacent to the active Sodar transducer detection surface at the antenna focus. The plotted noise data in Figure 3-43 are of interest primarily because they show the presence of a relatively consistent relationship between the Sodar noise level and the sound spectrum levels measured at the cylindrical Sodar transducer surfaces. The relationship of the latter levels to the true external ambient noise spectrum level is a complicated and unknown function of wind speed and of the directionality of the Sodar antenna relative to both the wind and the imaginary line to the largest source of turbulent ocean noise. In general the largest levels of Sodar output noise were obtained when the Sodar antenna faced directly into the wind. Thus, for example, measurements made on May 1 at the IOS dock under a 5 m/s wind directed outward toward the sea indicated a 800 mv increase in Sodar noise level when the antenna was rotated 180° from a direct seaward exposure surface into the wind. This effect also accounted for the generally much lower Sodar noise levels achieved at the Oak Bay Marina site relative to the Sheringham observations. In the former case, where a westerly or southwesterly wind trend was evident, almost all data were obtained with the axial wind component directed parallel to the outward propagating acoustic beam. Thus, for example, Sodar noise levels were only on the order of -750 mv during the May 21 periods which corresponded to the largest wind speeds (13 m/s) recorded during any of our studies. At Sheringham Lighthouse, on the other hand, considerable data were obtained on both June 13 an 18 for easterly and southwesterly winds with significant components antiparallel to the propagating beam. The resulting Sodar noise levels are plotted in Figure 3-44 show a roughly linear dependence on the axial wind velocity component directed into the antenna. These data provided an initial estimate for the Sodar noise which can be generated by a given relative (to the instrument) wind speed in a marine environment. Unfortunately the data limitation to speeds equal to or less than about 10 m/s still leaves open the question of appropriate Sodar noise levels for relative speeds of 20 to 25 m/s which quite commonly occur on board a vessel in the open ocean. In the absence of actual data, we shall use the linear extrapolation in the Figure to estimate Sodar noise levels at f = 2000 Hz for a given relative ship-to-air speed in the open ocean.

Extrapolations of the 2000 Hz noise limited of Figure 3-44 to both higher and lower frequencies can use the inverse square frequency dependence inferred from[21] the underwater data and as reported by Bogordski and Gavrilo[19] for noise measured at the water line of an icebreaker in open water for frequencies 150 Hz $\leq$ f $\leq$ 3000 Hz. (Curve 1 in Figure 3-38).

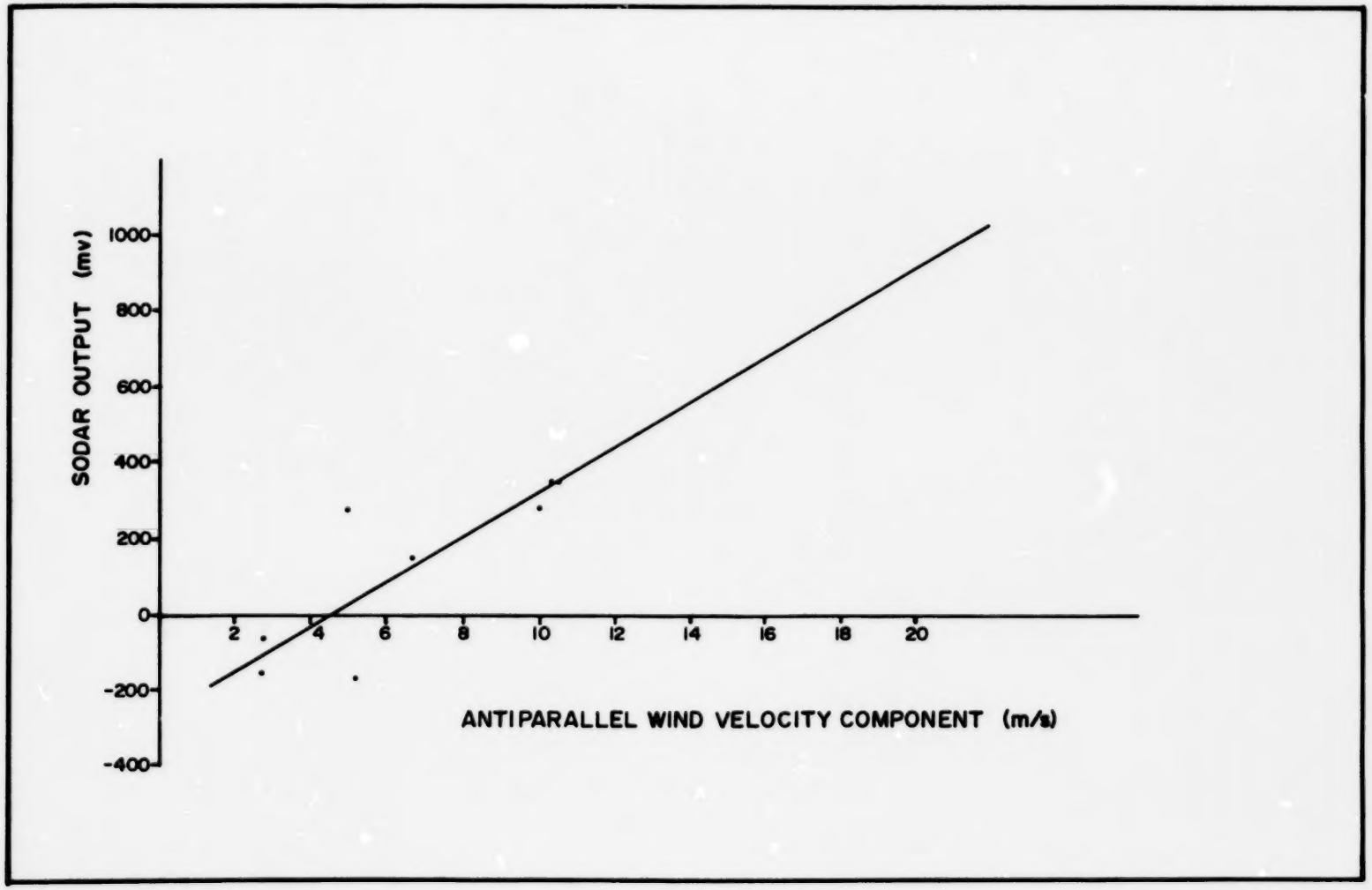

Figure 3-44: Experimental data on Sodar noise level at Sheringham Lighthouse site as a function of wind velocity component anti-parallel to Sodar antenna (wind directed ratio antenna).

Estimates of Sodar noise generated by the principal remaining noise source, namely icebreaking operations, can be derived from the noise spectrum curve of Figure 3-42 (which in all likelihood is an overestimate of actual on-deck noise levels). Further reductions are necessary to obtain appropriate values for the fraction of the acoustic energy which actually reaches the Sodar transducer. This fraction is determined by both the strength of the antenna receiving pattern side-lobes and by the position of the instrument on the vessel. Thus for example, a bow-mounted instrument may actually be forward of the noise source and the maximum possible Sodar noise would be expected to be equal to the noise voltage given by Eq. A-5 for an incident sound pressure level (SPL_A) given by the 10 Hz instrument bandwidth multiplying the sound spectrum levels of Figure 3-42 after reduction by the large negative beam rejection factors obtained from Figure 3-7 for large angles near 90°. Smaller reductions would be expected for an instrument located aft of the main ice fracturing portions of the vessel. In any case, the effective reduction of incident noise levels at a Sodar instrument printed directly forward of the ship is unlikely to be less than 20 dB.

3.5 INTERPRETATION AND COMPARISON WITH MODELS

3.5.1 INTRODUCTION

The data presented in earlier portions of this section represent a fairly detailed empirical evaluation of Sodar as a detector of navigational hazards in temperate marine and terrestrial atmospheres. Confidence in the extension and extrapolation of these results to evaluate the detection feasibility for icebergs in polar or sub-polar oceans requires additional environmental data and some demonstration that present levels of understanding are adequate for a meaningful evaluation. These tasks are carried out in the following subsections in the course of an overall summary and interpretation of the obtained data in the light of earlier work and of the theoretical understandings presented in an earlier report[1] and in published scientific literature.

3.5.2 TERRESTRIAL DATA

The terrestrial testing program was based on the assumption that the acoustic properties of a sea ice pack are well approximated by the physically hard surfaces of an asphalt composite road or a cement runway. Although there was little question of the validity of this assumption, similarity was less obtainable between the respective properties of the atmospheric surface boundary layers above pack ice and an airport runway under a summer sun. In the latter case air temperatures tended to decrease with height above the solar heated runway surface in contrast to the normal increase in temperatures found with elevation above an ice pack. In the absence of strong wind this temperature profile introduced upward refraction in the nominally horizontally propagating sound on both the outward and return paths from and to the Sodar transmitter/receiver. It is clear that results obtained under such circumstances represent an

underestimate of the actual returns which would have been obtained in the surface boundary layer lying above an equivalent pack ice surface. In the latter case except at high wind values, the vertical sound speed gradient is positive and downward refracting.

Under such circumstances therefore the initial demonstration (Figure 3-1) of the detectability of a small 5-10,000 tonne bergy bit-sized building in the midst of much "clutter" must be regarded as encouraging.

The more controlled and documented measurements made at the Boundary Bay Airport site using a 2.25 m^2 portable target provided quantitative measure of losses due to refraction and other effects such as beam broadening induced by wind-generated turbulence.

The transition from daytime (upward refractive) propagation conditions to nighttime (downward refractive caused by the positive vertical temperature gradients produced by the more rapid cooling of the runway surface) was studied in one particular set of measurements which illustrated both the complexities of the transition and the greater range generally associated with downward refractive conditions.

Detailed comparison of the measured propagation data and the corresponding propagation model predictions were complicated by the strong dependence of the model output on the vertical gradients in air temperature and in the beam-parallel wind component. Truly detailed comparisons required near-simultaneous temperature measurements at a number of different heights within the beam and, as well, at a number of points along the beam path. The collection of such amounts of data was not feasible during our experimental program.

An example of a typical set of boundary-layer meteorological data obtained in summer over a hard surface[6] is given in Figure 3-45. It can be seen from these data that our measurements of temperature and wind gradients over the 2 to 8 m or 2 to 9 m height intervals are primarily applicable only to the propagation in the upper portion of the beam originally centered in a horizontal 1.1 m height axis. The velocity shear in the lower 1 m of the atmosphere is typically concentrated immediately adjacent to the surface plane. As a result, except at very high wind speeds, the temperature gradient exerts the dominant influence in the great bulk of the lower portion of the boundary layer which, at Boundary Bay, contained approximately half the propagating acoustic energy. In the two periods of relatively stable atmospheric conditions 16:00 to 18:30 PDT, June 6 and 20:24 to 20:57 PDT June 26, sound speed gradients of +.04 S^{-1} and -.04 S^{-1} were calculated for the 2 to 8 m (or 9 m on June 6) layers respectively. In the latter case, the results corresponded to upward refraction for all portions of the beam on both the outward and return propagation paths. On June 6 however, the data suggest a more complex situation in which upward refraction in the lower portion of the beam existed simultaneously with downward and upward refraction in the upper portions respectively, of the outward and return beams.

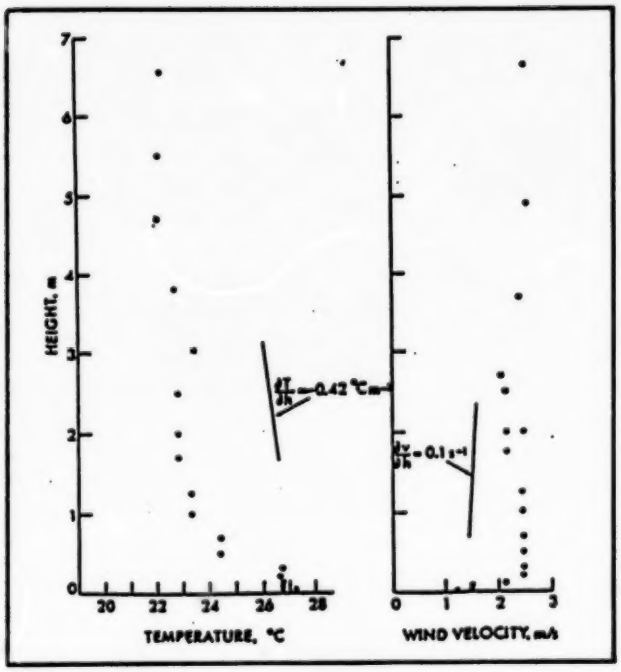

Figure 3-45: Detailed temperature and velocity versus height data as measured above an airport runway during a summer day[6].

Rather than attempting to model such situations with inadequate meteorological data, our comparisons will be carried out initially by assuming freely propagating (unrefracted) beams which, in all cases considered, would give the maximum attainable sound pressure levels both at the target and at the receiver. Experimental deviations from these maximum values will then be considered for consistency with additional losses expected in the presence of realistic gradients. The free propagation results for the 2.25 m^2 vertically inclined target at ranges 450 to 462 m and 715 m, calculated using the earlier derived[1] algorithm, are listed in the first row of Table 3-4. Model calculations assumed a transmitted power level of 70 acoustic watts and a 27.5 dB directional index. Measured data in the form of both peak (in brackets) and mean values are given in the other rows of the table for the times and dates of all Boundary Bay sound pressure level measurements.

Table 3-4: Model calculated and measured mean sound pressure levels in dB re 20 μPa. Measured at the target over the specified time intervals. Peak value intervals are given in brackets.

Origin of SPL Value	R = 341 m	R = 435-462 m	R = 715 m
Free Propagation Model	109.0	107.0	103.0
*Measured June 5, 16:30 PDT		91.8 (100)	
Measured June 6, 13:30 PDT		79.7 (87)	
Measured June 6, 16:20 PDT		82.0 (90)	
Measured June 6, 17:30 PDT		81.4 (90)	
Measured June 6, 19:15 PDT	81.9 (90)		
*Measured June 26, 20:21 PDT		91.0 (98)	
Measured June 26, 21:00 PDT			89.0 (92)
Measured June 26, 21:02-21:14 PDT			66.8 (77)
Measured June 26, 21:14-21:24 PDT			87.9 (96)

* Denotes periods of strong propagation.

It is seen that the strong propagation periods of June 5 and 26 (denoted by asterisk) were characterized by peak and mean values 7 to 9 dB and 15 dB respectively below the free propagation values which, at our measurement ranges, were equivalent to the "freefield plus pressure doubling" maximum values[6]. Such shortfalls are consistent with the measured or inferred existence of negative vertical sound speed gradients during the June 5 and 6 experiments. Additionally, even the $-.04\ s^{-1}$ gradient measured in the 2 m to 8 m layer on June 26 would theoretically have been expected to put all points at height = 1 m in the acoustical shadow at ranges greater than 250 m. As indicated in subsection 3.2, sound levels reaching points in such shadows can be reduced from the maximum free propagation plus pressure doubling (FPPD) value by anywhere from 10 to 30 dB depending upon the wind speed gradient and measurement height. Such reductions would bring the measured mean sound pressure levels close to or below the value measured during the strong propagation periods. The 10 to 12 dB lower values measured on June 6 are consistent with the additional approximate doubling of the beam width observed on this date presumably due to increased turbulence[8]. Such broadening would of itself cause an approximate 6 dB "loss" in sound pressure level at the target and thus account for a good portion of the excess attenuation observed on this date.

The events which occurred after 21:00 PDT on June 26 are, however, particularly difficult to explain in the absence of detailed parameter profiles in the 0 to 2 m layer and at points along the propagation axis.

Speculations in this respect and with regard to the strong propagation conditions of the following 21:14 to 21:24 PDT interval will be developed during our considerations of the received sound pressure level data.

Comparisons with the received signal data (taken from Table 3-3) and the free propagation model (FPPD) values are summarized in Table 3-5.

Table 3-5: Model calculated and measured mean sound pressure levels in dB re 20 μPα. Measured at antenna over specified time intervals.

Origin of SPL Value	R = 341 m	R = 435-462 m	R = 715 m
Free Propagation model	66.5	62.5	54.5
Measured June 5, 14:44-15:58 PDT		37.8 to 40.1	
Measured June 6, 11:25-12:26 PDT		37.4 to 38.9	
Measured June 6, 16:19-17:31 PDT		43.0 to 43.3	
Measured June 6, 17:32-18:47 PDT		44.0	
Measured June 6, 19:20-19:46 PDT	44.7		
Measured June 26, 20:11-20:29 PDT		49.8	
Measured June 26, 20:22-20:26 PDT		48.8	
Measured June 26, 20:45-20:57 PDT			37.5
Measured June 26, 20:57-21:02 PDT			38.9
Measured June 26, 21:04-21:10 PDT			31.7
Measured June 26, 21:10-21:13 PDT			43.0
Measured June 26, 21:14-21:19 PDT			49.3
Propagation model with dc/dz = +.05		58.5	51.3

The June 5 data in Tables 3-4 and 3-5 show that the ~15 dB reduction in the target SPL noted relative to the FPPD value increased to a total 22.4 to 25.1 dB total shortfall over the full two-way path. In the absence of adequate meteorological data, it was not possible to identify the mechanism whereby the return path losses were less than those that occurred in the outward path. The June 6 results were anomalous in that the 25 dB shortfall relative to the FPPD value measured at the target was actually reduced to 18.5 to 19.5 dB at the receiver. In fact, the approximately 10 dB drop in the sound level previously measured at the target on the latter date (relative to June 5) coincided with a corresponding increase of up to 3 dB in the levels recorded at the receiver. This anomaly in which the deviation from FPPD values was smaller at the receiver (by 3 to 4 dB) than at the target was also noted in the earliest June 26 data obtained during a period (before 20:57 PDT) of upward infractive conditions even in the 2 m to 8 m layer. The June 26 data (Table 3-5) did, however, show the higher return signal levels expected under the less upwardly refractive conditions of the evening hours relative to the primarily afternoon measurements of June 5 and 6.

The discrepancy between the one-way and two-way loss is most likely attributable to the known presence[6] of a strong vertical gradient in the sound pressure levels measured in the lower portions of an acoustical shadow. In this view the return signal would be disproportionately associated with reflection from the upper half of our ~ 2 m high target. Measurements of the magnitude of the height dependence were indicative of smaller (1 to 2 dB) differences in the one-way SPL values than would be inferred from our data (see Figure 3-46). Equally disconcerting in this respect is the fact that our own return signal data obtained on June 6 showed little difference between the return signals obtained alternatively with our target on the runway and at 5' elevation.

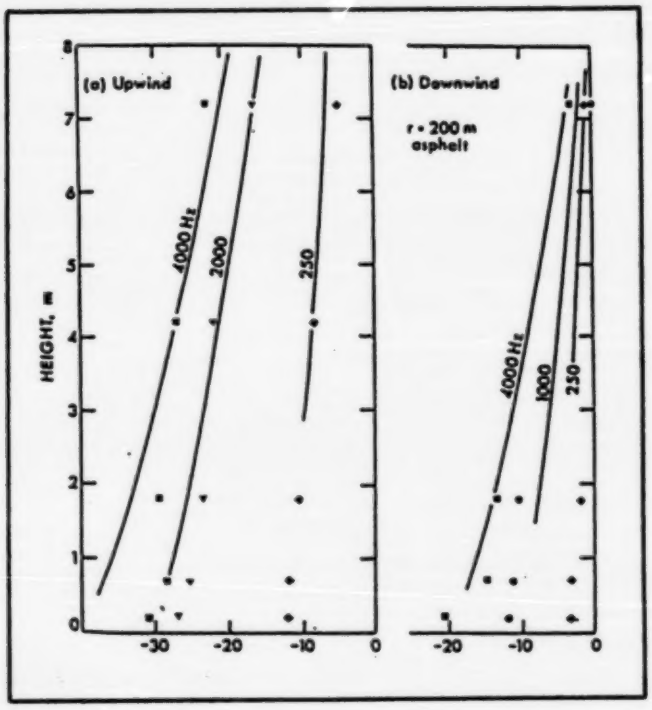

Figure 3-46: Data points represent sound pressure levels measured above hard ground. The temperature and wind velocity profiles shown in Figure 3-45 were measured simultaneously with these results. The curves are theoretical predictions. The sound pressure levels are relative to that for the point source placed on a perfectly hard surface, but allowing for geometrical spreading and molecular absorption[6].

The remainder of the June 26 return signal data were recorded during a period in which the 2 to 8 m upward refractive gradient decreased in magnitude until it changed in sign sometime before 20:51 PDT. Subsequently, the beam became more negative with time until the 21:21 cessation of Sodar measurements. The key feature of the SPL measurements at the target during this period was a larger than 20 dB drop in the sound pressure level over the 21:02 to 21:14 PDT interval. This interval included the 21:04 to 21:10 PDT period associated with the minimim signal return (see Table 3-5 and the detectability data of Figure 3-35a).

Again measurements of return signal during the latter interval indicated reductions of only 6.2 and 11.3 dB relative to the levels of the immediately preceding and following time periods. The highest level return recorded at the Boundary Bay site was obtained during the 21:14 - 21:19 PDT interval when (see Figure 3-35e) the 2 m - 8 m temperature difference reached a local minimum value of approximately -.5°C. The measured value was just over 5 dB below expections from the FPPD assumption and 2 dB below the value calculated from the earlier derived algorithm[1] assuming a sound velocity gradient $dc/dz = -.05\ s^{-1}$ consistent with the measured 2 m - 8 m temperature difference.

These results and the corresponding dramatic changes in the form of the return signal SPL's as a function of time after the transmission (see Figures 3-32 to 3-34) appear to be associated with a period of instability which accompanies the transition from upward to downward refraction. Large eddies containing masses of colder and/or warmer air drift through the beam producing transitions between the alternative upward and downward refractive modes. These conditions could, as well, induce hybrid or mixed modes of propagation. The resolution of the time-dependent signal returns into components carried out in Figure 3-30 would appear to be consistent with an overall transition to the dominance of downward refractive propagation during the 20:51 to 21:21 PDT interval. The extent of downward refraction increased both the amount of foreground clutter, i.e. the background line and the magnitude of the target return. The anomalous 21:04 to 21:10 drop appears to coincide with the rise of signal strenth from very distant reflecting objects (Figure 3-35b), (probably power line pylons), on the other side of a distant super highway. The subsequent falloff in this return coincided with the spectacular (20 dB) short-lived rise in noise during the 21:11 to 21:18 PDT interval.

The possibility that the anomalous noise originated at the super highway would be consistent with the presence of a long range skip-mode of sound propagation whereby the time dependent properties of a generally downward refractive atmosphere establishes low loss paths to specific spatial locations. In this view the interplay between the intensities of each of the components in Figure 3-35 a-d reflects shifts in the nodes and antinodes of the two-way propagation path beginning and ending at the Sodar antenna.

Speculation on the nature of the proposed modes of propagation must remain unconfirmed in the absence of much more detailed meteorological and acoustic measurements. Furthermore, such specific studies of the anomalous period of transition between daytime upward refractive and nighttime downward refractive conditions does not seem of immediate relevance to our evaluation of Sodar target detection above a hard surface. The data indicate that even in the presence of an unfavourable upward-refracting sound speed gradient, the reduction of the sound pressure levels at the Sodar antenna calculated assuming free field plus pressure doubling is never more than 20 dB and was often on the order of 10 to 12 dB. The difference between the maximum possible (FPPD) and observed values decreased with the apparent increase in the extent of downward refraction, reaching levels within 2 dB of model-calculated levels using sound speed gradients calculated from the 2 to 8 m temperature difference. Even during the anomalous period of very low incident power, target detectability was always maintained at ranges at least up to R = 715 m.

The changes in the appearance of the signal return as a function of time after the transmission which occurred during the transition from upward to downward-refraction conditions suggested that under the latter condition the detection of larger objects was possible out to ranges as large as 3 km even with a 1 m height beam.

3.5.3 MARINE DATA

The data obtained at the principal Oak Bay Marina and Sheringham Lighthouse marine test sites were of great value not only for preliminary testing of hazard detectability in an ice-free ocean but, as well, as a source of data on the range, wind speed and wind directionality dependences of the detection process.

Inspection of the sound pressure level-range relationships as measured at the targets (Figure 3-9) shows that the data exhibit the same R^{-2} range dependence noted at the terrestrial Boundary Bay site but are several decibels lower in magnitude at comparable ranges. On the other hand, lest these data be used to confirm a difference in the losses upon reflection at the alternative water and concrete runway surfaces, it should be noted that the marine return signal strengths (SPL values at the Sodar instrument) did not show reductions from the FPPD value any larger than those observed at the terrestrial site at comparable $\leq$ 715 m ranges. Direct comparisons of the measured ranges of marine signal level variability and the predictions of the free propagation model are facilitated by the listings of Table 3-6.

Except for those periods (May 21, and in the second listed interval of June 24 and 30) when moderate to strong winds were present parallel to the outward propagating beam, the returns from marker 2 were 11 to 15 dB below those obtained from the first marker. A further 4 to 6 dB drop was recorded between the second and third markers. The relative returns from marker 1 and 2 are relatively consistent with the expected R^{-4} range dependence and with the FPPD shortfalls recorded during the inferred

downward refractive periods of June 26. The more distant marker 3 returns on the other hand, were clearly too strong to be explained in terms of an R^{-4} dependence and the observed strengths of the nearer marker returns. This result is likely due to the mechanism(s) responsible for the anomalous appearance of distant targets noted during the apparent downward refractive period of June 26 at the Boundary Bay Airport site.

Table 3-6: Experimental and free propagation model* calculated values of SPL corresponding to signals corresponding to reflection from each marker detected at the Sodar antenna. Free propagation model values include corrections for marker cross-section intrinsic attenuation and beam alignment.

Date	Marker 1	Marker 2	Marker 3
Free Propagation Model May 21-June 24	61.5	50.1	36.4
Free Propagation Model June 30	59.5	52.1	38.4
May 21	42.6	trace	
May 23	47.2-49.3	34.3-36.7	28.2-30.5
May 30	51.6-54.8	39.5-43.9	35.0-40.5
June 24 (before 15:12 PDT) (H)	50.4-53.2	41.2-47.7	37.6-41.6
June 24 (after 15:12 PDT)	46.3-49.3	31.0-35.0	25.8-36.2
June 30 (15:28-15:46) (H)	49.8	35.1	32.6
June 30 (after 16:07 PDT)	47.8-48.0	33.1-33.7	21.5-26

* Separate model prediction estimates for May 21 to June 24 and for June 30 were made to account for the small changes (2 dB estimated) associated with the different beam alignments on markers 1 and 2 respectively, during these periods.

It is interesting to note that the returns during the cited period of strong returns at the Marina site were generally characterized by a broadness and oscillatory structure in the underlying initial decay curve (see for example Figures 3-15b, 3-16, 3-17a,b and 3-18a). The various bumps and dips in these curves sometimes complicated the extraction of equivalent SPL values for the discrete target reflections. At least some of these structures are believed to be associated with the reflections from the foreground and from previously insonifractions of more distant reflections similar to those encountered during the downward refractive study period at the Boundary Bay Airport.

On the other hand, the initial decays recorded during the low return periods (Figures 3-14, 3-17c and 3-18c,d,e) were relatively smooth and reminiscent of the "clean" returns observed at Boundary Bay throughout the June 5 and 6 experiments and during the early part of the June 26 measurements. Upward refractive conditions were present on both occasions.

Such returns were identified as being characteristic of upward refractive propagation on one or both segments of the two-way acoustic paths. By implication the returns received during the weak propagation periods at the Oak Bay site were similarly associated with the additional losses incurred by the necessity for propagation into the acoustic shadow. The reductions of the signal strength from the downward refractive, good propagation case, approximately 10 dB, were comparable to the differences noted between return strengths during alternatively downward and upward refractive propagation intervals at Boundary Bay airport on June 26.

It is possible to describe the data in Table 3-6 in a self-consistent empirical form which is consistent with the above interpretations in terms of periods of high and low sound propagation. In this approach the sound pressure level associated with returns from marker 1 is used to set the overall level of all returns. Its value, on the basis of the data in Table 3-6, can range anywhere from 6 to 19 dB below the FPPD or "free propagation" value. The extent of the latter reduction is a complicated function of atmospheric conditions but was generally on the order of or less than 13 dB except under the extreme winds of May 21. SPL values at the more distant markers were derived from the first marker level and the assumptions:

(a) that the marker 2 returns are 13 dB below the marker 1 value; and

(b) that the return from marker 3 can be obtained from the computed marker 2 level by:

1. subtracting 5 dB under "good" two-way, downward refractive conditions; and

2. subtracting 10 dB under "bad" upward refractive conditions on at least one one-way path.

The 13 dB decrease in (a) is slightly larger than expectations, 10 dB, for the marker 1 and 2 return difference in terms of the free propagation model. Both loss values given under (b) are significantly smaller than the approximate 14 dB difference in the marker 2 and 3 return SPL values expected in terms of the free propagation model.

Comparisons of this empirical range dependence with the spread of experimental values listed in Table 3-6 are illustrated in Figure 3-47a and b for all periods of high (H) propagation. Corresponding representations

for the low propagation periods of June 24 and 30 are given in Figure 3-47c and d. These last figures include representations of both a 5 dB and 10 dB falloff between markers 2 and 3. Our normalization of the empirical curve in all cases was to the mid-point of the range of values recorded for the marker 1 returns. The excellent fitting of the data suggests that although it is impossible to quantitatively explain the variations in the level of a given return as a function of time without extensive meteorological data, the range dependence results are consistent with theoretical expectations (i.e. R^{-4} law plus attenuation) at distances up to roughly 1 km. At greater ranges the rate of falloff with distance is dependent upon the presence or absence of an upward refractive segment in the two-way acoustic path.

This admittedly simplified description appears to be relatively consistent with observations made at both the terrestrial and marine sites. Thus, for example, the application of the algorithm to May 21 data predicts signal levels of 29.6 and 19 dB re 20μPa for markers 2 and 3 respectively. The absence of a marker 3 return in Figures 3-14c and d is thus not surprising since a return equal in magnitude to the baseline noise levels in the Figures would range from 34.8 (Figure 3-14a) to 36 dB (Figure 3-14c). Although it is difficult to estimate the magnitudes of trace signals, the long term average (180 pulses) marker 2 return on Figure 3-14a corresponds to a sound pressure level of approximately 27 dB, only slightly below the predicted value.

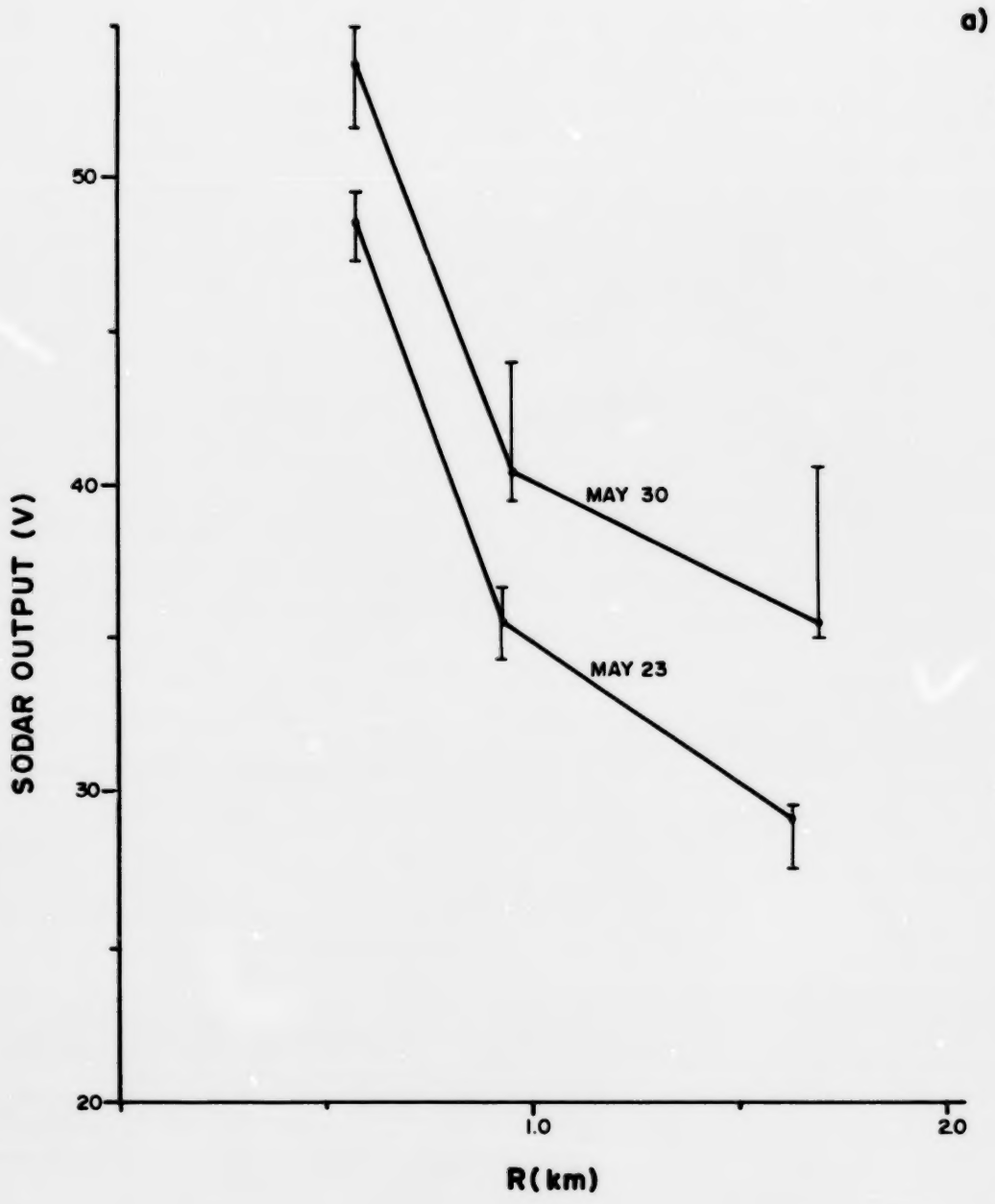

Figure 3-47: Experimental return signal ranges versus spatial target range recorded during high (H) propagation periods of a) May 23 and 30, and b) June 24 and 30. Corresponding ranges recorded during lower (L) propagation periods of c) June 24 and d) June 30. Solid line segments in all figures represent expectations on basis of empirical model described in text.

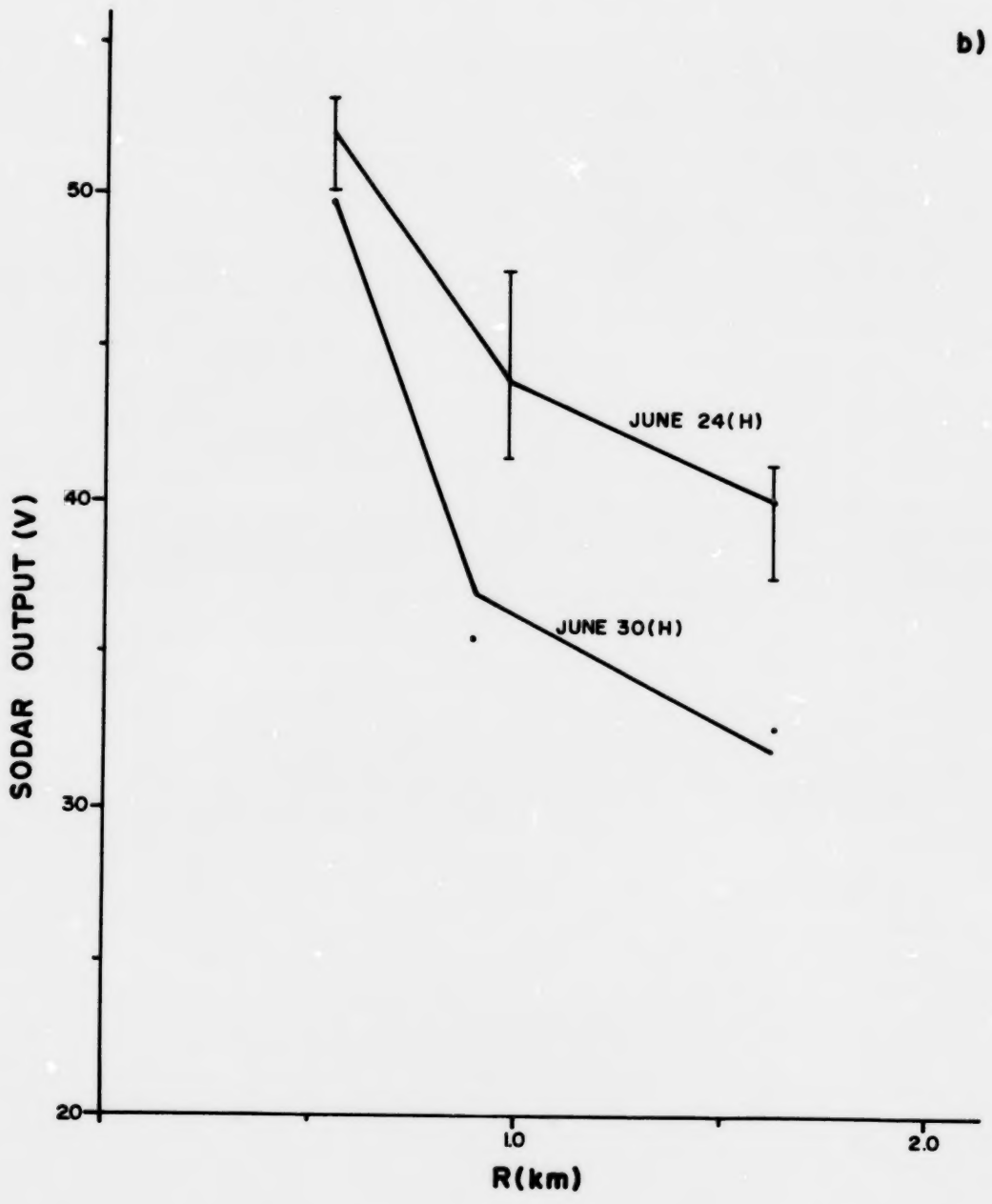

Figure 3-47: Experimental return signal ranges versus spatial target range recorded during high (H) propagation periods of a) May 23 and 30, and b) June 24 and 30. Corresponding ranges recorded during lower (L) propagation periods of c) June 24 and d) June 30. Solid line segments in all figures represent expectations on basis of empirical model described in text.

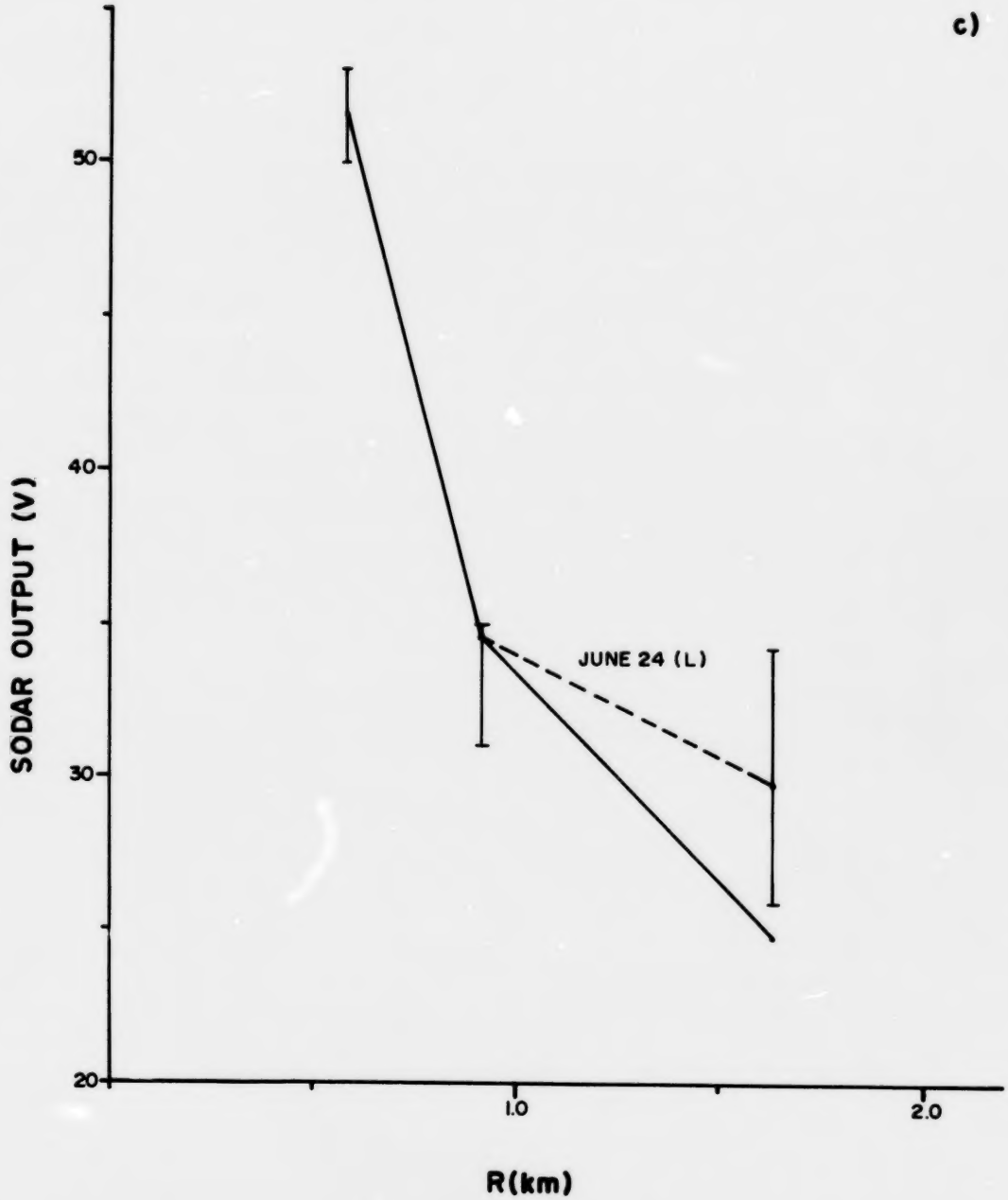

Figure 3-47: Experimental return signal ranges versus spatial target range recorded during high (H) propagation periods of a) May 23 and 30, and b) June 24 and 30. Corresponding ranges recorded during lower (L) propagation periods of c) June 24 and d) June 30. Solid line segments in all figures represent expectations on basis of empirical model described in text.

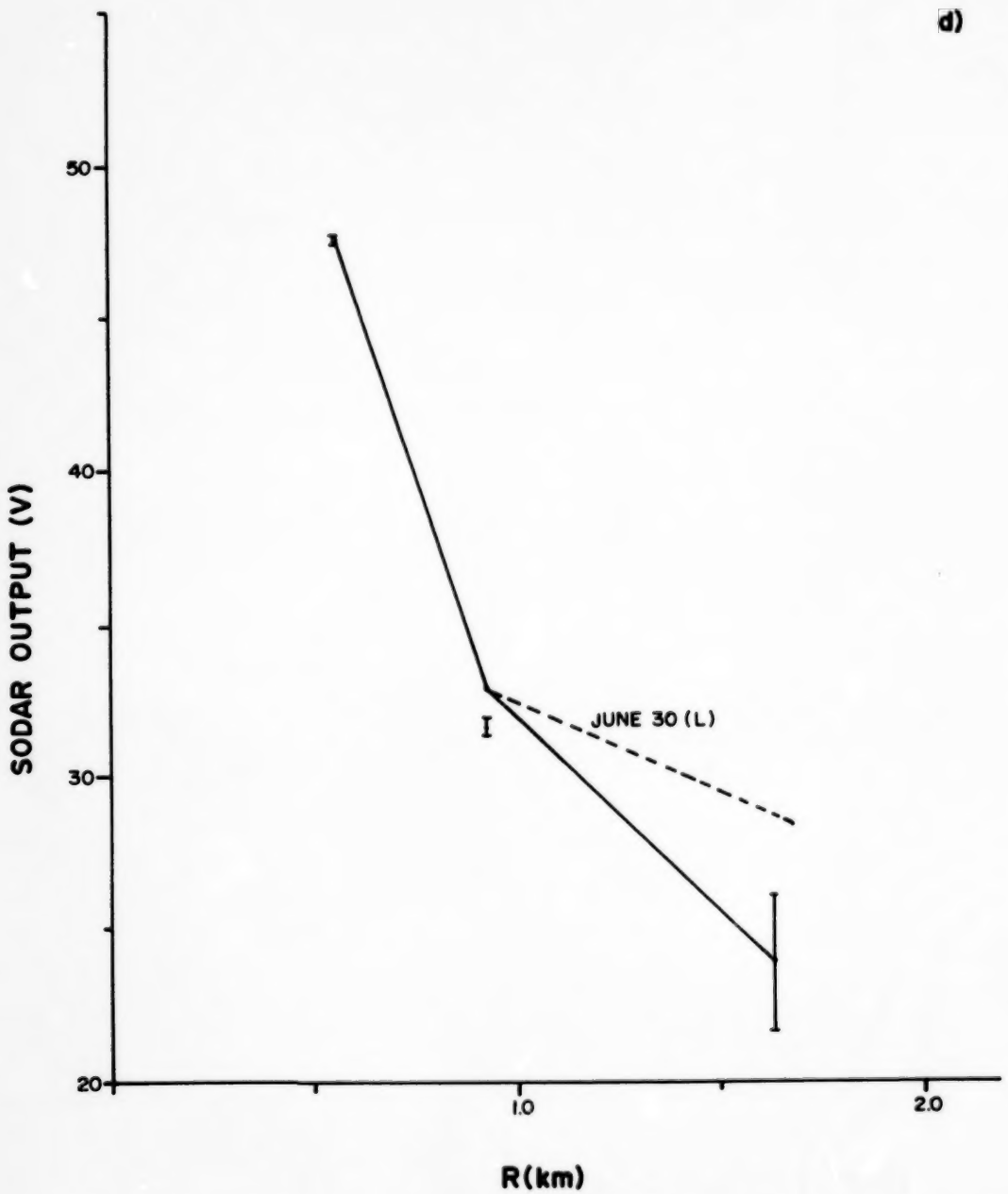

Figure 3-47: Experimental return signal ranges versus spatial target range recorded during high (H) propagation periods of a) May 23 and 30, and b) June 24 and 30. Corresponding ranges recorded during lower (L) propagation periods of c) June 24 and d) June 30. Solid line segments in all figures represent expectations on basis of empirical model described in text.

4. EVALUATION OF ACOUSTIC ICEBERG DETECTION

4.1 BACKGROUND

Before the data and interpretations of Section 3 are applied to feasibility evaluation, it is appropriate to review and outline the main features of the two basic types of usage anticipated for the iceberg detector and their respective difficulties.

In the first instance, the acoustic detection concept was originally proposed as a solution to the problems of detecting the presence of navigationally dangerous iceberg fragments in the midst of a pack ice environment. Evaluation of the instrument's applicability in this case required examination of its ability to distinguish sounds reflected from such fragments in the presence of both similar reflections from other less hazardous topographic ice features and environmental noise. The problem of reflection from non-hazardous ice objects such as ridges and rubble fields was in large part dealt with in the earlier theoretical treatment[1]. It was found that reflections from such objects were at least 20 dB smaller than returns from an 80° inclined iceberg surface of 50 m^2 total area oriented perpendicularly to the acoustic beam. The low magnitude of the ice feature returns was attributable to the inverse dependence of backscattering cross-section on the grazing angle of the incident beam. The large differences in the relative strength of the iceberg- and ridge-returns reflected the much larger (typically 80° to 90° as opposed to 20° to 30°) grazing angles formed by the nearly vertical iceberg side surfaces with the nominally horizontal acoustic beam. Physical arguments for this effect were also presented in terms of underwater sound data where the more nearly vertical surface of the underice ridges were found to totally dominate reflected sound mappings relative to much more extensive areas of more gradually sloping ice features. These results were strongly supported by our general observations of the near invisibility of low-lying rounded islands at the Oak Bay site and by the observations (subsection 3.3.2) that detectable returns from a 2.25 m^2 planar reflector were achieved only when the normal to the target surface deviated by 30° or less from the incident beam direction. These results do not preclude the occasional presence of strong returns from individual vertically upended floes of appropriate orientation. However, such returns should be, in most cases discernible from iceberg-related reflections by their magnitudes and by the much sharper dependence of these magnitudes on the changing angle (with vessel advance) between the reflecting floe surface and the acoustic beam direction.

The demonstration of the relative unambiguity of detected iceberg reflections reduced the principal task of our evaluation of the in-ice application to determining whether in fact, such detection is possible in the presence of the anticipated levels of noise introduced into the Sodar output by the interactions of the ship with the atmospheric and ice pack environments. It should be recognized that, in this application, the

minimum usable detection range for a given hazardous object is reduced relative to the second, open-water case discussed below because of the slower (by a factor of 3 or 4) speeds and shorter stopping distances characteristic of an ice passage.

The importance of the second area of application, namely, in nominally ice-free polar- or sub-polar-waters was emphasized by several members of the project review committee in November, 1985. Additional support for the existence of a need for such a detection capability was provided by the results obtained by Wadhams[22] of the Scott Polar Institute and Polar Oceans Associates Ltd. Dr. Wadhams is the editor of "The Iceberg Newsletter" and is an acknowledged authority on floating ice. In his evaluation of the effectiveness of marine radar in detecting Antarctic icebergs in the stormy waters of the southern oceans, Wadhams found that radar signals from even very large bergs often disappeared into the sea clutter at distances less than 1 or 2 nautical miles. Concerns arising from the failure to detect such icebergs have recently forced southern hemisphere marine traffic routes northward away from iceberg-inhabited zones into much rougher waters. The costs of the route adjustment have included additional fuel consumption, longer travel times and wave-induced damage. A more explicit description of this particular market for an effective detection device has been provided in a separate communication from Wadhams reproduced in Appendix C.

Similar "open" water detection requirements exist in the major north Atlantic shipping lanes and in the ice-free segments of the Arctic marine transport routes which include, for example, the southern and central offshore regions of West Greenland. Much of the motivation for navigational improvement in such areas is associated with the cost savings involved in maintaining the normal 15 to 20 knot speeds achievable in a truly ice-free open ocean. At such speeds avoidance may be a problem unless detection ranges are in the order of 1 km or more. The achievability of such detection ranges from a vessel moving rapidly through a turbulent ocean and atmosphere is the principal object in our evaluation of this instrumental application.

Our procedure separately addresses the in-ice and open ocean feasibility questions in subsections 4.2 and 4.3 respectively. The detection system considered in the evaluation is assumed to have characteristics identical to the instrument tested in our study with the exception of an assumed five-fold (7 dB) increase in transmitted power and the assumption that such power levels are also achievable at lower (1 kHz) and higher (8 kHz) transmission frequencies. This increase in the transmitted power to a level of 350 acoustic watts reflects improved transducer technology and is available in the latest version of the Sodar produced by the manufacturer. Other, possibly very significant, improvements in the performance of the tested unit will be considered in a concluding summary and recommendation subsection (4.4).

As indicated by the foregoing summary, the following evaluation of the tested system's likely performance will concentrate on the system's capability to detect reflected signals from small but hazardous iceberg fragments at distances sufficient to allow avoidance. The noise levels which set the limits of this detectability will be assumed to be determined by airborne sound and by sound generated close to or at the detecting transducer. Structure-transmitted sound, i.e. vibrations, will be assumed to be eliminated through the use of mechanical filters at the instrument mount. Such filtering has been successfully applied in marine applications of Sodar[23] to wind profiling and consultations with specialists in Vancouver B.C. indicated that elimination of this noise component through filtering and choice of instrument location was relatively straightforward.

Our test results consist of return signal estimates for reflections from a vertical iceberg face with an area of 50 m^2 oriented perpendicularly to the direction of the transmitted acoustic beam. The height of the transmitter relative to the surface would, in most applications, be 10 m or more but does not directly enter into our evaluation which is based on the empirical technique used to describe return signal levels at the Oak Bay site where transmitter elevations were 5 to 6 m. It is assumed that the transmissions are carried out at -20°C and that the observed empirical reflected signal relationships are maintained at lower (1 kHz) and higher (8 kHz) frequencies. In the first instance small corrections have to be applied to our free propagation results to account for the temperature dependence of the atmospheric attenuation. The extrapolation to other frequencies is probably only questionable at 8 kHz where the maintenance of the same electrical to acoustic power conversion efficiency would require a change in transducer properties and possibly in antenna dimensions. Further problems in this case could be associated with the known falloff with frequency of sound propagation into the acoustic shadow (Figure 3-46). Additional reductions of approximately 6 dB will be assumed applicable to return acoustic signal levels in all cases where one or more legs of the return path are upward refractive.

4.2 IN-ICE ICEBERG DETECTION

Estimation of signal returns from our 50 m^2 test iceberg surface and of the corresponding noise levels was carried out assuming the presence of upward refraction on at least one of the acoustic return path segments. At low wind speeds $\leq$ 4 m/s at h= 10 m, upward refraction is not present because of the predominance of strong [i.e. .22°C/m in Figure 6 of reference[1]] positive vertical temperature (and sound speed) gradients characteristic of the boundary layer above the ice surface. Under such conditions, returns from distances greater than 1 km are about 5 dB stronger than returns at higher wind speeds where upward refractive propagation would be present on one leg of the two-way path (see subsection 3.5.3). We have neglected this correction and assumed instead the worst case, upward-refractive transmission conditions giving a return

13 dB below the free propagation values from targets at R $\leq$ 1.0 km. Returns from more distant targets, on average, are describable by a further 10 dB reduction (23 dB in all) from the free propagation R = 1 km value. Noise level calculations were carried out similarly for worst case low and high wind scenarios namely where the vessel was assumed to be moving at 5 m/s directly into 3 m/s and 15 m/s winds. Contributions to noise were estimated for both the icebreaking and wind-driven ocean noise components using respectively Figure 3-42 (with appropriate bandwidth and 20 dB side lobe reduction values) and the relative wind-Sodar signal relationships of Figure 3-44. The calculated Sodar output signal levels at R = .5, 1.0 and 1.8 km are plotted in volts in Figures 4-1a,b,c for f = 1, 2 and 8 kHz respectively. The horizontal solid lines in each Figure represent the calculated noise levels for the worst case scenarios cited above in which the icebreaker is moving at 10 knots directly into 30 and 6 knot winds.

These results, first of all, indicate that, even in the most unfavourable ship heading, under 30 knot winds, signal returns are at least .1 v above the noise level out to .95, 1.25 and 1.4 km for f = 1, 2 and 8 kHz respectively. The detectability of such a signal elevation with a four pulse averaging scheme was illustrated in Figure 3-25.

At the 3 m/s wind speed the same .1 v signal elevation (relative to noise) criterion would give detection ranges of 1.4 , 1.7 and 1.8 km at the same transmission frequencies. These results strongly suggest that detection of icebergs at ranges much larger than the few hundred metres needed to effect avoidance, is readily achievable even with an only slightly more powerful version of the present Sodar system (the above detection ranges would be reduced by about .1 km if the present 70 acoustic watt transmission level were maintained). Moreover it should be noted that the limiting noise factor in the worst case studies is the wind-related noise component which on the basis of the discussion of subsection 3.4.2, is associated with wind generated noise in the vicinity of the transducer face. The installation of an open cell foam windscreen at this face and other design modifications are likely to reduce this noise to levels close to the ice-only noise values indicated by the dotted lines in Figures 4-1a,b.

The superiority of the f = 2000 Hz detection capability suggested by these results must be regarded with a good deal of caution because of a number of assumptions made regarding the freqency dependence of several calculation components. Thus, for example, questions can be raised as to the extent to which our f = 2000 Hz empirical results can be applied, with corrections limited to the effects of atmospheric attenuation as a function of transmission frequency. Similarly, our rather arbitrary imposition of an additional 6 dB reduction in the 8 kHz signal return represented an attempt to approximately account for the expected decreased levels of propagation into the acoustic shadow. The return data in the absence of this additional loss are indicated by the broken-line curve in Figure 4-1c. Further uncertainties are introduced when account is taken of possible additional losses of return signal intensity due to acoustic

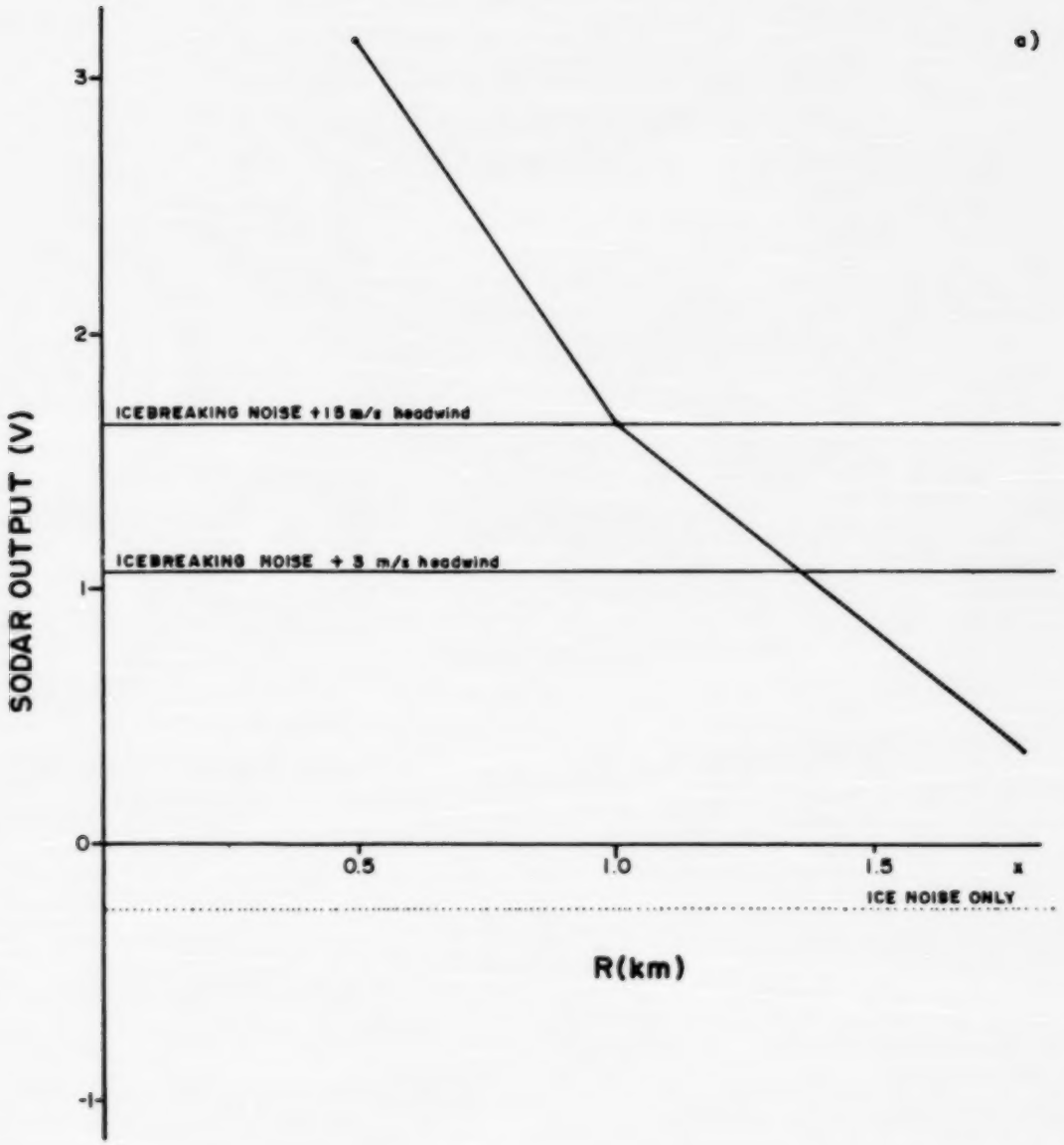

Figure 4-1: Plots of estimated noise and signal levels in the presence of icebreaking noise and 3 m/s and 15 m/s headwinds on an icebreaker underway through first year ice at 5 m/s (10 kts). Noise and signal levels are indicated by the horizontal (range-independent) solid sloping lines respectively for a) f = 1000 Hz, b) f = 2000 Hz and c) f = 8000 Hz. The broken line curve included in c represents the signal levels in the absence of the 6 dB additional loss assumed at f = 8000 Hz with respect to propagation into acoustic shadow (see text).

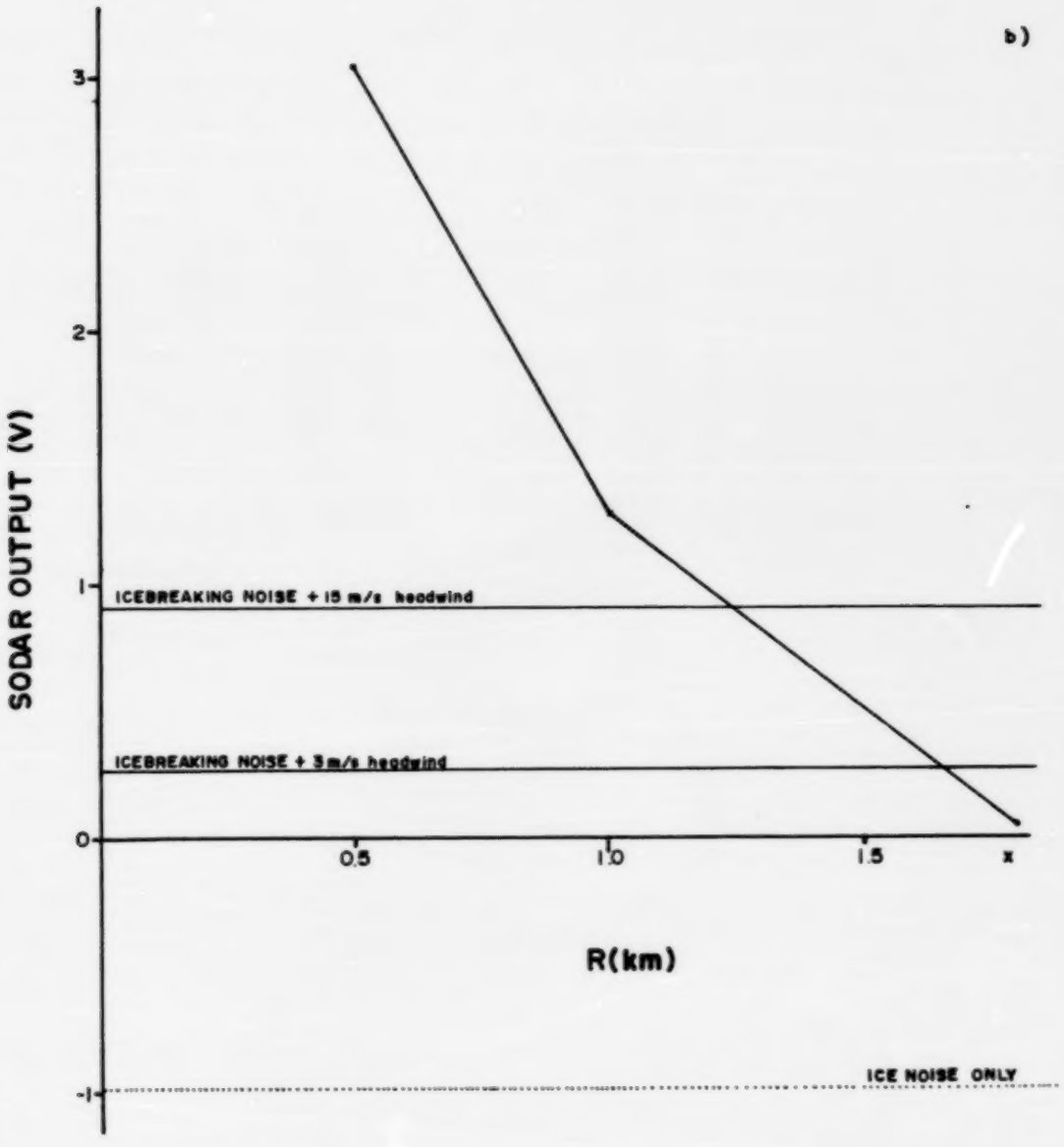

Figure 4-1: Plots of estimated noise and signal levels in the presence of icebreaking noise and 3 m/s and 15 m/s headwinds on an icebreaker underway through first year ice at 5 m/s (10 kts). Noise and signal levels are indicated by the horizontal (range-independent) solid sloping lines respectively for a) f = 1000 Hz, b) f = 2000 Hz and c) f = 8000 Hz. The broken line curve included in c represents the signal levels in the absence of the 6 dB additional loss assumed at f = 8000 Hz with respect to propagation into acoustic shadow (see text).

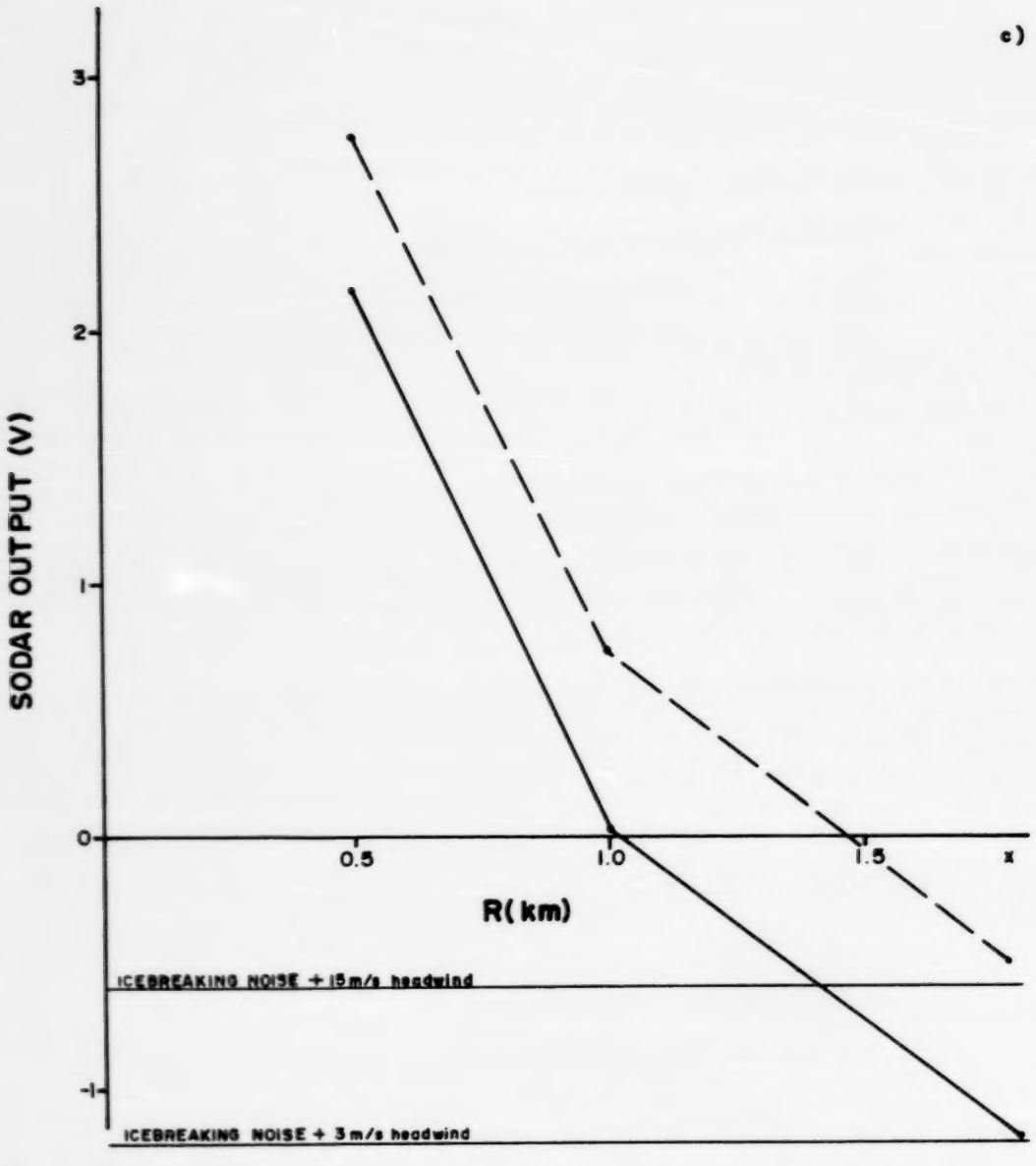

Figure 4-1: Plots of estimated noise and signal levels in the presence of icebreaking noise and 3 m/s and 15 m/s headwinds on an icebreaker underway through first year ice at 5 m/s (10 kts). Noise and signal levels are indicated by the horizontal (range-independent) solid sloping lines respectively for a) f = 1000 Hz, b) f = 2000 Hz and c) f = 8000 Hz. The broken line curve included in c represents the signal levels in the absence of the 6 dB additional loss assumed at f = 8000 Hz with respect to propagation into acoustic shadow (see text).

scattering off raindrops, droplets or snowflakes. Both theoretical calculations[23] and personal observations in noise propagation (Dr. T. Embleton, pers. comm.) and Sodar wind profiling (Dr. K. Underwood, pers. comm.) studies indicate that such losses will be small and unlikely to significantly affect our detection range estimates. Nevertheless, since their importance will undoubtedly increase with transmission frequency[24], judgements on the optimal detection frequency must await further field tests.

4.3 OPEN SEA DETECTION

The primary differences between the in-ice and open-ocean detection case is, of course, the absence of icebreaking noise and the additional presence (in very high seas) of clutter arising from reflection by wave surfaces within the 2 km detection range. Additionally, much larger noise levels can be generated by the larger relative wind speeds which are possible on a ship moving at, in our example, 20 knots into a 10 m/s (20 knot) headwind.

Our experimental data showed no detectable contribution from the highest observed sea states, corresponding to average significant wave heights of 4 to 5'. This situation may, of course, change under more extreme open-ocean conditions which may necessitate the use of statistical techniques to reduce the resulting clutter contributions.

The comparison of signal versus noise levels for this case is illustrated in Figure 4-2 for an f = 2000 Hz transmission frequency. Again, the noise results depend upon the experimental noise versus relative wind relationships of Figure 3-44 and, for the 10 m/s headwind case, upon extrapolation through the 10 m/s to 20 m/s relative wind speed range.

The results indicate that for wind speeds equal to or less than 20 knots, the minimum range of detectability (again using the .1 v elevation criterion) is between 1.4 and 1.5 km. Again, reduction in the Sodar noise level versus wind component relationships by improved screening and design could increase this value to close to 2 km.

4.4 SUMMARY AND RECOMMENDATIONS

Taken together, the experimental return signal data and extrapolations presented in Section 3 and in subsections 4.2 and 4.3 respectively, strongly suggest that acoustic iceberg detection is feasible in both ice-pack and open-ocean environments. The testing made the most unfavourable assumptions about wind speed, wind heading and noise generation and yet obtained likely detection ranges for a 50 m^2 iceberg surface greater than 1.0 km in pack ice and as least as large as 1.4 km in the open ocean. These performance estimates for the "as is" Sodar instrument (with a factor of five increase in power output) are particularly encouraging in view of several obvious changes in instrument

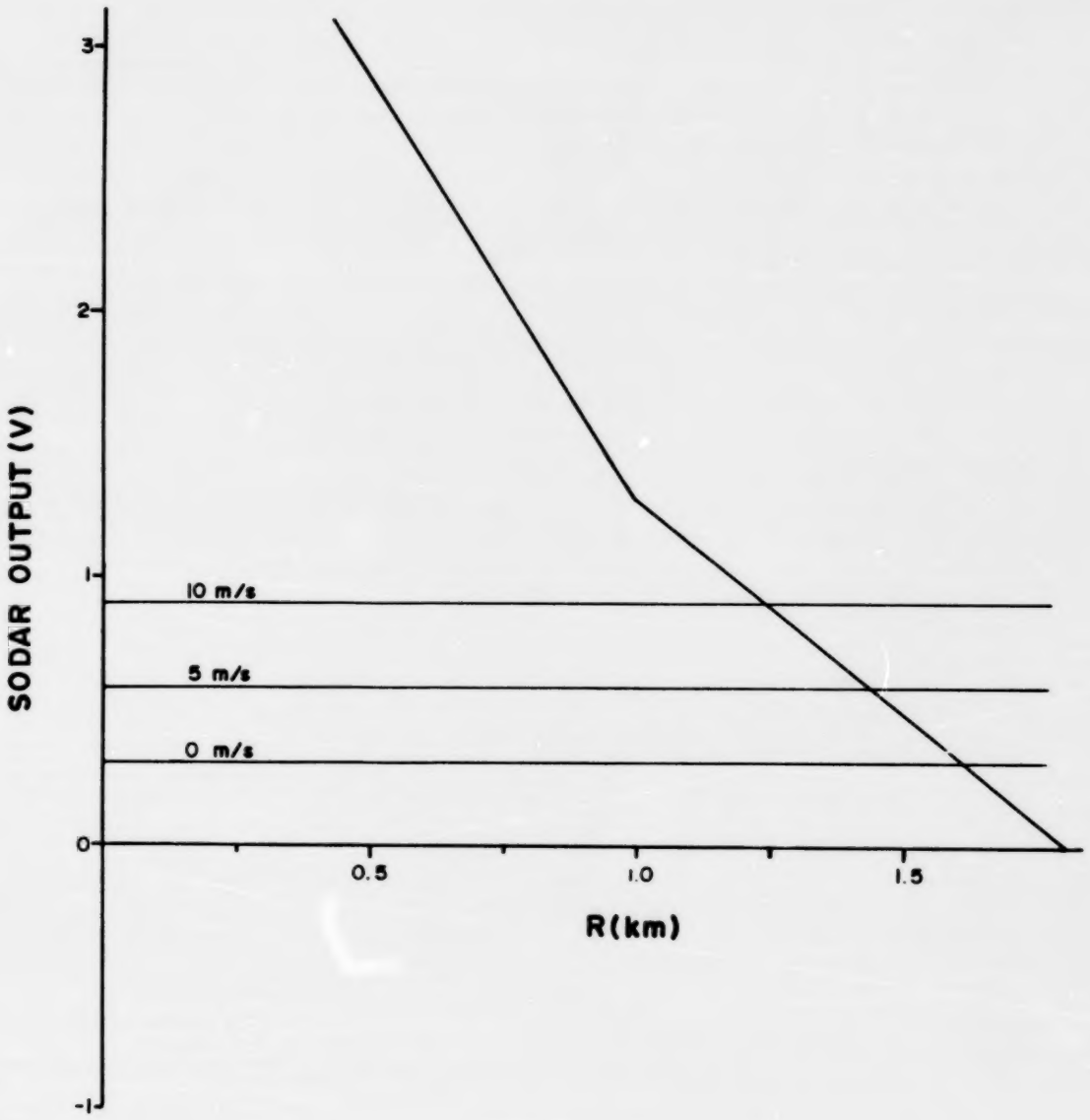

Figure 4-2: Plots of estimated noise and signal levels for a vessel moving at 20 knots (10 m/s) into 10.5 and 0 m/s headwinds.

design and operation such as the installation of windscreening and the use of spread-frequency enhancement techniques which could increase the experimental signal to noise ratio sufficiently to extend the worst case open-ocean detection range out to at least 2 km.

The translation of the detection concept into a functioning prototype navigational instrument should also be facilitated by the relative consistency of most of the recorded transmission and reception data with current models and understandings of long range sound propagation. Nevertheless, the development process will clearly require further testing and subsequent design and development work in three major areas:

(1) antenna location, mounting, protection and directional control;

(2) optimization of reflected signal detection and the deduction of reflector position from the timing and directionality of returns; and

(3) conversion of the received return signals into easily interpreted representations of reflector strength resident in specific areas forward of the ship's heading.

In the first instance it seems most likely that an optimal physical location for the antenna (and associated front-end electronics) would be in a far forward position such as on the elevated 60' tower at the rear of the fo'c'sle deck on the M.V. Arctic (Figure 4-3). Primary technical tasks would include achieving at least 30 dB isolation against structure transmitted vibration by suitable mechanical filters; maintaining good rejection figures with respect to airborne noise generated at the bow below and behind the forward looking antenna and the protection of delicate transducer coils against corrosion and other damage from spray and deckwash. Should the noise shielding and protection requirements preclude the use of more exposed, electronically directed multiple transducer arrays, the mounting will have to allow for mechanical scanning in a horizontal plane and perhaps gimbal suspension. Because of the considerable weight (approximately 700 lbs) of the tested single transducer unit, the mounting and other problems would be considerably simplified if detection was carried out at higher (5 to 8 kHz) frequencies because of the correspondingly much smaller dimensions of the antenna and shielding structures.

The optimization of the reflected signal reception would include making the fundamental decisions on the optimal transmission frequency and modification (i.e. the addition of a windscreen) and redesign of the antenna shield to minimize noise generation at or close to the detecting transducer. These considerations might include the use of separate transmitting and receiving antenna detectors. Additional decisions would have to be made regarding the use of spread-signal techniques such as frequency sweeping or optimally coded pulse sequences to increase the signal-to-noise ratio. Thus, for example, correlated detection of returns

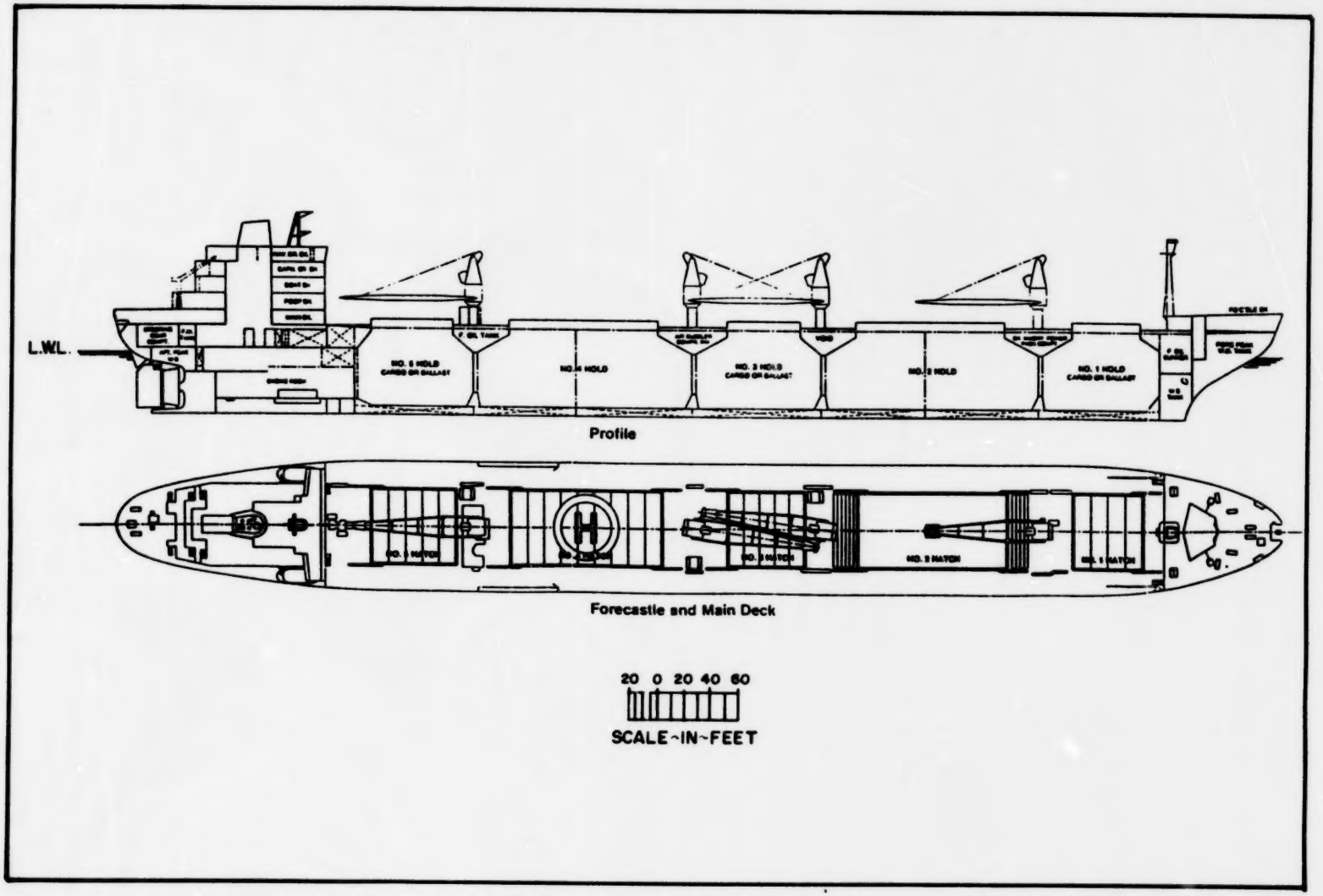

Figure 4-3: Side- and plan-views of the M.V. Arctic, a potential platform for an acoustic detection instrument.

relative to a transmitted sequence of 16 consecutive .1 second pulses each corresponding to one of two opposite phase values can give a signal to noise gain of 9 dB.* It should be noted however, that because of the slow propagation speeds of sound the transmission reception of such a sequence by a single antenna would result in the absence of observations for points at R < 300 m, close enough so that reflected signals reach the receiver during the transmission period. A slightly more complex pulsing scheme would have to be devised to provide coverage in this close-in region coincident with the use of the high process-gain detection.

A further 3 dB increase in processing gain is possible if data at R < .5 km are not required from every pulse sequence. Similar trade-offs between the desireability of long range detection and minimal confusion in interpretation would have to be made with regard to the observations reported in subsection 3.3.2 with respect to overlap effects associated with late arriving returns from reflections of previous pulses by very distant objects shorter-range reflection data. Clarification here could be achieved very simply by shifting the transmission frequencies of each successive pulse or pulse sequence. As well, some consideration should be given to methods of locking the narrow band detection system to the Doppler-shifted signals produced by the relative motion between the ship and the reflecting objects.

The initiation of antenna and mounting design studies and the development of efficient scanning strategies would require noise and signal return data (include frequency dependences) in the proposed operational environment.

Finally, assuming the overcoming of the mechanical, electrical and signal processing obstacles to the production of reliable interpretable acoustic signal returns, a processing and display scheme must be devised which:

a) correctly assigns each return to the appropriate range and direction by taking account of the motions of the ship attached antenna during the interval between the pulse transmission and the reception of the given portion of the signal return;

---

* It should be noted here that our empirical model for representing the reflected return signals already incorporates some processing gain since signal level values were deduced from interval-averaged returns incorporating typically 20 to 50 individual pulse returns. The processing gain from a 50 pulse average, for example, would be approximately 8.5 dB. Since averaging over this number of pulses with a typical pulse repetition interval of 15 seconds is impractical from a moving vessel, the processing gain achieved by the proposed coded-pulse scheme is probably necessary to retain the validity of the estimated return signal to noise estimates in feasible, shorter (i.e. .5 to 1 min.) averaging periods.

b) enters the magnitude of the return from each range and directional cell for each pulse (or pulse sequence) into the appropriate portion of a refreshable memory, the contents of which are displayed on a colour CRT display monitor.

Reflector strength entries would have to be shifted forward in the plan view display with vessel advance. Statistical treatment of individual entries will be necessary to reduce the effects of sea clutter and to allow for fluctuations and systematic changes in the strength of reflections and in the angular range cell width as the vessel advances. The quantity plotted or colour coded into each displayed forward range cell (Figure 4-4) should be a measure of the range-adjusted strength of the reflected sound from objects in that portion of the vessel foreground.

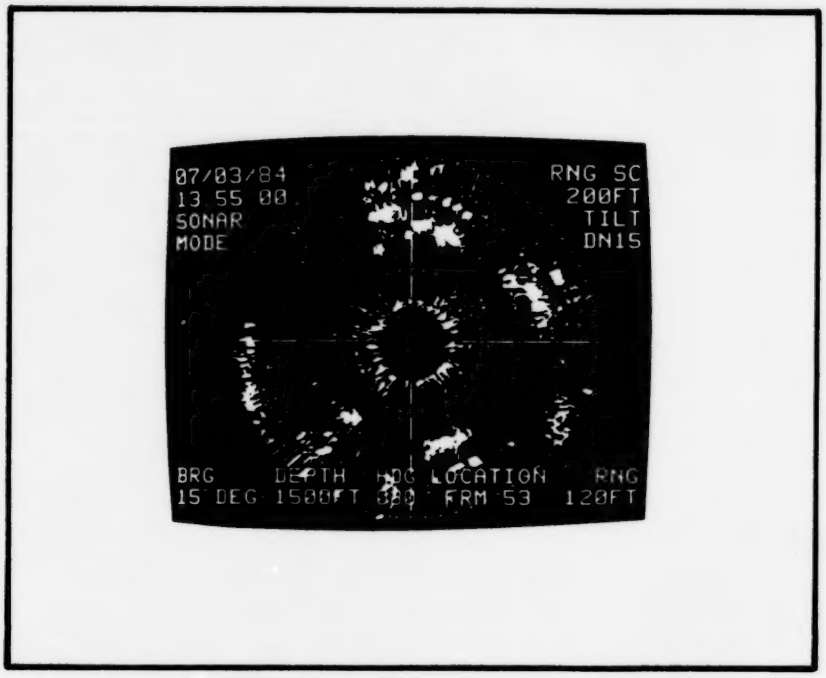

Figure 4-4: A representative modern marine radar display screen such as might be incorporated into an operational air acoustic detection system.

Of course, depending on the application, much simpler display (and scanning) systems are possible, giving, for example, reflectance values from each range cell along a single direction paralleling the instantaneous ship-heading as obtained from averaged individual sequences of coded pulse returns.

It is recommended that follow-up field experiments be initiated as soon as possible to generate the operating environment data necessary to confirm our calculated performance estimates and to allow the derivation of design specifications for a prototype detection instrument. The experiments would utilize a single transducer Sodar unit similar to that instrument used in the preliminary work. Modifications would include increased power levels to 350 acoustic watts and a capacity to operate over the frequency range 1.6 to 6 or 6 kHz with minimal hardware changes. A real-time hard copy display of individual acoustic pulse returns in a logarithmic range-corrected format (see Figure 3-11) is essential and should be incorporated in the tested system. It may also be worthwhile to pass the return pulse data through a data memory buffer to allow the operator the option of viewing time-averaged signal products. In addition to the disk storage of all return pulse data, storage and display capacities should be assured for the "wind-table or Doppler-shift data which are the principal product of a Sodar instrument in its normal meterological usage. Such data could be extremely useful in identifying atmospheric conditions associated with various qualities of instrument performance.

The experimental program would have two major field components to be carried out in the Victoria B.C. vicinity and on board a vessel in Arctic or sub-Arctic waters. The former work would carry out further testing of the slightly modified instrument in relatively convenient temperate latitude circumstance in order to assure proper functioning and to more economically determine the relative effectiveness of the three different test frequencies in detecting short- and long-range targets both in the presence and absence of precipitation. Testing could be carried out at the Oak Bay and Boundary Bay airport sites. In the latter case, at least one set of experiments will be carried out at night and in the early morning hours to compile more detailed data on return signal characteristics coincident with downward and neutrally-refractive conditions in the surface boundary layer.

The second part of the program will involve the installation of the Sodar instrument (self contained with its own trailer and power generation capacity) on a Canadian Coast Guard icebreaker or an icebreaking transport such as the M.V. Arctic. A third alternative would be to incorporate the instrument in any planned shipboard components of the broader FIDEX testing program. In any case, once installed at a forward portion in an icebreaking vessel, the Sodar instrument should be used to measure acoustic signal returns from various iceberg and sea-ice-related objects, both in the midst of pack ice and in open water and under all possible weather conditions including blizzard or "white-out" circumstances which

so frequently occur in Arctic waters. The frequency dependence of the detection process should be tested to an extent determined by the results of previous testings at temperate latitudes. Thus, if for example, the latter data indicate the general superiority of the performance of the instrument at one frequency, studies will be confined to a confirmation of this result under various Arctic conditions.

Measurements should be carried out both from the stationary vessel and while underway (assuming the availability of a vibration isolator). Monitoring of the ship's air-and structure-borne noise environment should be carried out during the Sodar detection measurements using the Sodar itself as well as a sound-level meter and, possibly, a broad-band tape-recorder. Basic meteorological-, shipspeed- and heading-data would be recorded coincident with the testing. All iceberg and sea-ice targets would be photographed and documented.

Emphasis in the experiments should be placed upon obtaining actual return data from various sized ice-objects under well documented and different weather and wind configurations.

Analysis of the data should be directed at the production of a report which describes the derived performance and parameter dependences and provides interpretation relevant to the specification of the basic characteristics of a prototype instrument, i.e. operating frequency, power level, beam width and scanning strategy together with a realistic assessment of its performance characteristics under various in-ice and open-ocean meteorological conditions.

The results of such a report would form the basis for deciding whether to proceed with prototype construction and testing.

In conclusion, the results of our study provide detailed technical evidence for the effectiveness of the air acoustic iceberg detection concept. In view of the apparently large market for a related navigational instrument, further research commitments certainly appear to be justified pursuant to possible eventual prototype design and construction.

5. REFERENCES

1. Marko, J.R. and R.D. Huston, 1985. An evaluation of the feasibility of air acoustic detection of icebergs in pack ice. Interim report prepared for the Transportation Development Centre, Montreal, Quebec. 75 pp.

2. Gentec Inc., 1985. Ultrasonic Doppler velocimeter for icebreakers. Transportation Development Centre, Montreal, Quebec, Rep. No. TP6787E.

3. Ingard, K.U., 1953. A review of the influence of meteorological conditions on sound propagation. JASA 25, pp. 405-411.

4. Parkin, P.H. and W.E. Scholes, 1965. The horizontal propagation of sound from a jet engine close to the ground at Hatfield. J. Sound Vib. 2, pp. 353-374.

5. Daigle, G.A., J.E. Piercy and T.F.W. Embleton, 1983. Line-of-sight propagation through atmospheric turbulence near the Ground. J. Acoustic. Soc. Am. 74, pp. 1505-1513.

6. Daigle, G.A., T.F.W. Embleton and J.E. Piercy, 1986. Propagation of sound in the presence of gradients and turbulence near the ground. J. Acoust. Soc. Am. 79, pp. 613-627.

7. Piercy, J.E., T.F.W. Embleton and L.C. Sutherland, 1977. A review of noise propagation in the atmosphere. JASA 61, pp. 1403-1418.

8. Brown, E.H. and S.P. Clifford, 1976. On the attenuation of sound by turbulence. JASA 60, pp. 788-794.

9. Hutchkins, D.A., H.W. Jones and L.T. Russell, 1983. Model studies of acoustic propagation over finite impedance ground. Acoustics 53, pp. 169.

10. Hall, F.F. Jr, and J.W. Westcott, 1974. Acoustic antenna for atmospheric echo sounding. J. Acoustical Soc. Am. 56, pp 1376-1382.

11. Bass, H.E., L.C. Sutherland, J. Piercy and L. Evans, 1984. Absorption of sound by the atmosphere. In: Physical Acoustics, Vol. XVII, pp. 145-228.

12. Horton, C.W., Sr. and T.G. Muir, 1976. Theoretical studies on the scattering of acoustic waves from a rough surface. JASA 41, pp. 27-634.

13. Horton,. C.W., Sr., S.K. Mitchell and G.R. Barnard, 1967. Model studies on the scattering of acoustic waves from a rough surface. JASA 41, pp. 35-643.

14. Greene, R.R. and A.P. Stokes, 1985. A model of acoustic backscatter from Arctic sea ice. J. Acoustical Soc. Am. 78, pp. 1199-1701.

15. Brown, J.R. and A.R. Milne, 1967. Reverberation under Arctic sea ice. J. Acoust. Soc. Am 42, pp. 78-82

16. Berkson, J.M., C.S. Clay and T.S. Kan, 1973. Mapping the underside of Arctic sea ice backscattered sound. AIDJEX Bull. 18, pp. 51-59.

17. Mandics, P.A. and F.F. Hall, Jr., 1974. An evaluation of the acoustic echo sounder in GATE. Internal paper, Wave Propagation Laboratory, NOAA, Boulder, CO.

18. Ottersten, H., M. Hurtig, G. Stilke, B. Brummer and G. Peters, 1974. Shipboard SODAR measurements during Jonswap 2. J. Geophys. Res. 79, pp. 5573-5584.

19. Bogorodski, P.V. and V.P. Gavrilo, 1979. Noise accompanying the breakup of ice by the hull of an icebreaker. Sov. Phys. Acoust. 25, pp. 73-74.

20. Edwards, R.Y, Jr., M.A. Dunne, G. Comfort, G. Tam, A.M. Nawwar, V. Bulat and M. Steele, 1979. Noise and vibration measurements on the CCGS Radisson. Report prepared for the Canadian Coast Guard.

21. Urick, R.J., 1975. Principles of Underwater Sound. McGraw-Hill Book Company, 2nd Edition, 384 p.

22. Wadhams, D. 1986. Observations of iceberg sizes and frequencies in the south Atlantic Ocean in winter. Iceberg Research. No. 13, pp. 1-5.

23. Mandics, P.A. and E.J. Owens, 1975. Observations of the marine atmosphere using a ship-mounted acoustic echo sounder. J. of Appl. Met. 14, pp. 1119-1117.

24. Little, C.G., 1972. Detectability of fog, cloud, rain and snow by acoustic echo sounding methods. J. Atmos. Sci. 29, pp. 748-753.

APPENDIX A

RELATIONSHIPS BETWEEN SODAR OUTPUT VOLTAGE AND SOUND PRESSURE LEVELS (SPL) RE: 20μPa AT THE RECEIVING ANTENNA

The relationship between the voltage input to the A/D converter (v_o) and input to the logarithmic amplifier, V_I, (Figure 2-2) shown in Figure A-1, can be written as:

$$V_I = \text{antilog}\ (.4v_o - 1) \qquad \text{(A-1)}$$

The voltage generated in the transducer coil can be derived from V_I by:

$$V_s = 10^{-G/20}\ V_I \qquad \text{(A-2)}$$

where G is the power gain introduced between the coil and the input to the logarithmic amplifier.

Since the difference in decibels between two signal voltages V_{SA} and V_{SB} can be written:

$$S_A - S_B \equiv 10\ \text{gb}\ V_{SA}^2 - 10 \log V_{SB}^2 = 20\ [\log V_{SA} - \log V_{SB}] \qquad \text{(A-3)}$$

Successive substitution of A-2 and A-1 for $V_{SA(B)}$ and $V_{IA(B)}$ respectively yields:

$$S_A - S_B\ (\text{in dB}) = 8\ [V_{OA} - V_{OB}] \qquad \text{(A-4)}$$

Letting S_B equal the 20 µPα reference pressure level we can write:

$$SPL_A\ \text{re}\ 20\ \mu\text{Pa} = 8\ [V_{OA} - V_{Oref}] \qquad \text{(A-5)}$$

where V_{OA} - V_{Oref} respectively represent the A/D input generated by signal A and by a 0 dB (re 20 µPα) sound pressure level.

Measurements of the sound pressure immediately beside the Sodar antenna were made using the B & K 2230 sound level meter and recorder on May 30, 1986 at the Oak Bay Marina site. Using the fast instrument response setting RMS SPL levels were recorded corresponding to the easily distinguishable returns from the strongest reflecting marker 1. Computated average SPL values associated with this reflection were used to provide values of SPL_A which could be used in conjunction with the corresponding interval-averaged (Xondar) output voltage V_{OA} associated with the marker 1 return to derive values for the unknown output voltage V_{Oref} corresponding to a 20 µPα sound pressure. Measurements in two sequences of 17 and 50 transmission pulses indicated V_{Oref} = 5.1 v η .2 v.

Using this value the usual 1300 mv to 2200 mv limits of the text's interval averaging signal return plots correspond to 30.4 and +58.4 dB re 20 µPα.

APPENDIX B

METEOROLOGICAL DATA AND MAPS OF OAK BAY AND BOUNDARY BAY AIRPORT SITES

Gonzales Observatory (adjacent to Oak Bay site) and Vancouver International Airport (10 miles from Boundary Bay Airport site, denoted by BB) Hourly Meteorological Readings

Date	Time (hours PDT)	Wind speed (m/s)	Direction	Temperature (°C)
May 16	10	4.5	N	18.8
May 16	11	5.0	NE	20.0
May 16	12	3.6	SE	20.9
May 16	13	2.8	NE	21.7
May 16	14	3.1	N	22.9
May 16	15	3.1	NE	23.7
May 16	16	1.4	SE	20.4
May 16	17	.8	SE	19.4
May 16	18	2.2	S	20.6
May 16	19	2.8	S	21.7
May 21	10	9.0	SW	10.8
May 21	11	9.0	SW	11.4
May 21	12	11.7	SW	12.2
May 21	13	9.8	SW	12.3
May 21	14	11.2	SW	12.5
May 21	15	13.1	SW	13.0
May 21	16	13.1	SW	13.2
May 21	17	13.1	SW	13.2
May 21	18	14.8	SW	12.2
May 21	19	12.6	SW	11.7
May 23	10	4.2	N	10.9
May 23	11	4.5	N	11.4
May 23	12	6.4	N	11.1
May 23	13	5.3	N	12.4
May 23	14	3.6	N	13.6
May 23	15	3.0	N	15.4
May 23	16	3.0	N	16.3
May 23	17	1.7	N	16.9
May 23	18	2.8	SW	12.8
May 23	19	3.6	SW	13.3
May 30	10	4.5	N	18.8
May 30	11	5.0	NE	20.0
May 30	12	3.6	SE	20.9
May 30	13	2.8	NE	21.7
May 30	14	3.0	N	22.9
May 30	15	3.0	NE	23.7
May 30	16	1.4	SE	20.4
May 30	17	0.8	SE	19.4
May 30	18	2.2	S	20.6
May 30	19	2.8	S	21.7

Date	Time (hours PDT)	Wind speed (m/s)	Direction	Temperature (°C)	
June 5	11	1.7	SE	17.0	BB
June 5	12	2.0	SE	18.0	BB
June 5	13	5.6	S	18.0	BB
June 5	14	5.0	SE	19.0	BB
June 5	15	6.2	S	20.0	BB
June 5	16	4.3	S	20.0	BB
June 5	17	5.0	SW	20.0	BB
June 5	18	5.0	W	19.0	BB
June 5	19	2.4	NW	17.2	BB
June 5	20	2.4	SW	16.1	BB
June 6	11	3.1	S	16.0	BB
June 6	12	3.1	S	17.0	BB
June 6	13	1.8	E	17.0	BB
June 6	14	0.6	E	18.0	BB
June 6	15	3.7	SE	18.0	BB
June 6	16	6.2	SE	17.0	BB
June 6	17	5.0	S	17.0	BB
June 6	18	3.0	S	17.0	BB
June 6	19	3.7	S	16.6	BB
June 6	20	3.7	S	16.2	BB
June 24	10	2.2	NE	14.4	
June 24	11	2.2	E	16.4	
June 24	12	3.1	E	16.8	
June 24	13	1.7	S	14.8	
June 24	14	1.7	S	16.3	
June 24	15	3.1	S	14.4	
June 24	16	4.2	SW	15.3	
June 24	17	4.5	SW	14.4	
June 24	18	5.3	S	13.9	
June 24	19	5.3	S	15.0	
June 30	10	2.2	E	14.3	
June 30	11	1.7	S	14.9	
June 30	12	1.7	S	16.3	
June 30	13	2.2	SE	16.4	
June 30	14	2.2	SE	17.3	
June 30	15	1.7	S	16.7	
June 30	16				
June 30	17				
June 30	18				
June 30					

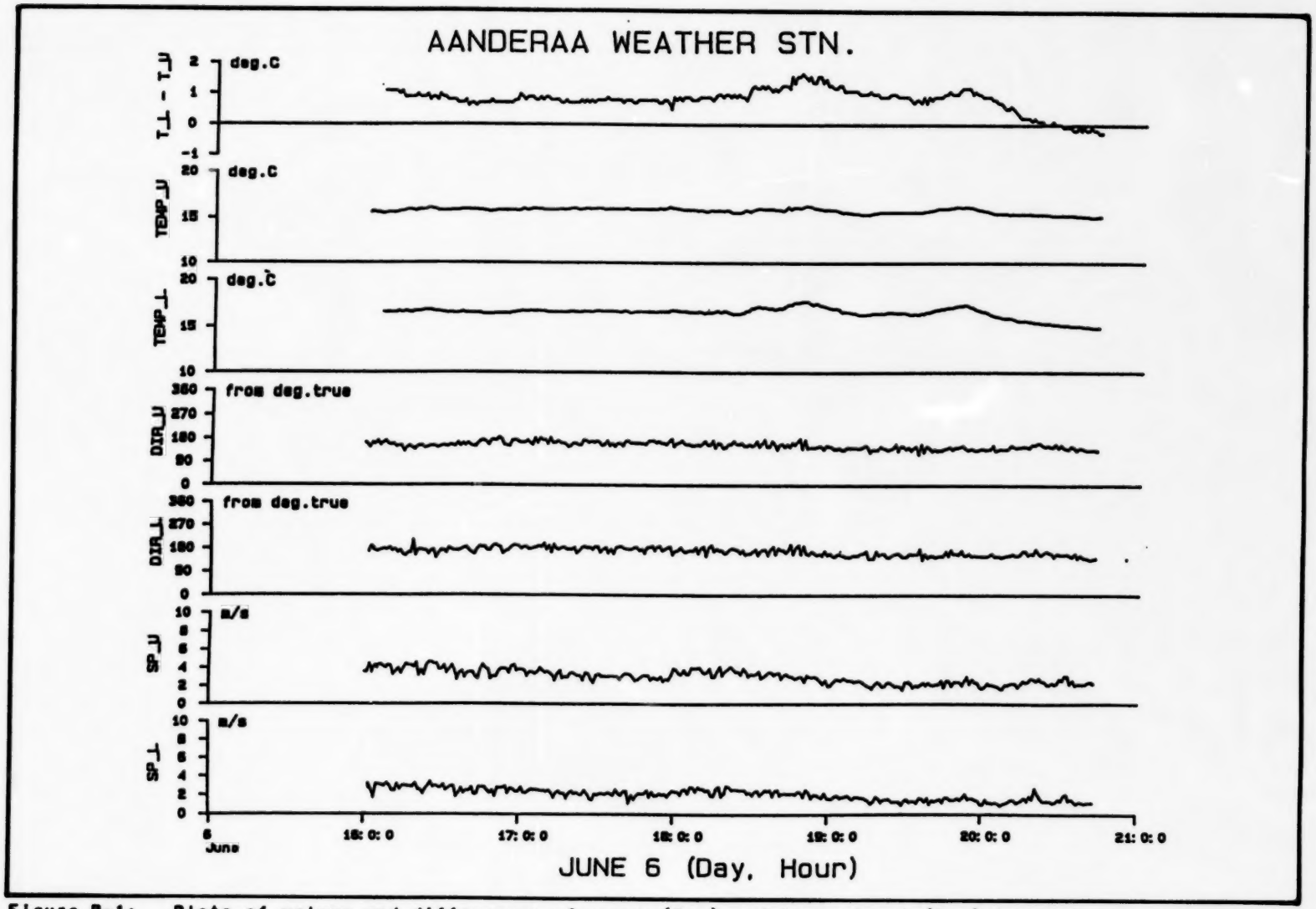

Figure B-1: Plots of values and differences of upper (9 m) and lower level (2 m) temperature, wind speed and direction as a function of time as measured at Boundary Bay Airport, June 6, 1986.

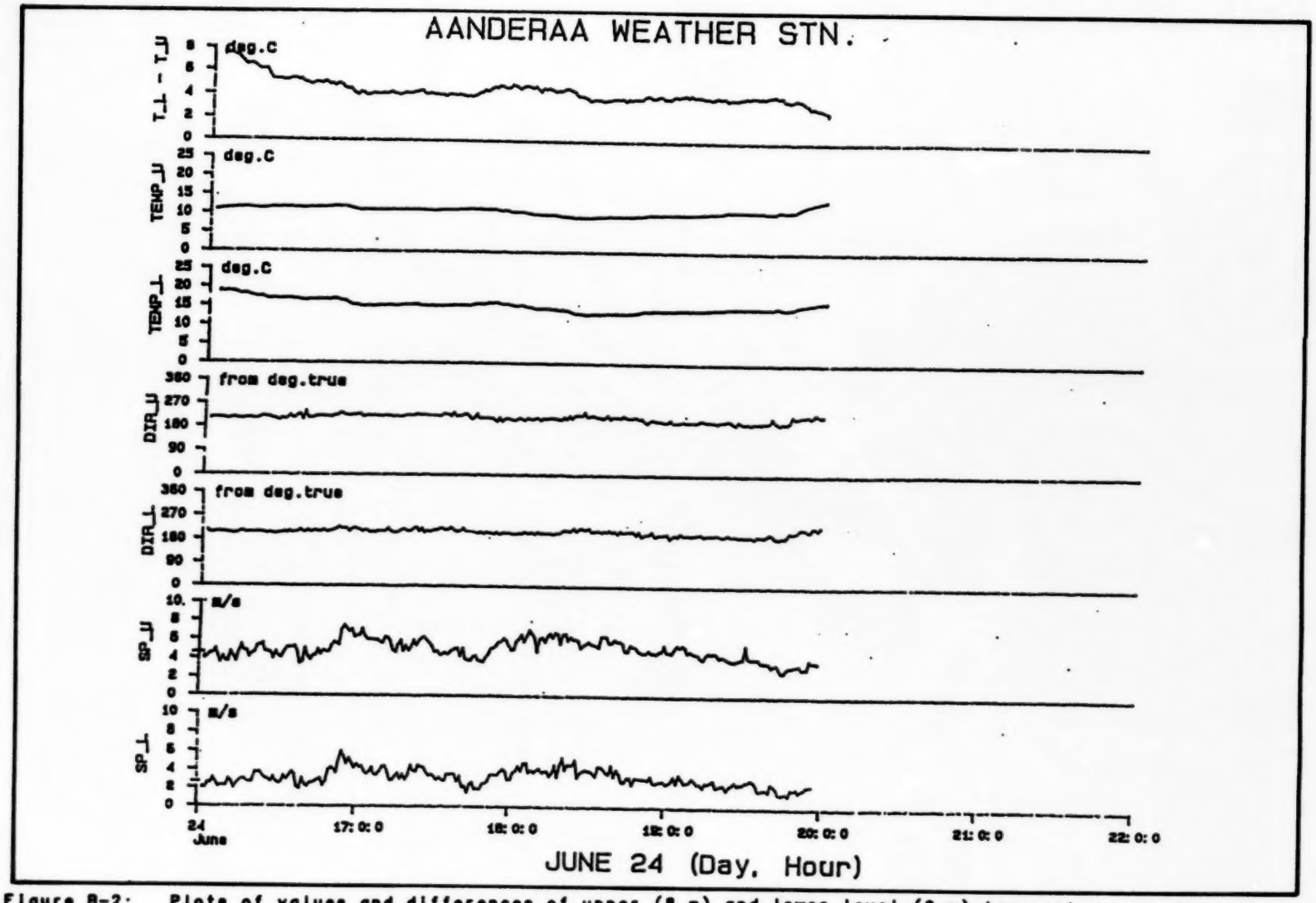

Figure B-2: Plots of values and differences of upper (8 m) and lower level (2 m) temperature, wind speed and direction as a function of time as measured at the Oak Bay Site, June 24, 1986.

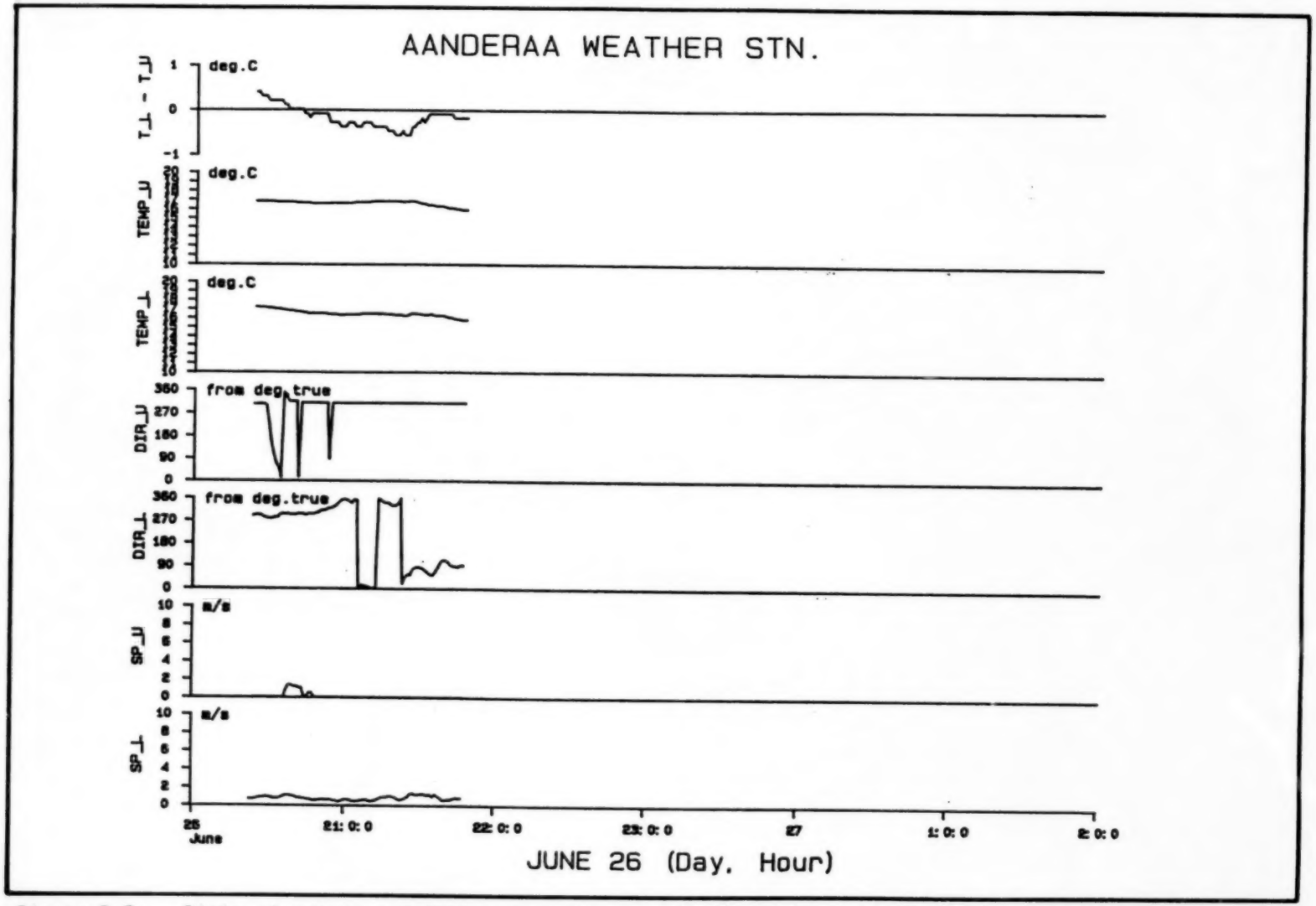

Figure B-3: Plots of values and differences of upper (8 m) and lower level (2 m) temperature, wind speed and direction as a function of time as measured at Boundary Bay Airport, June 26, 1986.

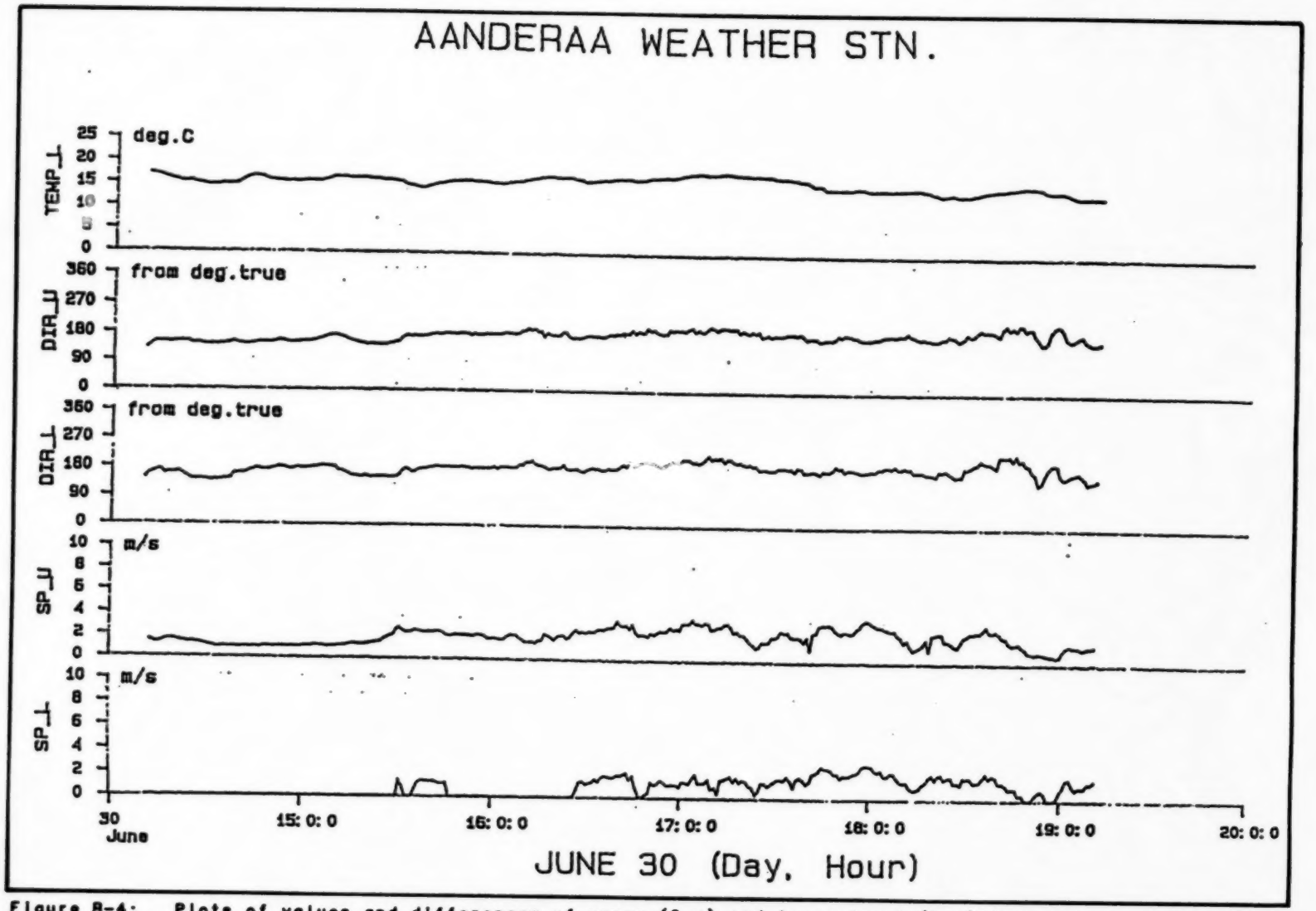

Figure B-4: Plots of values and differences of upper (8 m) and lower level (2 m) temperature, wind speed and direction as a function of time as measured at the Oak Bay site, June 30, 1986.

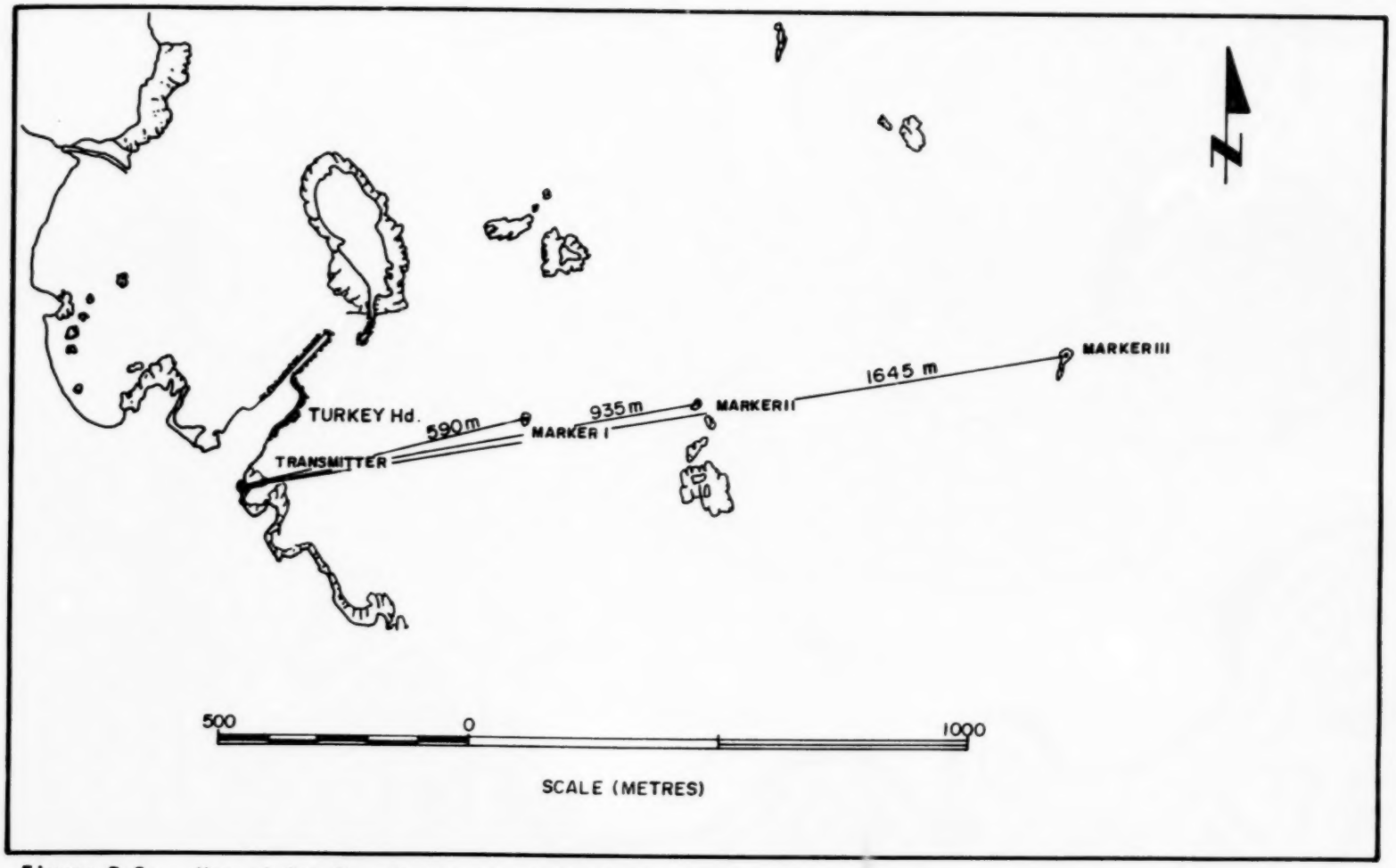

Figure B-5: Map of Oak Bay field site indicating ranges to markers.

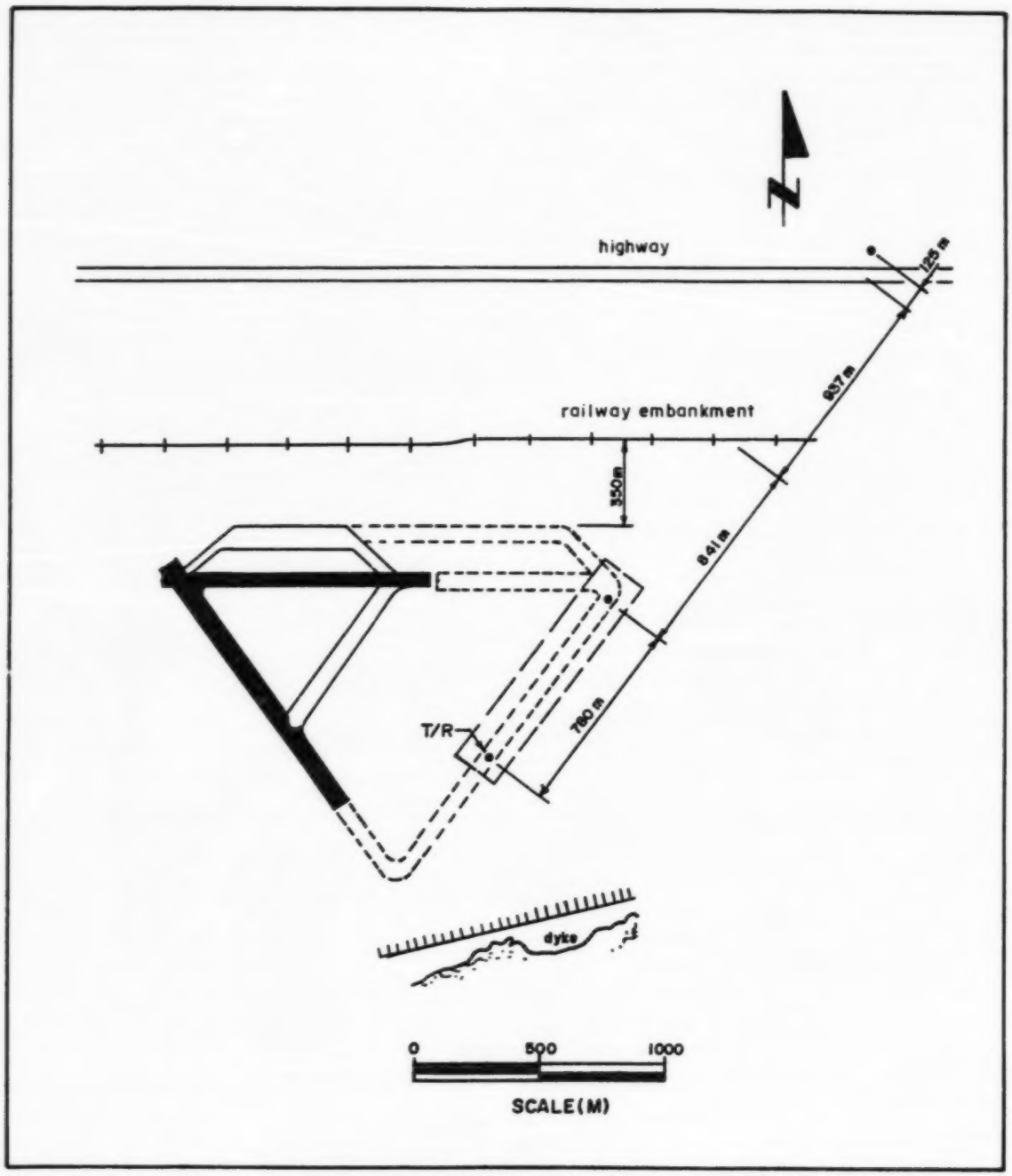

Figure B-6: Map of Boundary Bay Airport site showing position of transmitter/receiver (T/R) and a typical target position denoted by solid circle 780 m northeast of T/R.

APPENDIX C

OPEN MARKET EVALUATION

40, Grafton Street,
Cambridge CB1 1DS

Telephone: 0223 - 66716/322621

Polar Oceans Associates Limited

3 November 1986

Dr John Marko,
Arctic Sciences Ltd.,
1986 Mills Rd RR2,
Sidney B.C. V8L 3S1.

NOV 14 1986

Dear John,

In response to your enquiry, here is a brief assessment of the need for improved detection of icebergs at sea.

One of the chief problems in iceberg detection is the discrimination of a small ice target (growler or bergy bit, of low freeboard but sufficient mass to sink an unstrengthened ship) against sea clutter in the open ocean. The application to Arctic shipping is clear, but what is not often realised is that there is an important application to shipping in the Southern Hemisphere. One of our clients is an important container shipping company, whose main traffic is between New Zealand and Great Britain. Their vessels run a Great Circle route between New Zealand and Cape Horn, taking them through iceberg-infested regions of the Southern Ocean. A number of near-misses have been recorded. We have examined several ways of improving iceberg detectability, including the use of multifrequency radar, radars with improved digital storage and processing, underwater sonic methods, atmospheric sonic methods (your own system) and improved routing using satellite imagery. What is needed, we believe, is a combination of strategic avoidance by improved routing, and tactical avoidance through an improved close-range detection system for growlers. This is of great importance not only to shipping companies but also to shipping insurers. Another client is a major insurance company which deals with the insuring of Antarctic research and supply ships. Traffic of this type of vessel to the Antarctic is increasing and will increase further with the rapid growth in international interest in the Antarctic. Iceberg risks are an important component of the overall risk assessment.

I hope that these considerations can be given some weight in the assessment of the importance of supporting this area of research,

Yours sincerely,

Pete

Dr Peter Wadhams.